

THE UNIVERSITY OF THE SOUTH PACIFIC
LIBRARY

DIGITAL THESES PROJECT

Author Statement of Accessibility- Part 2- Permission for Internet Access

Name of Candidate : AWINESH MUNI SINGH

Degree : MASTER OF SCIENCE

Department/School : The University of the South Pacific

Institution/University : SCHOOL OF ENGINEERING AND PHYSICS
DIVISION OF PHYSICS

Thesis Title

Date of completion of requirements for award : OCTOBER, 2007

1. I authorise the University to make this thesis available on the Internet for access by USP authorised users.

Yes/No

2. I authorise the University to make this thesis available on the Internet under the International digital theses project

Yes/No

Signed: [Signature]

Date: 20/02/08

Contact Address

P.O. Box 2224

NAUSORI

PH: 9931686

e-mail: jams@unswired.com.fj

Permanent Address

P.O. Box 10208

NADI AIRPORT

PH: 9931686

e-mail: _____

THE UNIVERSITY OF THE SOUTH PACIFIC
LIBRARY

Author Statement of Accessibility

Name of Candidate : AWNESH MUNI SINGH

Degree : MASTER OF SCIENCE

Department/School : SCHOOL OF ENGINEERING AND PHYSICS
DIVISION OF PHYSICS

Institution/University : THE UNIVERSITY OF THE SOUTH PACIFIC

Thesis Title : TRANSPORTATION OF FINE SUSPENDED SEDIMENTS
IN THE SUVA LAGOON USING NUMERICAL MODELLING

Date of completion of requirements for award : OCTOBER, 2007

1. This thesis may be consulted in the Library without the author's permission ☒ Yes ☐ No
2. This thesis may be cited without the author's permission providing it is suitably acknowledged. ☒ Yes ☐ No
3. This thesis may be photocopied in whole without the author's written permission ☒ Yes ☐ No
4. This thesis may be photocopied in proportion without the author's written permission
Part that may be copied: ☒ Yes ☐ No

Under 10% -----

40-60% -----

10-20% -----

60-80% -----

20-40% -----

Over 80% -----
5. I authorise the University to produce a microfilm or microfiche copy for retention and use in the Library according to rules 1-4 above (for security and preservation purposes mainly) ☒ Yes ☐ No
6. I authorise the Library to retain a copy of this thesis in e-format for archival and preservation purposes. ☒ Yes ☐ No
7. After a period of 5 years from the date of publication, the USP Library may issue the thesis in whole or in part, in photostat or microfilm or e-format or other copying medium, without first seeking the author's written permission. ☒ Yes ☐ No
8. I authorise the University to make this thesis available on the Internet for access by authorised users. ☒ Yes ☐ No

Signed: 

Date: 20/02/08

Contact Address

P.O. Box 2224, NAUSORI

Email: jams@unwired.com.fj

Ph: 9931686

Permanent Address

P.O. Box 10208, NADI AIRPORT

Email: jams@unwired.com.fj

Ph: 9931686

TRANSPORTATION OF FINE SUSPENDED SEDIMENTS IN THE SUVA LAGOON USING NUMERICAL MODELLING

by

Awnesh Muni Singh

A thesis submitted in fulfillment of the
requirements for the degree of
Master of Science

School of Engineering and Physics
The University of the South Pacific

October, 2007

To my parents and my wife...



Table of Contents

<i>Declaration of Originality</i>	vi
<i>Acknowledgments</i>	vii
<i>Abstract</i>	ix
<i>List of Symbols and Abbreviations</i>	xi
<i>List of Figures</i>	xiv
<i>List of Tables</i>	xvi

Chapter 1

Introduction

1.1	Introduction	1
1.2	Objectives	2
1.3	Organization of Thesis	3
1.4	Conclusions	4

Chapter 2

Overview of the Suva Lagoon

2.1	Introduction	5
2.2	Climate of Fiji	6
2.3	Physical Geography and Bathymetry of the Suva Lagoon	7
2.4	Climatic Conditions over Suva	8
2.5	Tides	9
2.6	River Runoff and Sedimentation	10
2.7	Hydrodynamic Circulation and Effects of Sediments in Suspension	12
2.8	Conclusions	14

Chapter 3

Field Data and Results

3.1	Introduction	15
3.2	Wind Regime	15

3.3	River Runoff	18
3.4	Water Properties	20
3.4.1	Salinity	21
3.4.1.1	Wet-Warm Season	21
3.4.1.2	Dry-Cool Season	24
3.4.2	Temperature	25
3.4.2.1	Wet-Warm Season	25
3.4.2.2	Dry-Cool Season	28
3.4.3	Turbidity	29
3.4.3.1	Wet-Warm Season	29
3.4.3.2	Dry-Cool Season	31
3.4.4	Suspended Sediment Concentration	32
3.4.4.1	Wet-Warm Season	32
3.4.4.2	Dry-Cool Season	33
3.4.5	Turbidity and Suspended Sediment Concentration	34
3.5	Conclusions	36

Chapter 4

Governing Equations, Boundary Conditions and Numerical Discretization

4.1	Introduction	37
4.2	The 3D Hydrodynamic-Sediment Transport Coupled Model	37
4.3	Governing Model Equations and Boundary Conditions	38
4.3.1	Hydrodynamic Model	39
4.3.1.1	Model Equations	39
4.3.1.2	Boundary Conditions	41
4.3.2	Transport Model	44
4.3.2.1	Model Equations	44
4.3.2.2	Boundary Conditions	45
4.3.2.3	Critical Shear Stress for Deposition and Erosion	46
4.4	Transformed Equations and Model Grids	48
4.5	Model Bathymetry	52
4.6	Numerical Discretization	52
4.6.1	Temporal Discretization	53
4.6.2	Spatial Discretization	55
4.7	Model Validation and Implementation	57
4.8	Conclusions	58

Chapter 5

Model Results and Discussion		
5.1	Introduction	59
5.2	Model Parameters	59
5.2.1	Determination of the Critical Shear Stress for Deposition and Erosion	59
5.2.2	Determination of the Erosion Rate Coefficient	61
5.2.3	Sensitivity of the Sediment Fluxes to the Critical Shear Stress	63
5.2.4	Discussion of Deposition and Erosion for Different Forcings	64
5.3	Model Verification	66
5.3.1	Salinity Profiles	67
5.3.2	Effect of Model Resolution on Salinity Distribution	69
5.3.3	Turbidity Profiles	71
5.4	Implementation of the Model to the Suva Lagoon	74
5.4.1	Effect of the Presence of the Sandbank on Salinity Distribution	74
5.4.2	Effect of River Discharge on the Transport of Fine Suspended Sediments	76
5.5	Conclusions	80

Chapter 6

Conclusions		
6.1	What has been done in the Suva Lagoon?	85
6.2	Outcomes of this Project	86
6.3	Contributions to the study of the Suva Lagoon	88
6.4	Final Remarks	89

Bibliography	90
---------------------	----

Appendix

Deposition and Erosion Fluxes	97
-------------------------------	----



Declaration of Originality

I, Awnesh Muni Singh, hereby declare that this thesis is my own work and that to the very best of my knowledge, does not contain any material previously published or which subsequently overlaps with any other material submitted, for the award of any degree at any institution, except where due acknowledgment is made herein.

A handwritten signature in blue ink, appearing to read 'Awnesh Muni Singh', written over a horizontal line.

Awnesh Muni Singh

9th October, 2007



Acknowledgments

This thesis has been compiled through the assistance and guidance of many individuals who have helped me throughout my research work. Words do not suffice enough to express my gratitude and appreciation to these individuals. Nevertheless, I would like to record my sincere acknowledgment for their support in the compilation of this exposition.

The invaluable guidance, encouragement, advice and kindness from both my supervisors, Dr Than Aung (Physics Division, University of the South Pacific) and Dr Pascal Douillet (UR CAMELIA, IRD, Noumea) provided a strong foundation to my research work which was essential to get this thesis up to standard. It was an unparalleled effort from both these individuals to proof-read the draft chapters and to secure funding grants from various organizations to enable this research to be undertaken and completed within the required timeframe. My sincere appreciation goes to the Institut Français de Recherche pour l'Exploitation de la Mer (IFREMER) for allowing me to use the MARS3D model for my research work without which this thesis would not have been possible. I am also greatly thankful to my good friend Mr Shivanesh Rao, quoted repeatedly as Rao (2005) in this thesis, for his advice and comments throughout the course of this research. He made it easy for me to cope with the difficulties faced during data collection as well as when there were problems with the model.

I am indebted to the University of the South Pacific (USP) and Dr Sitaram Garimella (Associate Professor and Head of the School of Engineering and Physics) for allowing me the opportunity to complete my Masters degree by awarding me a scholarship as a Graduate Assistant in the Physics Division. My gratitude also goes to Professor Leon Zann (former Director, School of Marine Studies, USP) for allowing me to use the facilities at the School of Marine Studies (SMS) for collection and analysis of data. My heartfelt appreciation goes to Dr Edward Anderson (SMS) for sharing his knowledge and giving his consent for the use of the CTD probe. I am also thankful to Professor Moto Miyata from the Partnership for Observation of the Global Oceans (POGO) organization for allocating funds which enabled me to secure the boats for data collection.

My appreciation goes to the Faculty Research Committee of the Faculty of Science and Technology, and in particular to Professor Linton Winder, for allocating funds for my research and giving me a financial award to present my work at the 4th Annual Meeting of the Asia Oceania Geosciences Society in Bangkok, Thailand. I am also thankful to the organizing committee of the Pacific Science Association for providing me with the funding award to present my work at the 21st Pacific Science Congress in Okinawa, Japan. I am grateful to the French Embassy based in Suva for granting me funds to allow me to travel to Noumea to undertake training from my supervisor, Dr Douillet.

I would like to thank Mr Virendra Chand from the Fiji Hydrographic Service for providing river discharge data and Mr Azad Ali from the Fiji Meteorological Service for allowing me access to rainfall data. My sincere appreciation also goes to Mr Shiv Sharma, laboratory technician at SMS, for his assistance in providing equipment for the analysis of water samples. Thanks also to Mr Sunia Lavaki, chief technician at SMS, for arranging the boat used for data collection and Mr Sidney Malo, field technician at SMS, for allowing me to use the Niskin bottle and other equipment required for data collection.

Collecting oceanographic data in the Suva Lagoon is not an easy task and it was successfully conducted only through the assistance of hardworking and kind individuals which enabled this to eventuate. My gratitude and appreciation goes to Captains Netani and Joe for steering us safely through the waters, to the technicians from the Physics Division, Mr Neil Singh, Mr Amit Deo and Mr Rohit Lal, to Mr Justine Prakash, Mr Denise Chand (post-graduate students in the Physics Division) and Mr Pranil Sadal (my cousin) for their assistance in gathering data and to Mr Ravin Deo and Mr Anil Deo (of the Physics Division) for looking after my teaching workload at the Physics Division while I was collecting data in the Suva Lagoon.

Finally, I am greatly indebted to my parents, Mr Muni Singh and Mrs Shyam Singh, for their relentless and overwhelming support and guidance to bring me up to this point in my life. Furthermore, the backing and continual encouragement given by my wife Jyoti was a source of inspiration to my work. She has been a pillar of strength for me and I am deeply obliged to her for standing by my side.



Abstract

The city of Suva is a densely populated area, which is home to nearly a quarter of the population of the Fiji Islands thereby placing a lot of anthropogenic pressure on its lagoon. The Suva Lagoon has been subject to substantial sediment inputs generated by erosion and human activities. Freshwater input into the lagoon comes predominantly from the Rewa River, the largest fluvial system in the country. The high sedimentary load from the Rewa River, especially during the wet-warm season, has a strong impact on the water properties in the lagoon. The salinity, temperature and turbidity in the Suva Lagoon are some important parameters for water quality which are continuously changing with the seasons. They are also efficient indicators of variations in the lagoon and can transform the marine ecosystem.

This project involved gathering of river discharge and rainfall data, collection of wind and field data for the Suva Lagoon. Analysis of the results shows that the variations of CTD and turbidity measurements are dependent predominantly on the river discharge, while the dominant wind regime is the southeast trade winds. The mean monthly wind speed ranges from $4.4 - 5.6 \text{ m s}^{-1}$ during the dry-cool season and $3.3 - 4.5 \text{ m s}^{-1}$ during the wet-warm season. The discharge from the Rewa River is highly dependent on rainfall. A linear relationship with a correlation coefficient of 0.82 between the mean monthly river discharge and total monthly rainfall was established. The salinity range at the surface in the Suva Lagoon during the wet-warm season is between 23.6 – 34.4 psu and between 28.7 – 34.5 psu during the dry-cool season. The bottom salinity shows little horizontal variation. The field results also show that the temperature variations in the lagoon are due to the warm freshwater input from the Rewa River during both seasons. The surface temperature in the lagoon is lower in the dry-cool season (between $24.5 - 25.4 \text{ }^{\circ}\text{C}$) compared to the wet-warm season (between $28.9 - 30.2 \text{ }^{\circ}\text{C}$). The surface turbidity remains almost the same during both seasons with the Rewa Delta (2.6 FTU) and Laucala Bay (1.9 FTU) showing slightly higher turbidity than in Suva Harbour (0.8 FTU) and Nasese Channel (0.6 FTU).

A MARS3D hydrodynamic-sediment transport coupled model (built by IFREMER) was applied to the Suva Lagoon with the aim of simulating the water properties in the lagoon. The model is able to simulate the effects of bathymetry, bottom friction, turbulence, river runoff, tides and wind forcing on the salinity and suspended sediment concentration in the Suva Lagoon for the completeness of the model. Model parameters to simulate suspended sediment concentration in the lagoon were estimated

from the model trial runs. It was found that using the critical shear stress $\tau_{cr} = 0.020 \text{ N m}^{-2}$ and the erosion rate coefficient $ke_c = 6.5 \times 10^{-5} \text{ g m}^{-2} \text{ s}^{-1}$ showed good agreement with the percentage of fine sediments found at the bottom under the combined effect of the tide and wind. Using these values, the model was verified for salinity and turbidity distribution and the results showed good agreement between field data and model predictions. Increasing the model resolution from $\sigma = 10$ levels to $\sigma = 23$ levels shows a better representation of the vertical salinity profile, especially on the surface layer.

The verified model was used to simulate the effect of the presence of the sandbank in the Rewa Delta on the surface salinity distribution in the lagoon. Results showed that the sandbank is an important factor in determining the surface salinity variation in Laucala Bay. During high discharge rates, the surface salinity in Laucala Bay is in the range of 25.0 – 29.0 psu in the presence of the sandbank. Without the sandbank, model simulations show that the surface salinity range in the bay is between 28.0 – 32.0 psu. The presence of the sandbank in the Rewa Delta has the effect of channeling more freshwater from the Rewa River into Laucala Bay (through the Vunidawa River) than when there is no sandbank. This lowers the surface salinity in Laucala Bay significantly.

Model runs with different Rewa River runoffs were performed to observe the effect of river discharge on suspended sediment concentration in the Suva Lagoon. It was found that during low discharges ($80 \text{ m}^3 \text{ s}^{-1}$) from the Rewa River, the suspended sediment concentration in Laucala Bay is around 7 FTU at the Vunidawa River mouth. This high value is due to the resuspension of bottom sediments due to the tidal and wind effects. There is almost no input of suspended sediments from the Rewa River discharge as the sediments settle along the river channel due to the low river currents. A similar situation is observed for a discharge of $200 \text{ m}^3 \text{ s}^{-1}$, however, the SSC is more than 12 FTU at the Vunidawa River mouth. It is during high discharge rates from the Rewa River ($400 \text{ m}^3 \text{ s}^{-1}$) that the effects of river discharge on suspended sediment concentration can be clearly seen. The concentration of suspended sediments at the mouth of the Vunidawa River is more than 18 FTU. This high amount is due to the introduction of the sediments from the freshwater discharge of the Rewa River. The suspended sediments in Laucala Bay are transported further towards the passages by the tides and the wind. The discharge from the Rewa River is the most influential factor in determining the suspended sediment concentration in the lagoon. However, river discharge is directly related to rainfall, thus it can be said that rainfall is the deciding influence in the transport of fine suspended sediments in the Suva Lagoon.



List of Symbols and Abbreviations

$^{\circ}\text{C}$	-	degree Celsius
σ	-	vertical sigma layers of the model
σ_c	-	Schmidt number
ρ	-	density of seawater
ρ_a	-	density of air
ζ	-	free sea-surface elevation above mean sea-level
τ	-	bed shear stress
τ_{bx}	-	bottom friction in x -direction
τ_{by}	-	bottom friction in y -direction
τ_{cr}	-	critical shear stress
τ_{cd}	-	critical shear stress for deposition
τ_{ce}	-	critical shear stress for erosion
τ_{sx}	-	surface wind stress in x -direction
τ_{sy}	-	surface wind stress in y -direction
μ	-	kinematic molecular viscosity of water
A	-	cross-sectional area
ADI	-	Alternating Direction Implicit
C	-	suspended sediment concentration (SSC)
C_d	-	bottom drag coefficient
C_D	-	surface drag coefficient
D	-	total water depth
D_s	-	diameter of particles
f	-	Coriolis parameter

FTU	-	Formazin Turbidity Units
g	-	gravity
H	-	water depth at mean sea-level
i	-	east-west direction
j	-	north-south direction
k	-	vertical direction
k_0	-	von Karman's constant
ke	-	erosion rate coefficient
ke_c	-	fitting parameter
K_1	-	semi-diurnal principal lunar constituent of tide
K_2	-	semi-diurnal luni-solar constituent of tide
K_h	-	horizontal eddy diffusivity of particles
K_r	-	Strikler coefficient
K_z	-	vertical eddy diffusivity of particles
L	-	litre
m	-	metre
M_2	-	semi-diurnal principal lunar constituent of tide
M_f	-	lunar fortnightly constituent of tide
M_m	-	lunar monthly constituent of tide
N_2	-	semi-diurnal larger lunar elliptic constituent of tide
N_h	-	coefficient of horizontal eddy viscosity
N_z	-	coefficient of vertical eddy viscosity
NTU	-	Nephelometric Turbidity Units
O_1	-	semi-diurnal principal lunar constituent of tide
p	-	water pressure
psu	-	practical salinity units
P_1	-	diurnal principal solar constituent of tide
P_{mud}	-	percentage of mud
Q_1	-	diurnal larger lunar elliptic constituent of tide
R_d	-	mean monthly river discharge
R_D	-	river discharge

R_f	-	total monthly rainfall
s	-	seconds
s	-	ratio of density of particle to water
S	-	salinity
S_2	-	semi-diurnal principal solar constituent of tide
S_{sa}	-	solar semi-annual constituent of tide
SOI	-	Southern Oscillation Index
SPM	-	Suspended Particulate Matter
t	-	time
u_*	-	friction velocity
u	-	velocity in x -direction
v	-	velocity in y -direction
v_{av}	-	average current velocity
w	-	velocity in z -direction
W	-	wind speed
W_s	-	settling velocity
x	-	west-east direction
y	-	south-north direction
z	-	vertical direction
z'	-	distance from bottom
z_0	-	roughness parameter

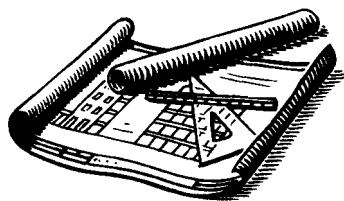
Symbols that have been used but which are not shown here have been explained at the places where they first appear in the text.



List of Figures

Figure 2.1	Map of Fiji.	5
Figure 2.2	Map of the Suva Lagoon.	7
Figure 2.3	Long term (1971 – 2000) average daily maximum and minimum temperatures (°C) and average total monthly rainfall (mm) at Laucala Bay, Suva [Source: www.met.gov.fj , 2005].	8
Figure 2.4	Water circulation during the wet season with a river discharge of $1000 \text{ m}^3 \text{ s}^{-1}$, 8 m s^{-1} southeast winds and M_2 , S_2 , K_1 and O_1 tides at the (A) surface and (B) bottom.	13
Figure 3.1	Two hourly wind stick plots showing magnitude and direction of wind during the (a, b) wet-warm season and (c, d) dry-cool season for the Suva Lagoon.	16
Figure 3.2	Percentage wind speed below 2 m s^{-1} for the period between August 2005 and August 2006.	17
Figure 3.3	Relationship between Rewa River discharge and rainfall.	19
Figure 3.4	Horizontal salinity variations on the surface (left column) and bottom (right column) in the Suva Lagoon during the wet-warm season.	22
Figure 3.5	Horizontal salinity variations on the surface (left) and bottom (right) in the Suva Lagoon during the dry-cool season.	24
Figure 3.6	Horizontal temperature variations on the surface (left column) and bottom (right column) in the Suva Lagoon during the wet-warm season.	26
Figure 3.7	Horizontal temperature variations on the surface (left) and bottom (right) in the Suva Lagoon during the dry-cool season.	28
Figure 3.8	Horizontal turbidity variations on the surface (left column) and bottom (right column) in the Suva Lagoon during the wet-warm season.	30
Figure 3.9	Horizontal turbidity variations on the surface (left column) and bottom (right column) in the Suva Lagoon during the dry-cool season.	32

Figure 3.10	Suspended sediment concentration at the surface in the Suva Lagoon during the wet-warm season.	33
Figure 3.11	Suspended sediment concentration at the surface in the Suva Lagoon during the dry-cool season.	34
Figure 3.12	Relationship between turbidity and suspended sediment concentration.	35
Figure 4.1	Modified Arakawa C-grid.	51
Figure 4.2	Bathymetry of the Suva Lagoon.	52
Figure 4.3	ADI algorithm.	53
Figure 5.1	The percentage distribution of fine sediments at the bottom in the Suva Lagoon.	60
Figure 5.2	Model distribution of the deposition flux (left column) and erosion flux (right column) cumulated over a tidal cycle for different forcings (a and d) tide, (b and e) wind 6 m s^{-1} and (c and f) tide and wind 6 m s^{-1} .	64
Figure 5.3	Field and model salinity profiles for $\sigma = 10$ levels at different locations in the Suva Lagoon using the same range for salinity at (a) Suva Harbour, (b) Nukubuco Passage, (c) Laucala Bay and (d) Rewa Delta.	68
Figure 5.4	Model salinity profiles for $\sigma = 10$ levels and $\sigma = 23$ levels at different locations in the Suva Lagoon (a) Suva Harbour, (b) Nukubuco Passage, (c) Laucala Bay and (d) Rewa Delta.	70
Figure 5.5	Field and model turbidity profiles for $\sigma = 10$ levels at different locations in the Suva Lagoon using the same range for turbidity at (a) Suva Harbour, (b) Nukubuco Passage, (c) Laucala Bay and (d) Rewa Delta.	72
Figure 5.6	Model surface salinity distribution with sandbank (left column) and without sandbank (right column) for a river discharge of (a and b) $80 \text{ m}^3 \text{ s}^{-1}$, (c and d) $200 \text{ m}^3 \text{ s}^{-1}$ and (e and f) $400 \text{ m}^3 \text{ s}^{-1}$.	75
Figure 5.7	Model surface turbidity distribution for a river discharge of (a) $80 \text{ m}^3 \text{ s}^{-1}$, (b) $200 \text{ m}^3 \text{ s}^{-1}$ and (c) $400 \text{ m}^3 \text{ s}^{-1}$.	78



List of Tables

Table 2.1	Characteristics of some of the principal tide-producing force constituents [Source: Pond and Pickard, 1983].	10
Table 3.1	Percentage wind direction for the period between August 2005 and August 2006.	17
Table 3.2	Summary of cruises showing the period, cruise date, total monthly rainfall R_f and mean monthly river discharge R_d .	20
Table 5.1	Summary of the minimum percentage difference between deposition and erosion fluxes for mean wind (6 ms^{-1}) and tide (M_2) conditions for several combinations of the critical shear stress τ_{cr} and coefficient of erosion ke_c .	62
Table 5.2	Deposition and erosion fluxes (D_f and E_f respectively) calculated by the model for the whole lagoon with different values of the critical shear stress and with $ke_c = 6.5 \times 10^{-5} \text{ g m}^{-2} \text{ s}^{-1}$. D_f and E_f are expressed in tonnes per tidal cycle.	63
Table 6.1	Summary of the salinity, temperature and turbidity range at the surface in Suva Harbour, Nasese Channel, Laucala Bay and Rewa Delta during the wet-warm and dry-cool seasons.	87



Chapter 1

Introduction

1.1 Introduction

Water properties in the coastal areas are constantly changing due to mixing of waters from different sources. Freshwater runoff from rivers gives coastal areas their relatively low salinity and high sediment concentrations (Bowden, 1983). Coastal zones are characterized by their shallow depths which place a great constraint on water movements. Bottom currents in the coastal areas are relatively large and bottom friction plays a significant role in resuspension of bottom sediments. The freshwater discharged from rivers into these areas perform vital functions in both societal and ecosystem terms, including personal water consumption, health and sanitation needs, agricultural, navigational and industrial uses, and various aesthetic, cultural, spiritual and recreational associations.

Sediments also play an important role in water quality management in coastal areas (Ouillon *et al.*, 2004). The major source of sediments in coastal zones is erosion of the shoreline and particulate matter carried by streams and rivers. Sediment alone degrades water quality for municipal supply, recreation, industrial consumption and cooling, hydroelectric facilities and aquatic life (Julien, 1998). In addition, chemicals and wastes are assimilated onto and into sediment particles by which they can be physically transported from the source (for example, factories, waste management facilities, etc.) to the marine environment. Sediments are a major source of water pollution and serve as a catalyst, carrier and storage agent of other forms of pollution.

Within the coastal area, a lagoon can usually be identified by the presence of three distinct zones: a freshwater zone that lies near the head of the lagoon where rivers enter, a transitional zone of brackish water that occurs near the middle of the lagoon, and a saltwater zone that lies close to the lagoon's mouth (Trujillo and Thurman, 2005). Urbanised coastal lagoons represent one of the most threatened global environments as some 60% of the world's

population lives within 60 km of the coast (Morrison, 2006). The Suva Lagoon is one of the most important water bodies in the South Pacific region (Morrison and Aalbersberg, 2006) and has been subject to substantial sediment inputs generated by erosion and human activity. These activities have a dramatic impact on the water quality and thus sediment studies need to be carried out to understand the long term effects on the lagoon environment.

The ability to predict suspended sediment concentrations in the water column is very important to improve the understanding of water quality dynamics in water bodies such as the Suva Lagoon. A comprehensive picture of a lagoon can be obtained when natural processes such as wind, river discharges and tides are simultaneously taken into account in any lagoon study. One effective way of such a study can be done through a combination of experimental observations and numerical modelling. As a result, a detailed pattern of the transport of suspended sediments can be obtained. Hydrodynamic equations are solved numerically in this method using local properties, such as bathymetry, as constraints. The output of the numerical model is compared with the field measurements and consistency in the two sets of information acts as verification of the model. Once verified, the model can be used to predict sediment transport under different tidal and wind forcings and river runoff.

1.2 Objectives

The main task of this project is to gather field data and to use the boundary conditions to validate a 3D hydrodynamic-sediment transport coupled model for the Suva Lagoon, which would then be used to understand the transport of fine suspended sediments in the lagoon. The model can be used in future to predict the water properties and the areas of sedimentation in the lagoon without having to collect *in situ* data. The outline of the objectives can be specified as follows:

- To analyze seasonal variations of rainfall, freshwater discharge and wind velocity in the study area and use the results to validate the model.
- To gather salinity, temperature and turbidity data using a SBE 19 CTD probe and water samples using a Niskin bottle at various locations in the Suva Lagoon during the different seasons.
- To determine the seasonal variations of salinity, temperature, turbidity and suspended sediment concentration in the lagoon.

- To establish a relationship between surface turbidity and suspended sediment concentration.
- To estimate the erosion rate coefficient and the critical shear stresses for deposition and erosion to be used in the model.
- To validate the model by comparing field data with model output.
- To use the model to predict the effect of model resolution and the presence of the sandbank in the Rewa Delta on salinity distribution in the lagoon.
- To find out the effect of different river discharges on suspended sediment transport in the Suva Lagoon.

1.3 Organization of Thesis

The thesis is prepared as follows:

- Chapter 2 gives an overview of the Suva Lagoon. The climate, physical geography, bathymetry, wind regime, tidal influence and freshwater runoff into the Suva Lagoon are discussed. Previous hydrodynamic studies that have been carried out in the lagoon are mentioned in brief as literature review.
- Chapter 3 presents the results of field data collected. The wind speed and direction during the different seasons are analyzed and the water properties are discussed. A relationship between surface turbidity and suspended sediment concentration is determined.
- Chapter 4 discusses the governing equations, boundary conditions and numerical discretization used in the model. The equations and assumptions used in the hydrodynamic and transport models are presented comprehensively.
- Chapter 5 highlights the model results. The model parameters used to calibrate the model for the Suva Lagoon are determined through model test runs. These parameters are verified by comparing the areas of sediment deposition and erosion with the percentage of fine sediments found at the bottom. The model is validated by comparing field salinity and turbidity with the model output. Having validated the model, it is used to determine the effect of model resolution and the presence of the sandbank in the Rewa Delta on salinity distribution in the lagoon. The effect of the river discharge on fine suspended sediment transport is discussed.

- Chapter 6 summarizes the results of the field measurements and the model output. A brief summary of the contributions of the present study to the understanding of the hydrodynamics and transport of fine suspended sediments in the Suva Lagoon using a numerical model is presented.

1.4 Conclusions

Rivers have been used by man since the dawn of civilization as a source of water (for food and transport), as a defensive barrier, as a source of power to drive machinery, and as means of disposing of waste (www.wikipedia.org, 2006). Sustained abuse has resulted in significant alarm for river health (Brierley and Fryirs, 2005). River health, defined as the ability of a river and its associated ecosystem to perform its natural functions, is a measure of catchment health, which in turn provides an indication of environmental and societal health (Brierley and Fryirs, 2005). The water quality in the Suva Lagoon is vulnerable as the lagoon has been subject to substantial sediment input from the Rewa River, erosion and human activity. It is important to study the effects of river discharge on coastal lagoons as majority of the world's population reside near coastal areas. A 3D hydrodynamic-sediment transport coupled model is required to determine the influence of river discharge on the water quality, and especially for this project, the transport of fine suspended sediments in the Suva Lagoon.



Chapter 2

Overview of the Suva Lagoon

2.1 Introduction

Fiji is an island group located in the Pacific Ocean between latitudes 15°S – 22°S and longitudes 177°W – 175°E. The country consists of 844 islands and islets of which 105 are permanently inhabited with 90% of the population living on the two main islands of Viti Levu and Vanua Levu. Most of the islands are of volcanic origin and are generally mountainous and rugged. Its total land area is 18 272 km² dispersed in its territorial waters of 141 800 km² (Raj, 2004). The population of Fiji estimated for July 2007 stands at 918 675 (www.cia.gov, 2007).

All major economic activities are based on its two main islands of which Viti Levu is the largest in size (10 388 km²) with more than 75% of the total population and hosts the capital city of Suva, as can be seen in Fig. 2.1. The city is home to nearly a quarter of the population of Fiji (www.factbites.com, 2005) thereby placing a lot of anthropogenic pressure on its lagoon.

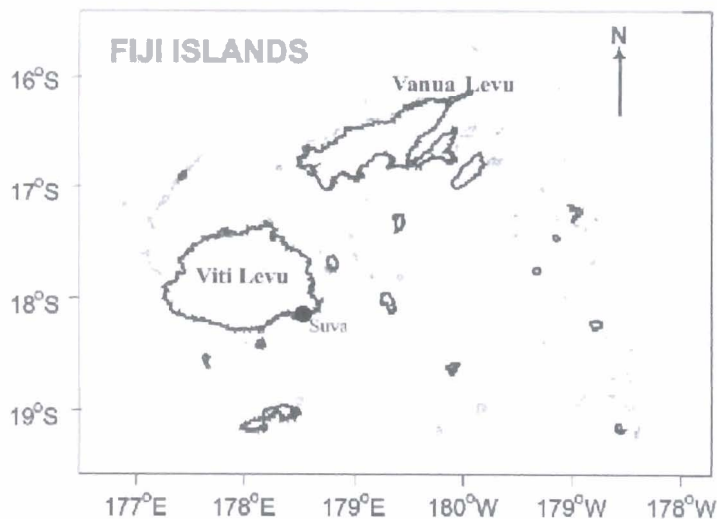


Figure 2.1 Map of Fiji.

2.2 Climate of Fiji

Fiji enjoys a tropical climate without great extremes of heat or cold. The country experiences a distinct wet and dry season, controlled largely by north and south movements of the Inter Tropical Convergence Zone (ITCZ), the main rainfall producing system for the region.

During all seasons, the predominant winds over Fiji are the southeast trade winds. On the coast of the two main islands, day-time sea breezes blow across with great regularity. Winds over Fiji are generally light or moderate; stronger winds are far less common and are most likely to occur in the period June to November when the trade winds are most persistent. However, tropical cyclones and depressions can cause high winds, especially from November to April when the trades die down (www.met.gov.fj, 2005).

Rainfall is highly variable from region to region and is mainly influenced by the island topography and the prevailing southeast trade winds. These trades are often saturated with moisture and any high land mass lying in their paths receive much of the precipitation. The mountains of the larger islands create wet climatic zones on their windward sides and dry climatic zones on their leeward sides resulting in wet and dry zones that are fairly well defined (www.met.gov.fj, 2005). The principal influences on the seasonal rainfall pattern are tropical disturbances and cyclones while the El Niño Southern Oscillation (ENSO) phenomenon is also known to intensify these effects (Raj, 2004).

Temperatures throughout Fiji are fairly uniform. In the lee of the mountains on the larger islands, however, the day-time temperatures are often 1 – 2 °C above those on the windward side. Also, the humidity on the lee side tends to be somewhat lower. Due to the influence of the surrounding ocean, the changes in the temperature from day to day and season to season are relatively small. The average temperatures change only about 2 – 4 °C between the coolest months (July and August) and the warmest months (January and February). Around the coast, the average night-time temperatures can be as low as 18 °C and the average day-time temperatures can be as high as 32 °C. In the central parts of the main islands, average night-time temperatures can be as low as 15 °C (www.met.gov.fj, 2005).

2.3 Physical Geography and Bathymetry of the Suva Lagoon

The city of Suva is perched on a hilly peninsula between Laucala Bay and Suva Harbour, which together comprise majority of the Suva Lagoon in the southeast corner of Viti Levu. Suva Harbour lies on the west of the lagoon and in between its fringing reefs of Nukusaga and Vunivau lies the Suva Passage, as can be seen in Fig. 2.2. The Nasese Channel links Suva Harbour and Laucala Bay and is bounded by the Suva Peninsula and the Nawanada Reef. To the east lies Laucala Bay. The Sosoikula and Nukubuco barrier reefs and the Nasigasiga and Ucuisila barrier reefs are broken by the Nukubuco and Nukulau Passages respectively. The small islets of Nukubuco and Nukulau form emerged caps on the barrier reef dipping gently into the lagoon, while Makaluva Island is close to the reef front (N’Yeurt, 2001).



Figure 2.2 Map of the Suva Lagoon.

The average water depth in Laucala Bay is 9 m deepening to more than 40 m in the Nukubuco and Nukulau Passages. Laucala Bay is connected to Suva Harbour by the narrow

Nasese Channel that is 5 – 10 m deep. Suva Harbour has an average depth of 15 m with depths of 80 – 100 m in the Suva Passage (Penn, 1983).

2.4 Climatic Conditions over Suva

At Suva, the long term (1971 – 2000) averaged daily maximum and minimum temperatures generally have a direct correlation with the average total monthly rainfall for each month, as can be seen in Fig. 2.3.

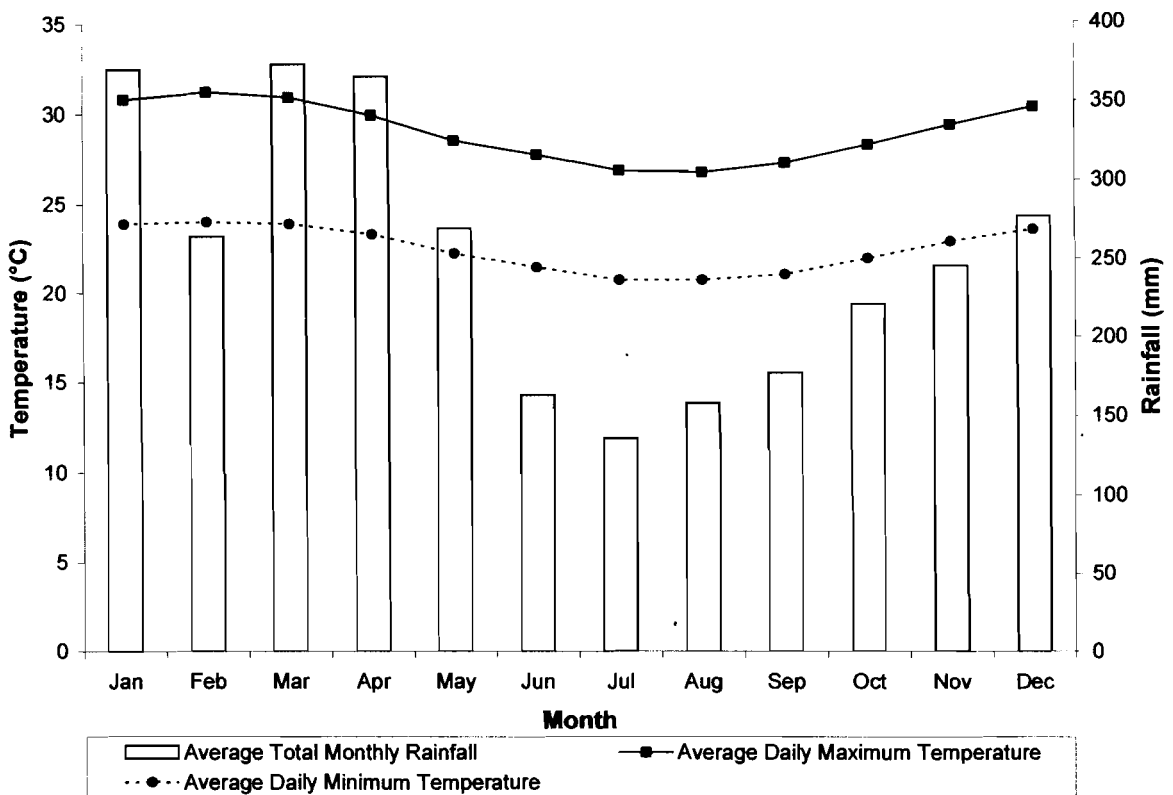


Figure 2.3 Long term (1971 – 2000) average daily maximum and minimum temperatures (°C) and average total monthly rainfall (mm) at Laucala Bay, Suva [Source: www.met.gov.fj, 2005].

The discrepancy during the month of February can be attributed to the lower number of tropical cyclones affecting Fiji during that month as when compared to January and March. Furthermore, tropical cyclones in January and March were more severe and frequent than those in February and since severe tropical cyclones are more likely to bring higher rainfall, the total rainfall for the month is affected. The average total monthly rainfall during the cooler months of May to October is low compared to the warmer months of November to

April. The rainfall pattern is influenced by the north and south movements of the ITCZ. During the cooler months, the ITCZ moves away from the Fiji group and the formation of heavy rain is less frequent. However during the warmer months, the ITCZ moves closer to the Fiji group thereby increasing the formation of heavy rain (www.met.gov.fj, 2005). Fiji can therefore be said to have two distinct seasons in a year; the dry and cool season (between the months of May and October) and the wet and warm season (between the months of November and April).

The wind regime over the Suva Lagoon is dominated by the southeast trade winds. The mean monthly wind direction, measuring from the north, is between 90° – 170° (between east to southeast) indicating the dominance of the southeast trade winds throughout the year with mean monthly wind speeds between $3 - 6 \text{ m s}^{-1}$.

2.5 Tides

Tides are dominantly produced by a combination of time-varying gravitational potential of the Moon and Sun (Bowden, 1983). Tides are most commonly seen as a regular rise and fall of sea-level at the coast. Tides produce tidal currents which move water from one place to another to accommodate the sea-level changes. The tide, because it is a permanent phenomenon, is one of the most important factors essential in the analysis of particle transfer and in the interpretation of sedimentology (Douillet, 1998).

Tides everywhere are made up of a number of constituents of different periods (Bowden, 1983). Each constituent has different tidal amplitudes. Constituents that have large tidal amplitudes have a more significant effect on the water column than those with small tidal amplitudes. Some of the more important tidal constituents (divided into three species: semi-diurnal, diurnal and long period) with their size relative to the largest, the M_2 or principal lunar constituent taken as 100, are given in Table 2.1. It should be noted that the tidal amplitude of each tidal constituent is not the same everywhere. Some places have two high and two low tides a day and some have one high and one low tide a day. The latter is due to the presence of amphidromic points of semi-diurnal tides.

Table 2.1 Characteristics of some of the principal tide-producing force constituents [Source: Pond and Pickard, 1983].

Species	Name	Symbol	Period (solar hours)	Relative Size
Semi-diurnal	Principal lunar	M_2	12.42	100
	Principal solar	S_2	12.00	47
	Larger lunar elliptic	N_2	12.66	19
	Luni-solar	K_2	11.97	13
Diurnal	Luni-solar	K_1	23.93	58
	Principal lunar	O_1	25.82	42
	Principal solar	P_1	24.07	19
	Larger lunar elliptic	Q_1	26.87	8
Long Period	Lunar fortnightly	M_f	327.90	17
	Lunar monthly	M_m	661.30	9
	Solar semi-annual	S_{sa}	4383.00	8

At Suva, as in most other places, there are two tides per day (semi-diurnal tides). The tidal amplitudes at Suva due to the M_2 , S_2 , K_1 and O_1 constituents are 0.565 m, 0.091 m, 0.094 m and 0.046 m respectively (www.tidesandcurrents.noaa.gov, 2006). These four constituents have larger amplitudes than all others and will be used to represent the total tidal effect on the Suva Lagoon when using the numerical model. The other constituents have a minimal effect compared to the M_2 , S_2 , K_1 and O_1 constituents and are not used in this study.

The area occupied by the water in the lagoon varies with the tide with a mean tidal range of 1.164 m (www.tidesandcurrents.noaa.gov, 2006). At high tide, the area is $6.34 \times 10^7 \text{ m}^2$ and $5.57 \times 10^7 \text{ m}^2$ at low tide, with the capacity to hold a mean volume of the lagoon of about $7.77 \times 10^8 \text{ m}^3$ (Campbell *et al.*, 1982). Generally, the rise and fall of water level due to tides acts as a major flushing mechanism for a lagoon (Li and Gu, 2001). According to Rao (2005), the flushing rate of the Suva Lagoon during the wet and dry seasons is $-502.4 \text{ m}^3 \text{ s}^{-1}$ and $-24.6 \text{ m}^3 \text{ s}^{-1}$ respectively. Ideally the water in a lagoon does not empty or overflow with time, therefore the flushing rate must be zero in any season. This discrepancy is attributed to the non-inclusion of freshwater runoff from smaller rivers discharging into Laucala Bay and Suva Harbour (Rao, 2005).

2.6 River Runoff and Sedimentation

The Rewa River is the longest river and the largest fluvial system in Fiji. Its drainage basin covers one-third of the island of Viti Levu and originates in Tomanivi (Mount Victoria), the highest peak in Fiji (maximum height above sea-level is 1323 m), and flows southeast for 145

km before splitting up two-thirds on its way downstream into several tributaries. One of these tributaries is the Vunidawa River, which channels 15% of the total discharge of the Rewa River into Laucala Bay while the remainder flows into the Rewa Delta (Campbell *et al.*, 1982).

The dynamics of the Rewa River are affected by dredging of the riverbed and the construction of the Rewa Bridge approximately 15 km upstream from the mouth of the Vunidawa River. Dredging of the riverbed is a major structural flood management measure to increase flood discharge capacity (Raj, 2004) while the construction of a bridge across a river can significantly change the river hydraulics as well as the river morphology (www.dhi.dk, 2006).

The transport, erosion and deposition of sediments are key elements for describing and understanding the behavior of rivers (www.dhi.dk, 2006). Rivers transport not only the water itself but also materials in suspension downstream. The spreading of sediments of a certain quality can be very important for resuspension and transport of contaminated sediment, deposition, erosion and transport of fine sediments containing organic material which influence the oxygen demand in the water, and transport, dispersion and sedimentation of fine sediments, rich in nutrients, which is favorable to agricultural production on the flood plains (www.dhi.dk, 2006).

The freshwater input from the Vunidawa River carries a large amount of fine sediments and organic particulate matter into Laucala Bay (Squires, 1962). The bay area is subject to much sedimentation with a substratum of clayey-silty ooze caused by siliciclastic fluvial input by the Rewa River (Schneider *et al.*, 1995). The Samabula, Nasinu and Vatuwaqa Rivers also deposit sediments into Laucala Bay and have a combined runoff of over $3 \text{ m}^3 \text{ s}^{-1}$ (Naidu *et al.*, 1991). Because of the weak currents in the bay, these sediments are deposited easily and this causes the dirty waters to stay in the bay for a long time (Gendronneau, 1985). Sediments in Laucala Bay are generally very fine while coarser-grained sediments are found close to the barrier reefs (N'Yeurt, 2001). Bay muds are about 25 – 40 m thick at Suva Harbour (Shorten, 1993).

Cohesive sediments are a blend of clay, silt, sand and organic matter. They form mud when mixed in water. These cohesive sediments are predominantly fine-grained and the electromagnetic characteristics of the clay minerals cause aggregation of these particles into flocks. These sediment particles, however, in general, are not solid particles but flexible flocks which can aggregate or break-down depending on various external factors, such as turbulent shear, concentration and salinity of the ambient water (www.kuleuven.be, 2007). Their size, structure and strength are thus variable, much in contrast to non-cohesive particles like sand and gravel, therefore, the sediment mechanics of cohesive particles is different and much more complex than that of sand (www.kuleuven.be, 2007). As these sediments are so fine, they are often transported by the river all the way down to their mouth, where they ultimately deposit often massively forming typical mud banks and intertidal flats. The percentage distribution of these fine-grained sediments in the Suva Lagoon is generally high near the river mouths and gradually decreases towards the reef passages. In order to simulate the transport of fine sediments in any coastal area, model mathematical equations are used to represent the transport of sediments as accurately as possible by generalizing and using approximations as to the type and nature of the sediment being transported. It is difficult to ascertain, at this stage, the nature of the sediment being transported, thus approximations in the model equations will be used.

2.7 Hydrodynamic Circulation and Effects of Sediments in Suspension

Studies done on the Suva Lagoon by Campbell *et al.* (1982), Penn (1983), Gendronneau (1985), Smith *et al.* (1994) and Kumar (2000) focused on the water properties and water circulation in Laucala Bay. Rao (2005) took the study of the hydrodynamic circulation in the lagoon even further by using a 3D hydrodynamic model built by the Institut de Recherche pour le Développement (IRD) in Noumea. He concluded that the surface water circulation is dominated by wind while tides dominate the whole water column at all times. Also, the discharge from the Vunidawa River is dominant only in the surface layer especially during the wet season when freshwater discharge is significantly high. Figure 2.4 shows the surface and bottom water circulation during flooding tide in the wet-warm season from Rao's (2005) work.

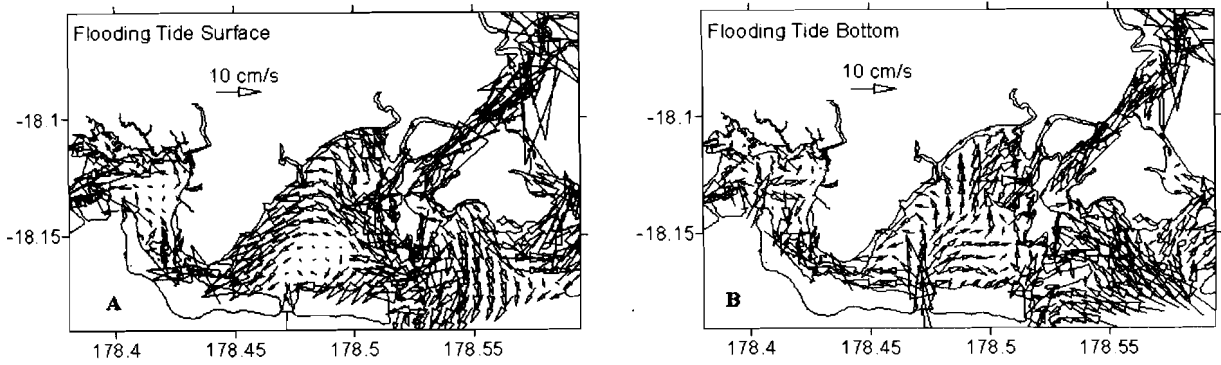


Figure 2.4 Water circulation during the wet season with a river discharge of $1000 \text{ m}^3 \text{ s}^{-1}$, 8 m s^{-1} southeast winds and M_2 , S_2 , K_1 and O_1 tides at the (A) surface and (B) bottom.

Laucala Bay represents a depositional environment that is mainly controlled by the Rewa River Delta and the Suva Barrier Reef (Schneider *et al.*, 1995). The Rewa River, which provides a high siliciclastic and chemical input into the lagoon (Schneider *et al.*, 1995), has deleterious effects on the reef and reef community (Squires, 1962). The effects of sediments in suspension are mainly in reduction of light penetration restricting the depth of coral growth (Squires, 1962) and limiting coral reef development (Penn, 1983). The ability to predict suspended sediment concentrations in the water column is very important to improve the understanding of water quality dynamics and biological processes in water bodies (Hu and Wang, 1998).

One important parameter for measuring water quality is turbidity. Turbidity is a measure of the degree to which the water loses its transparency due to the presence of fine suspended particles (www.lenntech.com, 2006). The greater the amount of total suspended solids in water, the murkier it appears and the higher the measured turbidity (www.waterontheweb.org, 2006). Some parameters influencing turbidity include clay, silt, finely divided organic and inorganic matter, soluble colored organic compounds, plankton, microscopic organisms, sediments from erosion, resuspended sediments from the bottom, freshwater discharge, algal growth, dredging operations and flooding. Suspended particles absorb heat from the sunlight making turbid waters become warmer and so reducing the oxygen concentration in water making it difficult for organisms to survive. The oxygen concentration is lowered even further as suspended particles scatter the light decreasing the photosynthetic activity of plants and algae.

2.8 Conclusions

Sediments can be very good indicators of water quality because polluting agents such as trace (toxic) metals and organochlorine residues tend to concentrate in these materials and are thus easier to detect (Naidu *et al.*, 1991). Effective management of contaminated sediments requires a quantitative understanding of the transport of sediments (www.qeallc.com, 2006). This can be done by using a 3D hydrodynamic model which defines the transport of suspended sediments in the Suva Lagoon.

The first application of a hydrodynamic model (built by IRD) to the Suva Lagoon was done by Kumar (2000). He used a 2D model to define the water circulation due to the M_2 tidal constituent (without river runoff or wind). Rao (2005) built up on the work done by Kumar (2000) by using the application of a 3D hydrodynamic model (also built by IRD) to determine the water properties and water circulation in the Suva Lagoon by considering the effects of river runoff, wind stress, bathymetry, bottom friction and the M_2 , S_2 , K_1 and O_1 tidal constituents. A similar type of work using the same model has been done on the southwest lagoon of New Caledonia by Douillet *et al.* (2001).

This project will further build up on the work of Rao (2005) by applying a 3D hydrodynamic-sediment transport coupled model to the Suva Lagoon. The 3D coupled model, which is an extension of the model used by Rao (2005), will be used to understand sediment related processes including advection, vertical mixing, settling, deposition, erosion and transport of fine suspended sediments in the Suva Lagoon.



Chapter 3

Field Data and Results

3.1 Introduction

Salinity, temperature and turbidity are important parameters which are continuously changing with the seasons and need to be studied because they are efficient indicators of variations in the lagoon and can transform the marine ecosystem. Several cruises were conducted to collect necessary data for water quality analysis and the results obtained will also be used to calibrate a numerical model. The data collected were filtered and analyzed and the results are presented in this chapter.

3.2 Wind Regime

The wind data was monitored at the School of Marine Studies (SMS) at the University of the South Pacific under technical assistance of *Research Unit: Characterization and modelling of exchanges in lagoons subject to terrigenous and anthropogenic influences* (UR CAMELIA), IRD in Noumea. The wind speed and direction were recorded at regular intervals of 10 minutes at a height of 10 m above mean sea-level. The stick plots in Fig. 3.1 show the magnitude and direction of the wind during the wet-warm season (November – April) and the dry-cool season (May – October).

During the dry-cool season, the southeast trade winds are dominant, blowing with great regularity over the lagoon, as seen in Fig. 3.1c, d. However, during the wet-warm season, the southeast trade winds weaken and the winds generally blow across from the northeast (Fig. 3.1a, b).

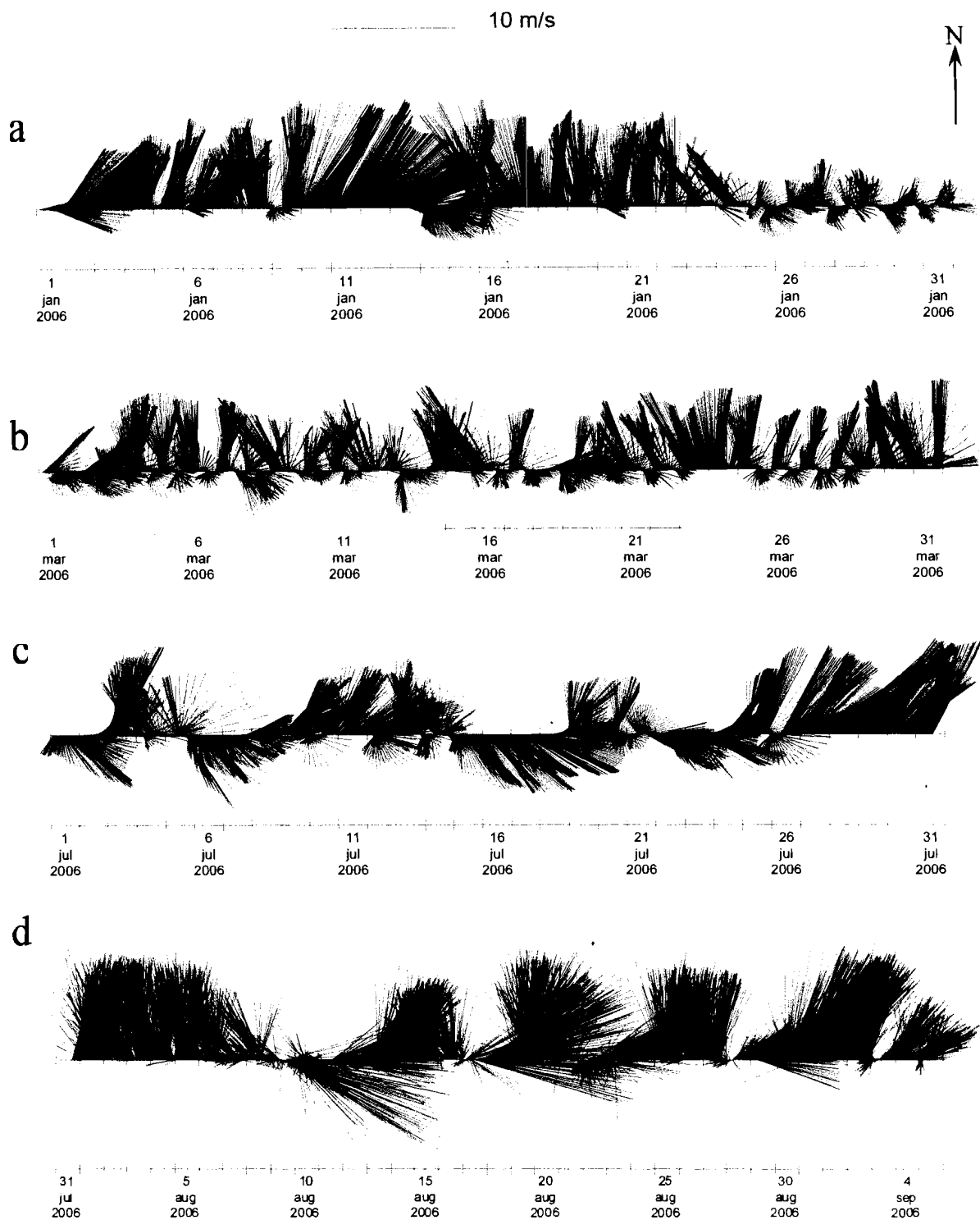


Figure 3.1 Two hourly wind stick plots showing magnitude and direction of wind during the (a, b) wet-warm season and (c, d) dry-cool season for the Suva Lagoon.

Table 3.1 shows the percentage wind direction over the Suva Lagoon. It can be seen that in both seasons, there is generally a high percentage of wind blowing from the southeast (SE) direction.

Table 3.1 Percentage wind direction for the period between August 2005 and August 2006.

Period	Month/Year	NE (%)	NW (%)	SE (%)	SW (%)
Dry-cool	Aug - 2005	24	11	48	18
	Sep - 2005	25	6	66	3
	Oct - 2005	32	12	51	4
Wet-warm	Nov - 2005	18	13	62	6
	Dec - 2005	22	12	59	7
	Jan - 2006	41	9	43	7
	Feb - 2006	27	21	33	19
	Mar - 2006	49	21	25	6
	Apr - 2006	38	23	29	10
	May - 2006	29	12	46	12
Dry-cool	Jun - 2006	25	13	52	10
	Jul - 2006	16	13	47	24
	Aug - 2006	35	7	50	8

Further analysis of wind data is made by plotting the percentage wind speed below a benchmark of 2 m s^{-1} for each month during the wet-warm and dry-cool seasons. The result is shown in Fig. 3.2.

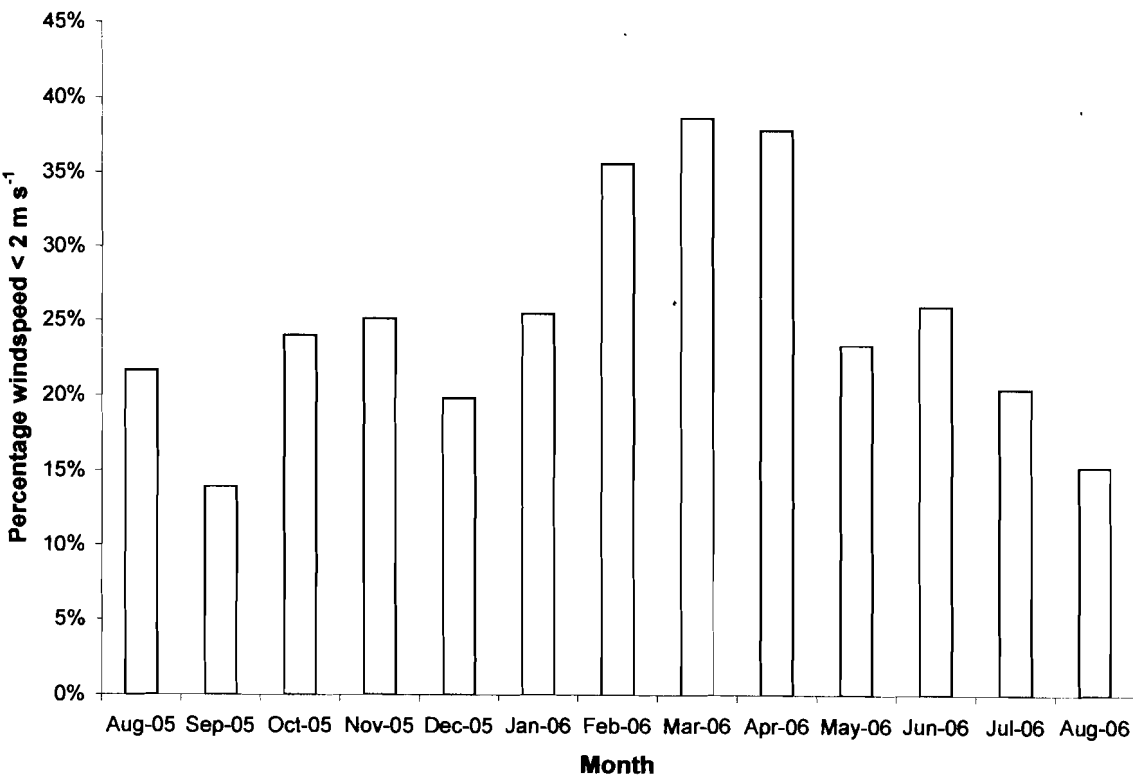


Figure 3.2 Percentage wind speed below 2 m s^{-1} for the period between August 2005 and August 2006.

Figure 3.2 shows that the percentage wind speed below 2 m s^{-1} during the wet-warm season is higher than in the dry-cool season. This indicates that stronger winds persist during the dry-cool season than in the wet-warm season. This can also be observed from the stick plots in Fig. 3.1a, b where the wind speed is lower, and in Fig. 3.1c, d where the wind speed is higher. The mean monthly wind speed ranges from $4.4 - 5.6 \text{ m s}^{-1}$ during the dry-cool season and $3.3 - 4.5 \text{ m s}^{-1}$ during the wet-warm season.

3.3 River Runoff

The Rewa River discharges freshwater into Laucala Bay through the Vunidawa River (refer to Fig. 2.2 in Chapter 2). The Vunidawa River is the major source of variations in salinity, temperature and turbidity in Laucala Bay. It is therefore important to study the freshwater runoff in order to understand the water properties and the transport of fine suspended sediments into the bay.

The Rewa River is fed by several rivers before it reaches the Suva Lagoon. These rivers include the Waidina, Wainimala, Wainibuka and Waimanu Rivers (located further north of Suva therefore not shown in Fig. 2.2), which introduce a significant amount of freshwater into the Rewa River. Although direct measurements of river discharge at the Rewa River mouth is not available, the discharge from the Rewa River can be determined by adding up the individual runoffs from these rivers. However, due to the lack of continuous discharge data of these contributing rivers into the Rewa River, the Rewa River discharge during the sampling time was determined by plotting a relationship between available discharge data between years 2000 and 2005 (from the Fiji Hydrology Department) and rainfall data for the same period (from the Fiji Meteorological Service). Figure 3.3 shows a least squares fit plot of the mean monthly discharge of the Rewa River (for months with continuous discharge data) and the corresponding total monthly rainfall.

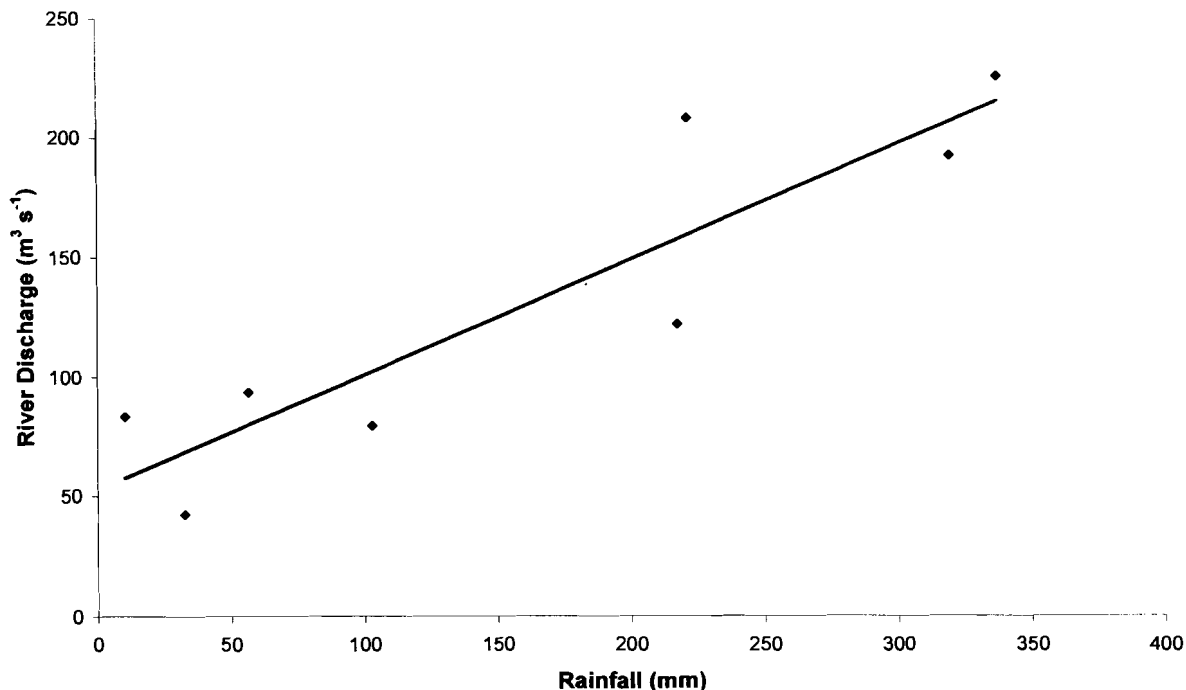


Figure 3.3 Relationship between Rewa River discharge and rainfall.

Assuming a linear relationship exists between river discharge and rainfall, a correlation coefficient of 0.82 was obtained. Equation (3.1) shows the relationship between river discharge and rainfall.

$$R_d = 0.4794 R_f + 52.755 \tag{3.1}$$

where R_d is the mean monthly river discharge from the combined runoffs of the Waidina, Wainimala, Wainibuka and Waimanu Rivers in $\text{m}^3 \text{s}^{-1}$ and R_f is the total monthly rainfall in mm. Looking at Fig. 2.3 (in Chapter 2) and equation (3.1), it can be said that there is high discharge during the wet-warm season and low discharge during the dry-cool season. Tropical cyclones are frequently encountered during the wet-warm season and associated heavy rainfall leads to flooding which increases river discharge thereby changing the water properties in the lagoon significantly.

Rao (2005) also deduced a similar relationship between the mean monthly river discharge R_d (in $\text{m}^3 \text{s}^{-1}$) for the same area and rainfall R_f (in mm) and is given by equation (3.2).

$$R_d = 0.4393 R_f + 31.722 \quad (3.2)$$

However, Rao (2005) used only five consecutive months (November 2000 – March 2001) of data for his work.

3.4 Water Properties

The water properties in the Suva Lagoon were determined by collecting *in situ* data using a standard SBE 19 CTD probe and a Niskin bottle. The CTD, which measures conductivity (salinity), temperature and pressure, was fitted with an additional sensor to measure turbidity. The Niskin bottle was used to collect water samples, which were analyzed for suspended sediment concentration (SSC).

A total of five cruises were dedicated to collecting data in the lagoon. Four cruises were undertaken during the wet-warm season and one during the dry-cool season. The total monthly rainfall taken prior to the cruise date and the mean monthly river discharge calculated using equation (3.1) for each cruise is shown in Table 3.2.

Table 3.2 Summary of cruises showing the period, cruise date, total monthly rainfall R_f and mean monthly river discharge R_d .

Season	Cruise Date	Cruise Name	Total monthly rainfall R_f (mm)	Mean monthly river discharge R_d (m ³ s ⁻¹)
Wet-warm	15-Mar-2006	<i>Cruise 1</i>	364.4	227.4
	03-Apr-2006	<i>Cruise 2</i>	252.4	173.8
	05-Apr-2006	<i>Cruise 3</i>	261.8	178.3
	07-Apr-2006	<i>Cruise 4</i>	257.1	176.0
Dry-cool	06-Sep-2006	<i>Cruise 5</i>	110.6	105.8

Table 3.2 shows that river discharge during the wet-warm season is significantly higher than during the dry-cool season. This implies that the water properties in the lagoon are expected to be influenced more by the freshwater discharge during the wet-warm season than during the dry-cool season. The variations of salinity, temperature and turbidity in the lagoon for *Cruise 2*, *Cruise 3* and *Cruise 4* will be discussed together as they were done on consecutive days to observe the effect of freshwater discharge on water properties in the lagoon. The white dots in Figs. 3.4 – 3.11 indicate the sampling sites during the respective cruise. It is to

be noted that sampling was taken at different times during the day so there can be variations in the water properties due to the tidal effect and solar heating.

3.4.1 Salinity

The salinity in the Suva Lagoon is largely controlled by the freshwater input from the Rewa River. During the wet-warm season there is high rainfall resulting in high freshwater discharge, therefore salinity in the lagoon is expected to be low. The low discharge during the dry-cool season due to low rainfall is expected to affect the lagoon salinity to a lesser extent.

3.4.1.1 Wet-Warm Season

The salinity variations in the lagoon were analyzed for the wet-warm season and are plotted in Fig. 3.4.

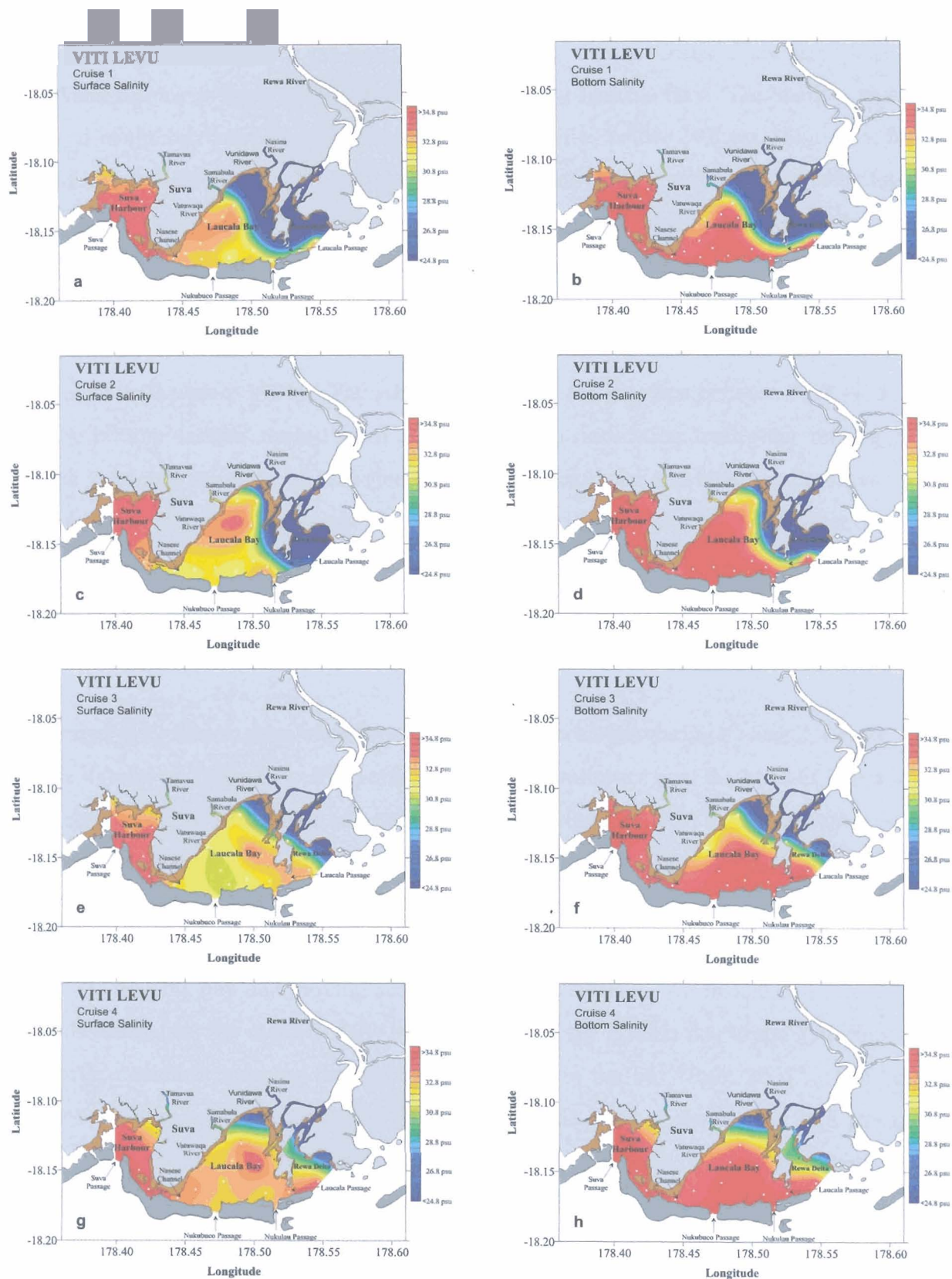


Figure 3.4 Horizontal salinity variations on the surface (left column) and bottom (right column) in the Suva Lagoon during the wet-warm season.

The low salinity waters near the head of Laucala Bay during *Cruise 1* are due to the high freshwater discharge from the Vunidawa River entering Laucala Bay. The shallow waters at the head of the bay kept the surface and bottom salinities below 24.8 psu (Fig. 3.4a, b). A path of low salinity water at the surface near the head of the bay was observed to be forming along the shallow Laucala Bay coast. The path is more evident in the bottom layer (Fig. 3.4b). This path indicates that freshwater discharged from the Vunidawa River enters the bay and begins to flow seaward along the coast. The presence of the coastline acts as a lateral constraint on the water movement, tending to divert the currents so that they flow nearly parallel to it (Bowden, 1983). The surface salinity in the bay was between 31.2 – 33.3 psu and the bottom salinity ranged from 32.4 – 34.9 psu, indicating freshwater mixing at the surface layer and an influx of seawater, through the Nukubuco and Nukulau Passages, in the bottom layer. Suva Harbour seems to be isolated from the effects of the freshwater discharge from the Rewa River. However, freshwater discharge from the Tamavua River affects the surface salinity near the head of the harbour (Fig. 3.4a). The surface and bottom salinities in the Suva Passage was found to be 34.4 psu and 34.9 psu respectively.

Compared to *Cruise 1*, there were lower freshwater discharges during *Cruise 2*, *Cruise 3* and *Cruise 4* (refer to Table 3.2). The surface and bottom salinities near the head of Laucala Bay were observed to be above 24.8 psu (more than that during *Cruise 1*) in the three cruises. The surface salinity at the head of Laucala Bay decreased from 32.2 psu during *Cruise 2* to 31.6 psu during *Cruise 3*. The surface salinity in Laucala Bay during *Cruise 3* was also lower than that during *Cruise 2*. This is due to the effect of the freshwater discharge from the Vunidawa River entering the bay and moving seaward along the surface. An instance of high salinity water is found near the middle of the bay (Fig. 3.4c, e, g). This is due to the gyre formed by the surface currents trapping the high salinity water in the bay (Rao, 2005). The bottom salinity in Laucala Bay ranged from 32.0 psu near the head of the bay to 34.8 psu at the Nukubuco Passage. A similar case was observed during *Cruise 3*, however, a path of low salinity water along the bottom was also found along the Laucala Bay coast (Fig. 3.4f). This is the path taken by freshwater discharged from the Vunidawa River as it enters the bay and moves towards the Nasese Channel. By obstructing the flow of water towards it, the coastline causes surface slopes to develop and these in turn react on and modify the water movement (Bowden, 1983).

During *Cruise 4*, the freshwater discharge from the Rewa River was less than that during *Cruise 2* and *Cruise 3* (refer to Table 3.2). Hence, the surface and bottom salinities in Laucala Bay were found to be more than those found during *Cruise 3*. This implies that the influx of seawater through the Nukubuco and Nukulau Passages along the surface (32.6 – 33.0 psu) and bottom (34.8 – 34.9 psu) was more dominant in determining the salinity distribution than the freshwater discharge (< 31.5 psu) from the Vunidawa River. Figure 3.4e, g shows that the surface and bottom salinities in the bay were higher during *Cruise 4* than in *Cruise 3*. The surface gyre remains near the middle of the bay and the path of freshwater along Laucala Bay coast is still present, but to a smaller extent due to the lower freshwater discharge.

Suva Harbour is isolated from the freshwater discharge of the Rewa River (Fig. 3.4c-h) but the effect of the freshwater discharge from the Tamavua River on the surface salinity at the head of the harbour is evident. The surface salinity at the head of the harbour decreased from 34.1 psu during *Cruise 2* to 33.8 psu during *Cruise 3* due to the increased discharge from the Tamavua River. However, the surface salinity increased during *Cruise 4* due to lower discharge from the Tamavua River and an influx of seawater through the Suva Passage.

3.4.1.2 Dry-Cool Season

The salinity variations in the lagoon were analyzed for the dry-cool season and are plotted in Fig. 3.5.

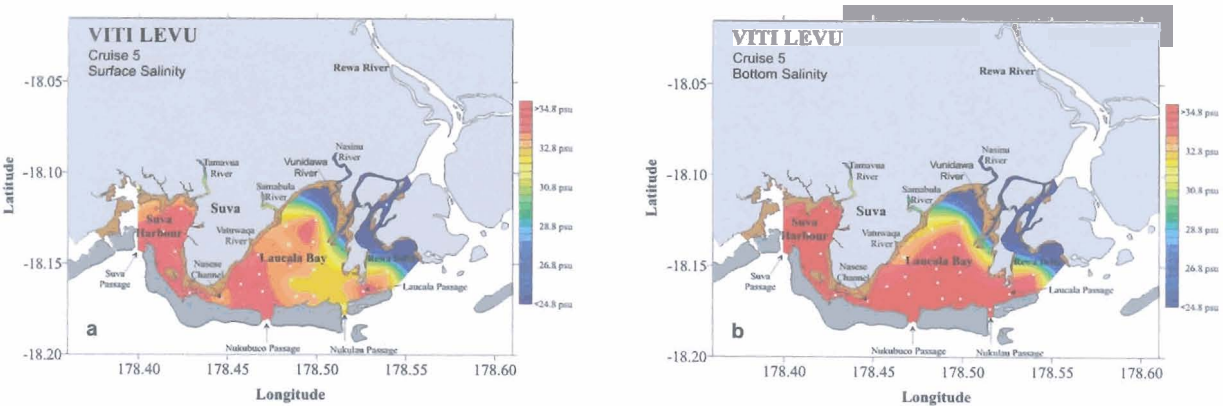


Figure 3.5 Horizontal salinity variations on the surface (left) and bottom (right) in the Suva Lagoon during the dry-cool season.

Due to the low freshwater discharge from the Rewa River during *Cruise 5* (refer to Table 3.2), the salinity in Laucala Bay was generally found to be higher than during *Cruise 1*, *Cruise 2*, *Cruise 3* and *Cruise 4*. The surface salinity in Laucala Bay ranged from 33.7 psu near the head of the bay to 34.5 psu at the Nukubuco Passage. The high salinity waters entering through the Nukubuco Passage at the surface can be seen to move towards the Laucala Bay coast in Fig. 3.5a. This highly saline water extends towards the head of Laucala Bay mixing with the freshwater discharged from the Vunidawa River. An instance of high salinity water is found in the middle of the bay due to the gyre formed by the surface currents (Fig. 3.5a). Although the freshwater discharge is low during the dry-cool season, it still influences the salinity in the bay. Suva Harbour is unaffected by the freshwater discharge from the Rewa River but the freshwater discharge from the Tamavua River does affect the surface salinity (34.0 psu). The bottom salinity in the harbour shows little horizontal variation and remains uniform at around 35.0 psu.

3.4.2 Temperature

The water temperature in the Suva Lagoon is expected to be higher in the wet-warm season than in the dry-cool season (refer to Fig. 2.3 in Chapter 2). The freshwater input from the Rewa River is the major source of temperature variations in the lagoon.

3.4.2.1 Wet-Warm Season

The temperature variations in the lagoon were analyzed for the wet-warm season and are plotted in Fig. 3.6.

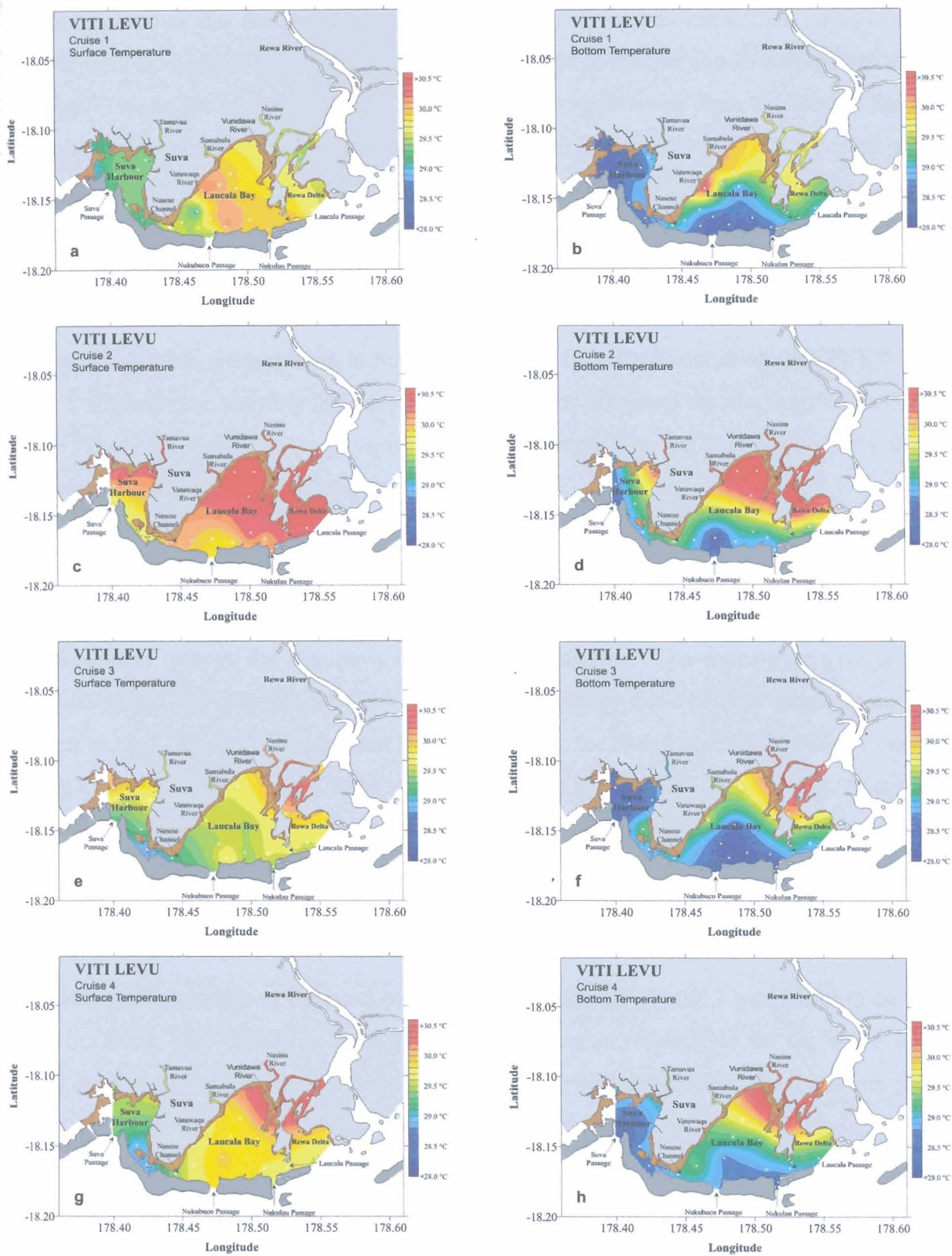


Figure 3.6 Horizontal temperature variations on the surface (left column) and bottom (right column) in the Suva Lagoon during the wet-warm season.

Figure 3.6a shows that the surface temperature in Laucala Bay during *Cruise 1* ranges from 30.0 °C near the head of the bay to 30.2 °C in the middle of the bay and 29.3 °C at Nukubuco Passage. This is due to the movement of warm surface water away from the head of the bay towards the Nukubuco and Nukulau Passages. Figure 3.6a also shows that there is an influx of cold seawater from Nukubuco Passage moving towards the middle of the bay. This is more evident in the bottom layer (Fig. 3.6b). Figure 3.6b shows cooler water entering through the Nukulau Passage and moving towards the head of the bay. A path of warm freshwater is observed to be moving along Laucala Bay coast towards Nasese Channel. The surface and bottom temperatures in Suva Harbour are fairly uniform, at around 29.3 °C and 28.5 °C respectively, showing little or no influence of the effects of the discharge of the Rewa River. There are, however, small variations in temperature near the head of the harbour due to warm freshwater discharge from the Tamavua River.

The surface temperature at the Nukubuco Passage during *Cruise 2* was 29.8 °C reaching a maximum value of 30.8 °C at the head of Laucala Bay. Figure 3.6c clearly shows the input of warm water through the Vunidawa River into Laucala Bay. The warm waters reside near the head of the bay and are carried towards the Nukubuco and Nukulau Passages and are evident in Fig. 3.6c, e, g. The bottom temperature near the Nukubuco and Nukulau Passages during *Cruise 2*, *Cruise 3* and *Cruise 4* remain between 28.4 °C and 28.9 °C (Fig. 3.6d, f, h). This cold seawater entering from the passages extends into the bay and mixes with the warm waters discharged from the Vunidawa River near the middle of the bay. A path of warm water can clearly be seen flowing towards the Nasese Channel (Fig. 3.6f).

The surface temperature at the head of Suva Harbour during *Cruise 2* was found to be 30.2 °C (Fig. 3.6c). The discharge from the Tamavua River is responsible for the warm water found at the head of the harbour. As the warm water discharged from the Tamavua River enters the harbour, it mixes with cold seawater entering through the Suva Passage. The surface temperature at the Suva Passage was found to be 29.5 °C. A similar condition was observed during *Cruise 3* where the surface temperature at the head of the harbour was found to be 29.7 °C and 29.1 °C at the Suva Passage (Fig. 3.6e). However, the surface temperature during *Cruise 4* showed little horizontal variation ranging between 29.3 °C at the Suva Passage to 29.5 °C near the head of the harbour (Fig. 3.6g). This is due to the lower discharge from the Tamavua River and an increased influx of cold seawater through the Suva

Passage. The bottom temperatures in the harbour were generally lower than the surface temperatures as expected. The bottom temperature near the head of the harbour during *Cruise 2* was found to be the same as the surface temperature of 30.2 °C. This is due to vertical mixing with warm surface waters discharged from the Tamavua River at depths less than 3 m. The bottom temperature reaches a minimum of 28.5 °C at the Suva Passage. The bottom temperature in Suva Harbour during *Cruise 3* was found to be more uniform at around 28.5 °C. A similar situation was observed during *Cruise 4*.

3.4.2.2 Dry-Cool Season

The temperature variations in the lagoon were analyzed for the dry-cool season and are plotted in Fig. 3.7.

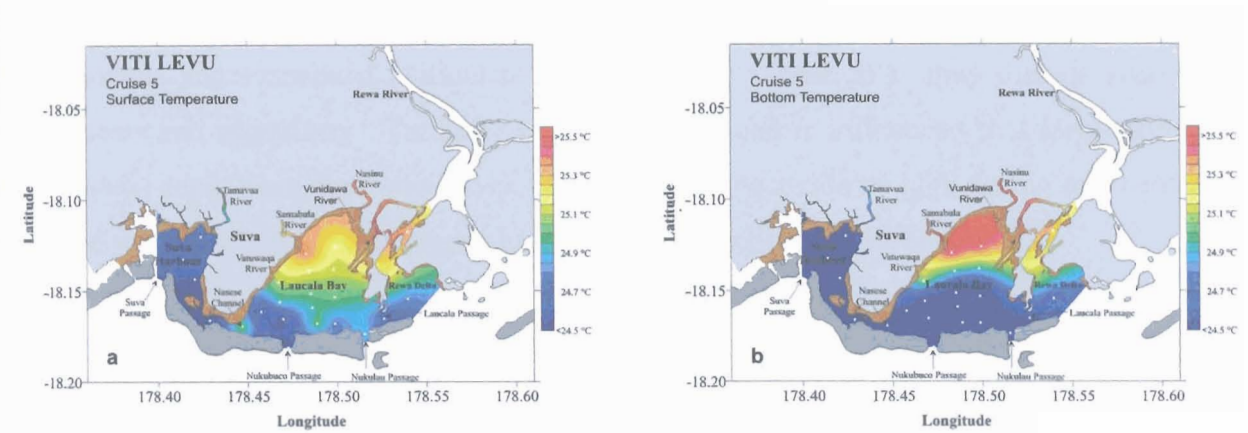


Figure 3.7 Horizontal temperature variations on the surface (left) and bottom (right) in the Suva Lagoon during the dry-cool season.

The surface and bottom temperatures in the Suva Lagoon during the dry-cool season were expectedly lower than during the wet-warm season. The surface temperature in Laucala Bay during *Cruise 5* ranged from 24.5 °C near the Nukubuco and Nukulau Passages to 25.2 °C near the head of Laucala Bay (Fig. 3.7a). Due to the low discharge during the dry-cool season, the warm waters discharged from the Vunidawa River during *Cruise 5* remained near the head of the bay. Cooler waters entering through Nukubuco Passage extended to the middle of the bay where it mixed with the warm waters discharged from the Vunidawa River. Density is dependent on salinity and temperature. Normally, high density waters at the bottom have high salinity and low temperature and vice versa for low density waters at the surface. However, if the salinity and temperature at the bottom are both higher than those at

the surface, then the high density water will remain at the bottom regardless of the temperature at the bottom. This occurrence is observed near the head of the bay where the bottom temperature is higher than the surface temperature. A path of warm freshwater was observed to be forming along the Laucala Bay coast (Fig. 3.7b). The cool water entering through the Nukubuco and Nukulau Passages can be seen to extend towards the middle of the bay. The surface and bottom temperatures at Suva Harbour were uniform at 24.7 °C and 24.4 °C respectively.

3.4.3 Turbidity

Turbidity is a measure of water clarity. It is an optical property that expresses the degree to which light is scattered and absorbed by molecules and particles (www.ozestuaries.org, 2006). Turbidity in the water column is a result of the presence of soluble colored organic compounds and suspended particulate matter (SPM). These SPM may include suspended sediments and organisms. Turbidity in the Suva Lagoon is influenced to a large extent by freshwater input from the Rewa River. Turbidity is expected to be high during the wet-warm season when freshwater discharge is high and low during the dry-cool season.

Turbidity is measured in Nephelometric Turbidity Units (NTU) or Formazin Turbidity Units (FTU), depending on the method and equipment used (www.ozestuaries.org, 2006). Turbidity measured in NTU uses nephelometric methods that depend on passing specific light of a specific wavelength through the sample. FTU is the unit of measurement when using absorptometric methods (spectrophotometric equipment) and is the one that was used in this project.

3.4.3.1 Wet-Warm Season

The turbidity variations in the lagoon were analyzed for the wet-warm season and are plotted in Fig. 3.8.

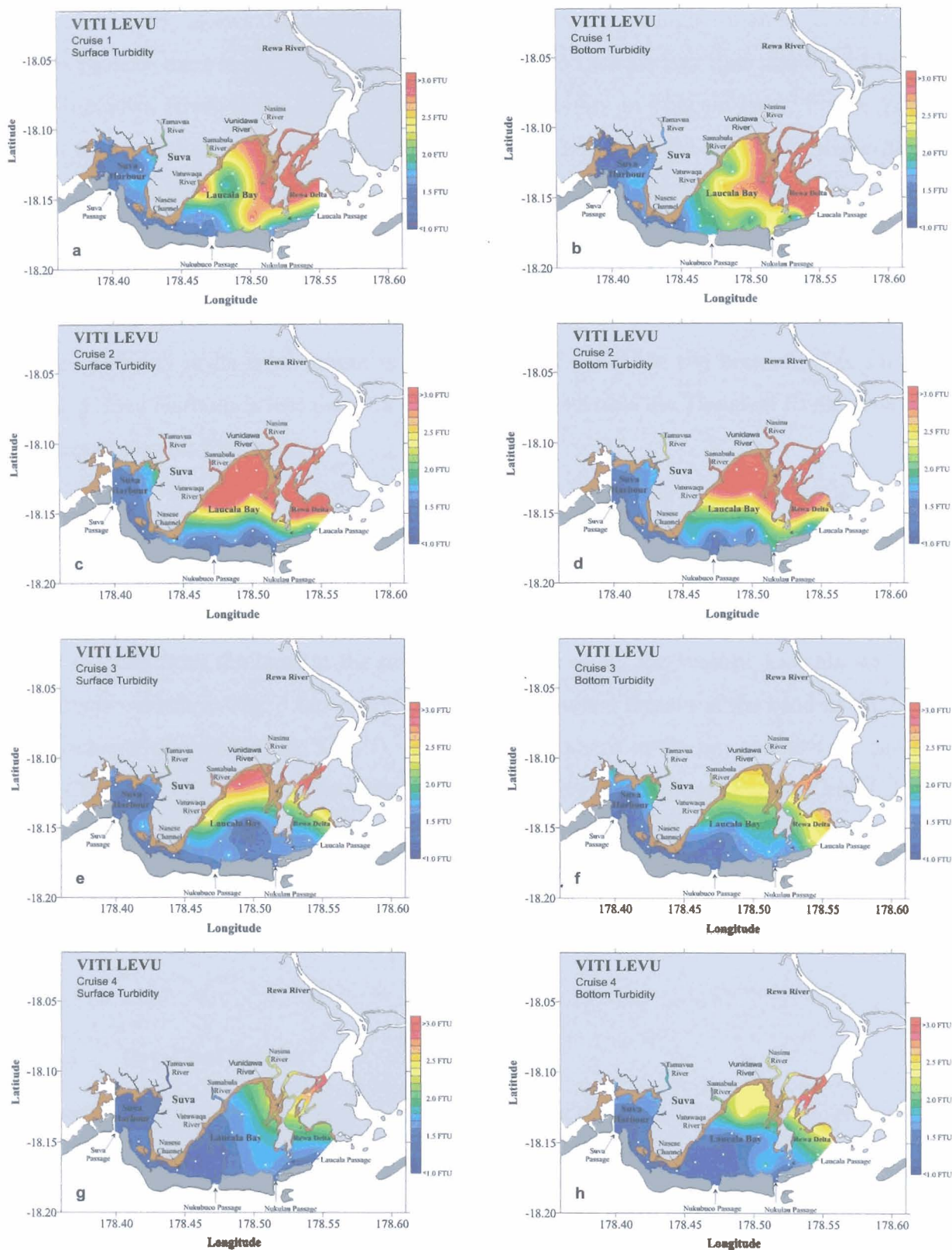


Figure 3.8 Horizontal turbidity variations on the surface (left column) and bottom (right column) in the Suva Lagoon during the wet-warm season.

Figure 3.8 clearly shows that turbidity in Laucala Bay is always higher than in Suva Harbour. This is because there is higher freshwater discharge into Laucala Bay than into Suva Harbour. The Vunidawa River is the major source of high turbidity in Laucala Bay. Figure 3.8a, b shows that turbidity in Laucala Bay during *Cruise 1* is high at the Vunidawa River mouth. The surface turbidity is 2.0 FTU while the bottom turbidity is 2.8 FTU. There is higher turbidity at the bottom due to resuspension of bottom sediments in the water column. Much higher turbidity (3.6 FTU) is observed in the shallow Rewa Delta. There are also discharges from smaller rivers, like the Vatuwaqa River, and this is evident in Fig. 3.8a where the surface turbidity at its river mouth is 2.9 FTU and 2.0 FTU at the bottom. The turbidity found at Suva Harbour is less than 1.8 FTU with maxima near the Tamavua River mouth and the west of Nasese Channel.

Figure 3.8c, d shows high turbidity at the surface (6.5 FTU) and bottom (4.4 FTU) at the head of Laucala Bay during *Cruise 2*. It can be clearly seen that the path of freshwater from the Vunidawa River entering the bay is responsible for the high turbidity. The high turbidity water extends from the head to the middle of the bay along the shallow Laucala Bay coast and this is evident in Fig. 3.8e. Some high turbidity waters remain at the head of the bay as the discharge decreases (Fig. 3.8e, f). The turbidity pattern in the bay remains the same up until *Cruise 4* (Fig. 3.8g, h) but there are low turbidity waters compared to *Cruise 2* (Fig. 3.8c, d) due to the decreased discharge of freshwater from the Rewa River. Suva Harbour remains undisturbed by the discharge from the Rewa River but some high turbidity waters can be found at the head of the harbour due to the freshwater discharge from the Tamavua River.

3.4.3.2 Dry-Cool Season

The turbidity variations in the lagoon were analyzed for the dry-cool season and are plotted in Fig. 3.9.

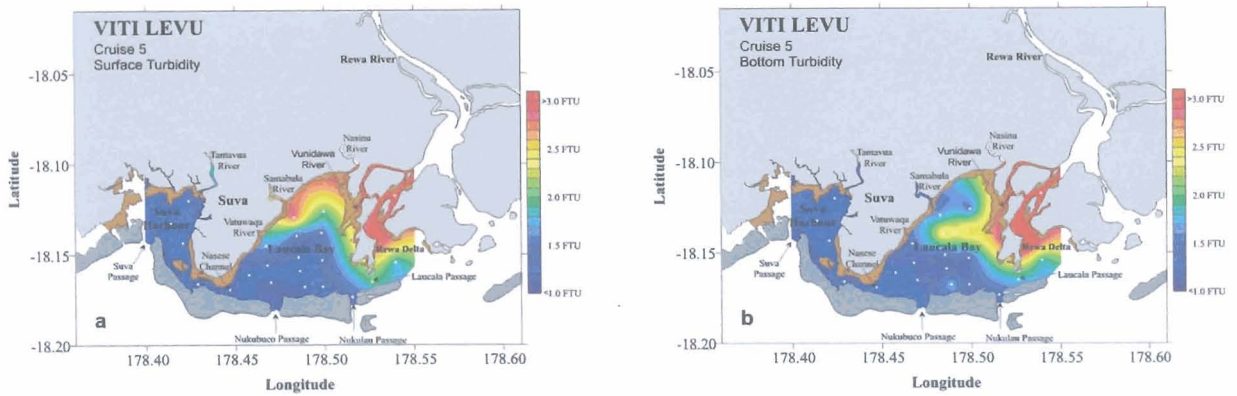


Figure 3.9 Horizontal turbidity variations on the surface (left column) and bottom (right column) in the Suva Lagoon during the dry-cool season.

Due to lower freshwater discharge during the dry-cool season, the turbidity in Laucala Bay is less (Fig. 3.9a, b). However, turbid waters (2.9 FTU) were observed at the surface at the mouth of the Samabula River. The bottom turbidity at the Vunidawa River mouth was found to be higher than the surface turbidity. This is due to resuspension at the bottom stirring up the bottom sediments. Lower turbidity in Laucala Bay is due to lower freshwater discharge during the dry-cool season. Suva Harbour shows uniform turbidity of 1.2 FTU from the surface to a depth of 30 m.

3.4.4 Suspended Sediment Concentration

Turbidity was also measured by determining the suspended sediment concentration (SSC) in a given volume of sample. The water samples were taken a meter below the sea-surface and were filtered using a Whatman nuclepore polycarbonate track-etch membrane filter paper, which has a diameter of 47 mm and porosity, made by laser beams, of $0.4\ \mu\text{m}$ (values cited from the filter paper package box). The SSC was measured in mg L^{-1} .

3.4.4.1 Wet-Warm Season

The filter paper used in analyzing the water samples for *Cruise 1*, *Cruise 2*, *Cruise 3* and *Cruise 4* was an ADVANTEC MFS borosilicate microfiber filter paper. This was not the preferred filter paper but was used as the Whatman filter paper needed was not available at that time. Nevertheless, the water samples were analyzed and the results are plotted in Fig. 3.10.

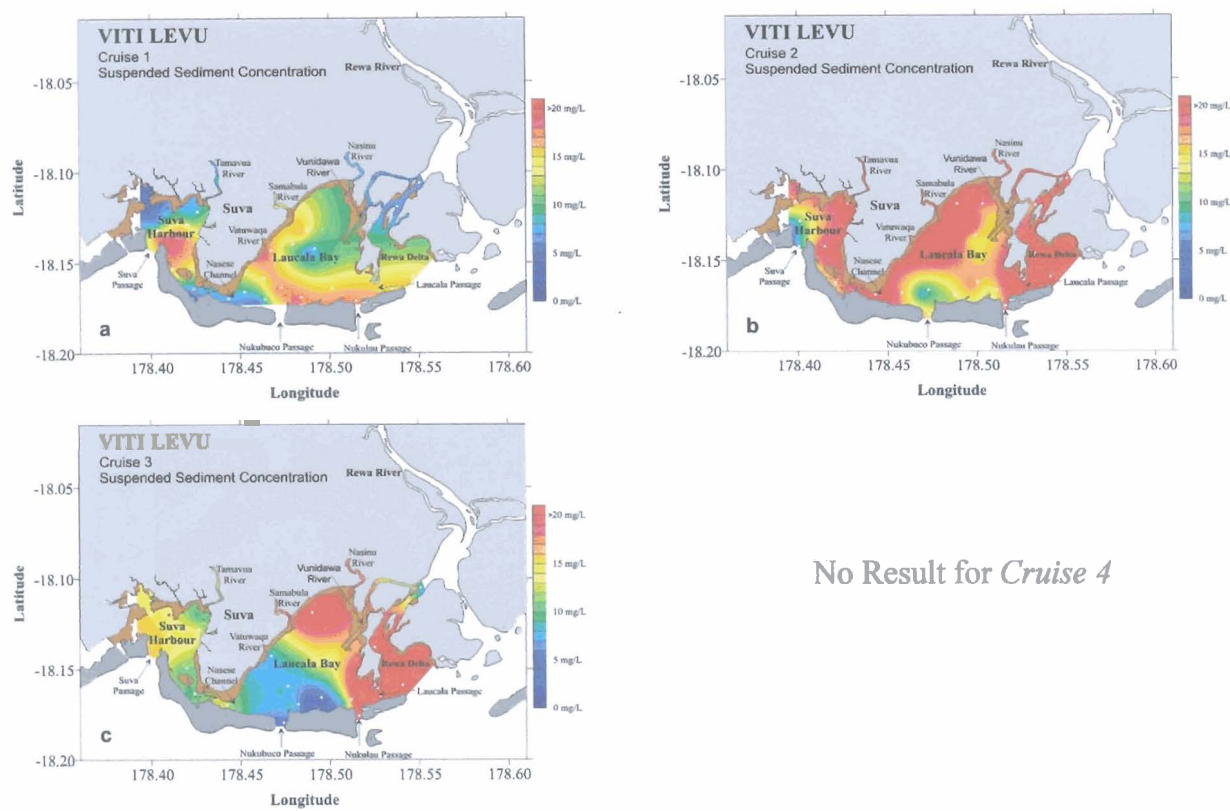


Figure 3.10 Suspended sediment concentration at the surface in the Suva Lagoon during the wet-warm season.

The results from Fig. 3.10 show that high suspended sediment concentration, hereafter denoted as SSC, can be seen near the river mouths and along the coastline. Figure 3.10a shows that high SSC is found at the mouth of the Vatuwaqa River during *Cruise 1*. Similarly during *Cruise 2*, high SSC is observed in the Rewa Delta, along the Laucala Bay coast, through Nasese Channel and at the mouth of the Tamavua River. The head of Laucala Bay shows a zone of high SSC during *Cruise 3*. It can be said that the Nasinu, Tamavua, Vatuwaqa, Samabula and Vunidawa Rivers all contribute to the high SSC in the Suva Lagoon. The shallow Laucala Bay coast and the head of Laucala Bay are regions where high SSC can be found. The shallow Rewa Delta is also a high SSC region. There was no result obtained for *Cruise 4* because the samples were analyzed a week after data collection and the sediments had settled to the bottom thereby giving inaccurate results. Shaking the sample bottles did not help in resuspending the settled sediments.

3.4.4.2 Dry-Cool Season

The SSC values for *Cruise 5* during the dry-cool season were obtained by using the Whatman filter paper and the result is plotted in Fig. 3.11.

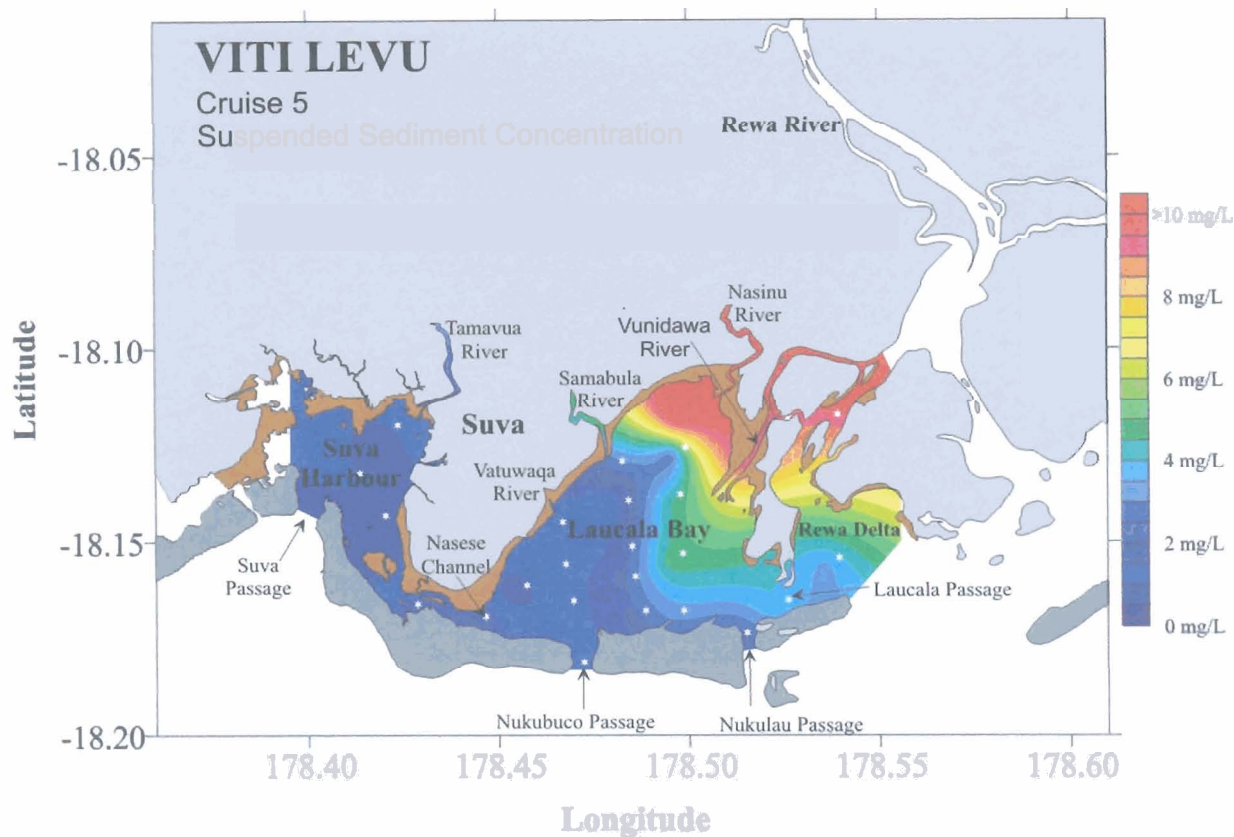


Figure 3.11 Suspended sediment concentration at the surface in the Suva Lagoon during the dry-cool season.

Figure 3.11 shows the relative concentrations at various places in the Suva Lagoon. High SSC is found at the head of Laucala Bay and the mouth of the Vunidawa River. The Rewa Delta also shows regions of high SSC. The passages, Nasese Channel and Suva Harbour show relatively low SSC.

The variations in the SSC are due to two main factors. The first is the resuspension of bottom sediments (where there is a high percentage of fine particles at the bottom), which increases the SSC in the water column. And the second is the effect of the high sediment input from the Rewa River, which increases the turbidity of water.

3.4.5 Turbidity and Suspended Sediment Concentration

If we compare the surface turbidity measured using a CTD probe from Fig. 3.8a, c, e and Fig. 3.9a with the measured SSC using filtration in Fig. 3.10a-c and Fig. 3.11 respectively, we can see that the best comparison between turbidity and SSC is between Fig. 3.9a and Fig. 3.11. A graph of surface turbidity against SSC for *Cruise 5* is plotted in Fig. 3.12.

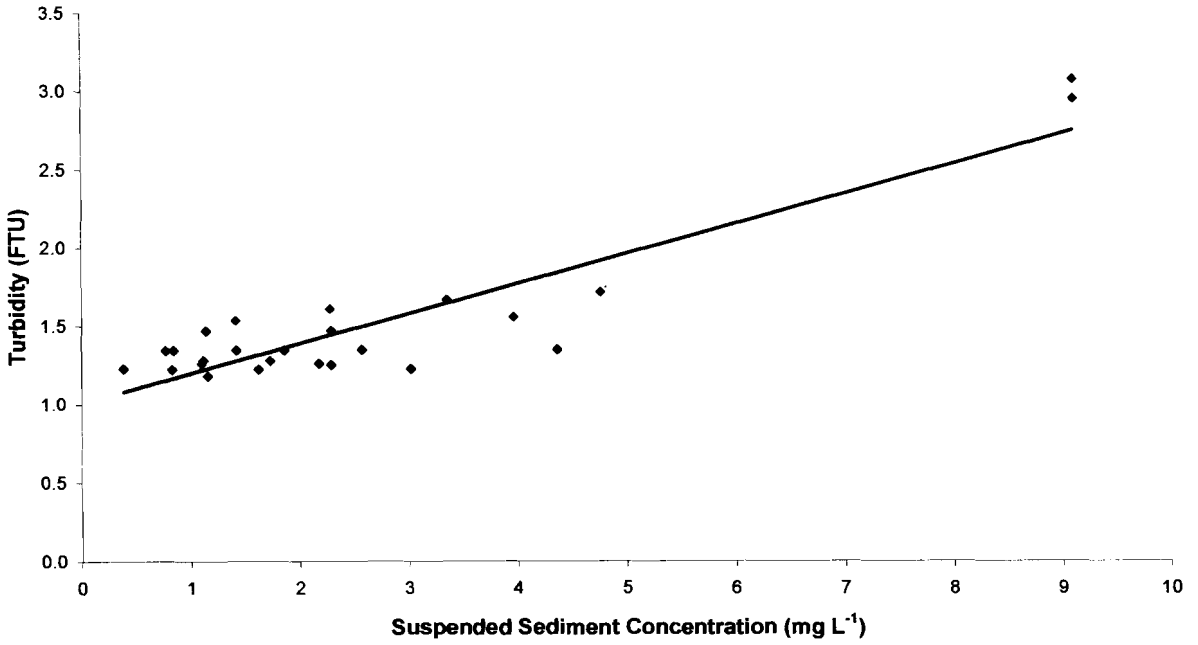


Figure 3.12 Relationship between turbidity and suspended sediment concentration.

As mentioned earlier, turbidity is a measure of the total suspended solids in water. Therefore, assuming a linear relationship between surface turbidity and SSC, there is a correlation coefficient of 0.82 between the two variables. The suspended sediment concentration is related to surface turbidity as given by equation (3.3).

$$T_{urb} = 0.1895 \text{ SSC} + 1.0069 \quad (3.3)$$

where SSC is the suspended sediment concentration in mg L^{-1} and T_{urb} is the turbidity in FTU. It can be said from equation (3.3) that seawater has a turbidity of approximately 1 FTU when the SSC is 0 mg L^{-1} . This however contradicts that turbidity in the water column is a result of the presence of suspended particulate matter. Therefore, a reading of 1 FTU would probably indicate that the turbidity sensor has an error of 1 FTU whereby it is the background turbidity of water in the absence of any suspended particulate matter. This perhaps is the case because the sensitivity range of the turbidity sensor is quite large, between 0 – 400 FTU. Ideally, the vertical axis intercept in Fig. 3.12 should pass through the origin.

3.5 Conclusions

The mean wind direction over the Suva Lagoon is generally from the southeast. These southeast trade winds have a mean annual wind speed of about 6 m s^{-1} and are an important component in the distribution of salinity, temperature and turbidity in the lagoon. River runoff is also an important factor which influences the distribution of these parameters. The high discharge from the Rewa River during the wet-warm season is seen to affect the lagoon water properties more than during the dry-cool season, especially for Laucala Bay.

The southeast trade winds tend to push the freshwater discharged from the Vunidawa River towards the head of Laucala Bay resulting in high temperature and turbidity and low salinity waters being accumulated there. The piled-up water flows along the Laucala Bay coast and towards Nasese Channel. This path of freshwater discharged from the Vunidawa River is evident in Figs. 3.4 – 3.9. These figures also show that the influx of seawater through the Nukubuco and Nukulau Passages extend up to the middle of the bay beyond which there is mixing with freshwater at depths of less than 3 m. The freshwater input from the Rewa River is warmer than the oceanic water entering through the passages during both seasons.

Suva Harbour, unlike Laucala Bay, is protected from the full brunt of the southeast trade winds by the hilly Suva Peninsula. The harbour water properties are more homogenous than in the bay due to lower freshwater discharge from the Tamavua River (compared to the Rewa River) and weaker southeast trade winds. The harbour is isolated from the effects of the freshwater discharge from the Rewa River. Thus, it can be said that Suva Harbour and Laucala Bay exists as two separate water bodies.

The water properties in the Suva Lagoon are influenced by a combination of factors which include river runoffs, winds and tides. A numerical model can be used to determine the impact that these factors have on the water properties in the lagoon. The results presented in this chapter would be used to validate a 3D hydrodynamic-sediment transport coupled model for the Suva Lagoon. The model theory is presented in detail in the following chapter.

Chapter 4



Governing Equations, Boundary Conditions and Numerical Discretization

4.1 Introduction

Numerical modelling is a powerful method of visualizing and analyzing the dynamic behavior of physical systems (www.aslenv.com, 2004). The distribution and behavior of key properties can be readily simulated within the numerical model, including tidal currents and circulation, salinity, temperature and suspended sediment concentration (SSC – mass of suspended sediments per unit volume of water). A 3D numerical model is used in this project to predict the transport of fine suspended sediments in the Suva Lagoon.

4.2 The 3D Hydrodynamic-Sediment Transport Coupled Model

The MARS3D multilayered model used for this project was developed by the Institut Français de Recherche pour l'Exploitation de la Mer (IFREMER) and is presented extensively by Douillet *et al.* (2001). The model has hydrodynamic, transport and turbulence components and is able to predict sea-level heights, current velocities, salinity and SSC due to river runoff and different tidal and wind forcings at the grid points at discrete time intervals.

The governing equations of the hydrodynamic model component express the conservation of mass, momentum and salinity and assume the hydrostatic and Boussinesq approximations (for example, Blumberg and Mellor, 1987; Ruddick *et al.*, 1995; Estournel *et al.*, 1997). The MARS3D model is made up of two inter-related sub-models: a depth-integrated 2D model (Douillet, 1998) and a 3D model which uses the same horizontal axis. The 2D model solves the shallow water equations (Blumberg and Mellor, 1987), calculates the free surface water elevation and horizontal velocity at all grid points and supplies these to the 3D model.

The transport model component calculates the spatial and temporal distributions of salinity and suspended sediment concentration (Douillet *et al.*, 2001; Ouillon *et al.*, 2004). In this component, the suspended sediment transport is modeled by an equation expressing the local variation of the sediment concentration due to the advective motion and turbulent diffusion of surrounding sediments.

The turbulence model used is of the Mellor and Yamada (1982) type, which characterizes the turbulence by equations for the turbulent kinetic energy. The bottom stress is parameterized by means of a quadratic function of the velocity that is consistent with the existence of a logarithmic layer adjacent to the bottom (Blumberg and Mellor, 1987; Deleersnijder and Beckers, 1992; Douillet, 1998). A wind friction condition is applied at the surface (Douillet *et al.*, 2001). Open boundary conditions are the same to those applied in the 2D model (Neumann type for velocity and Dirichlet for water height).

The model resolution is based on the Alternating Direction Implicit (ADI; Leenderstse, 1967) method for time discretization and on the finite difference method for space discretization. A modified Arakawa C-grid (Lazure and Salomon, 1991) is used which is able to automatically handle emerging tidal flats as a result of the combined use of a test during the ADI procedure and the above mentioned grid modification. The horizontal grid spacing used in this study is 200 m. The model is able to simulate the effects of bathymetry, bottom friction, turbulence, river runoff, tides and wind forcing. The source code of the model is written in the FORTRAN programming language and is run on the Windows XP operating platform.

4.3 Governing Model Equations and Boundary Conditions

The equations for the model are initially written in a Cartesian coordinate system (x, y, z, t) with the x -axis directed to the east, the y -axis to the north, the z -axis as the vertical direction and t denotes time. The hydrodynamic model solves the primitive continuity and momentum equations for the surface elevation and 3D velocity field for incompressible flow assuming hydrostatic equilibrium and the Boussinesq approximation. The computed flow field transports salinity and SSC using the advection-diffusion equation in the transport model.

Appropriate boundary conditions need to be provided for the interpretation of transport phenomenon through a numerical model (Fernandes, 2005). The boundary conditions are specified for the surface, bottom and lateral boundaries and can be closed, open or moving.

4.3.1 Hydrodynamic Model

4.3.1.1 Model Equations

The hydrodynamic model uses the equations of motion, known as the Navier-Stokes equation, together with the equation of continuity of volume to determine the water surface elevation and the current velocity. The Navier-Stokes equation, which is valid basically for all flow conditions (Burchard, 2002), has its general form given by equation (4.1).

$$\frac{\partial q}{\partial t} + (\nabla \cdot q)q = F - \frac{1}{\rho} \nabla p + D_i \quad (4.1)$$

where q is the velocity component (u, v, w) in the x , y and z directions respectively at any grid locations in space, $F = (fv, -fu, g)$ with f being the Coriolis parameter and g the acceleration due to gravity, ρ is the *in situ* water density, p is the pressure of the fluid and D_i is the diffusion term given by equation (4.2).

$$D_i = \frac{\partial}{\partial x} \left(N_h \frac{\partial q_i}{\partial x} \right) + \frac{\partial}{\partial y} \left(N_h \frac{\partial q_i}{\partial y} \right) + \frac{\partial}{\partial z} \left(N_z \frac{\partial q_i}{\partial z} \right) \quad (4.2)$$

where N_h and N_z are the horizontal and vertical eddy coefficients of viscosity respectively. The four unknowns in the above equations are the velocity components (u, v, w) and pressure p . The vertical velocity is calculated from the continuity of volume equation given by equation (4.3).

$$\frac{1}{\rho} \frac{d\rho}{dt} + \left[\frac{\partial u}{\partial x} + \frac{\partial v}{\partial y} + \frac{\partial w}{\partial z} \right] = 0 \quad (4.3)$$

To simplify the governing equations, the Navier-Stokes equation is solved using the Boussinesq approximation and the hydrostatic pressure distribution assumption. The Boussinesq approximation implies that density differences are neglected unless the differences are multiplied by gravity. This approximation is shown in equation (4.4). The initial density of seawater used in the model is $1027.34 \text{ kg m}^{-3}$.

$$\frac{1}{\rho} \cdot \frac{d\rho}{dt} = 0 \quad (4.4)$$

Using the Boussinesq approximation, the equation of continuity is reduced from equation (4.3) to equation (4.5).

$$\frac{\partial u}{\partial x} + \frac{\partial v}{\partial y} + \frac{\partial w}{\partial z} = 0 \quad (4.5)$$

The hydrostatic pressure distribution assumption implies that the weight of the fluid identically balances the pressure as shown by the momentum equation in equation (4.6).

$$\frac{\partial p}{\partial z} = -\rho g \quad (4.6)$$

The hydrostatic assumption allows pressure to be replaced by the total water depth D as shown in equation (4.7).

$$p = \rho g D = \rho g (H + \zeta) \quad (4.7)$$

where ζ is the free surface elevation above mean sea-level and H is the measured water depth from mean sea-level. The Navier-Stokes equation in equation (4.1) can be further divided into components in the x and y directions as shown in equations (4.8) and (4.9) respectively.

$$\frac{\partial u}{\partial t} + u \frac{\partial u}{\partial x} + v \frac{\partial u}{\partial y} + w \frac{\partial u}{\partial z} - fv - \frac{\partial(N_z \partial u)}{\partial z^2} = -g \frac{\partial \zeta}{\partial x} + F_x \quad (4.8)$$

$$\frac{\partial v}{\partial t} + u \frac{\partial v}{\partial x} + v \frac{\partial v}{\partial y} + w \frac{\partial v}{\partial z} + fu - \frac{\partial(N_z \partial v)}{\partial z^2} = -g \frac{\partial \zeta}{\partial y} + F_y \quad (4.9)$$

where ζ is the free sea-surface elevation and F_x and F_y are the other forces, including the frictional and tidal forces, acting on a unit mass. Equations (4.5), (4.6), (4.8) and (4.9) are used in the model to solve for the unknown velocity components (u, v, w) and sea-surface elevation ζ .

4.3.1.2 Boundary Conditions

Boundary conditions are set for the sea-surface and for the sea-bottom. Elevation at the open boundary is specified with 4 tidal constituents. At the river boundary, a volume flow is imposed and river salinity is fixed. At coastal boundaries, a free-slip condition is imposed by specifying a zero normal component of mass and momentum flux. The subscripts s and b are used to denote the surface and the bottom respectively.

To calculate the vertical velocity from the equations of motion, it is necessary to relate the shearing stress components τ_{xx} and τ_{yy} to the velocity components u and v as shown in equation (4.10). A fluid for which the friction law of equation (4.10) holds is called a Newtonian fluid.

$$\tau_x = \rho N_z \frac{\partial u}{\partial z} \quad \tau_y = \rho N_z \frac{\partial v}{\partial z} \quad (4.10)$$

Frictional effects arise from the shearing stress of wind acting on the sea-surface and the shearing stress at the bottom caused by the flow of water over the seabed (Bowden, 1983). These stresses are transmitted to the rest of the water column by internal shear stresses due to turbulence. At the sea-surface, the surface horizontal velocity is governed by the stress at the air-sea interface and is given by equation (4.11).

$$\tau_{sx} = \rho_o N_z \frac{\partial u}{\partial z} \quad \tau_{sy} = \rho_o N_z \frac{\partial v}{\partial z} \quad (4.11)$$

The stress is imposed by means of the wind shear stress τ_s , and is calculated according to a quadratic friction law given in equation (4.12). This equation is used to determine the surface horizontal velocity in equation (4.11).

$$\tau_s = C_D \rho_a W^2 \quad (4.12)$$

where C_D is the drag coefficient at the air-sea interface, ρ_a is the density of air which is taken as 1.25 kg m^{-3} and W is the wind speed in m s^{-1} at a 10 m height above mean sea-level. The wind affected Ekman layer is 62 m in the Suva Lagoon (Rao, 2005). The net transport in this layer is in the direction perpendicularly to the left (in the Southern hemisphere) of the wind direction. However in shallow waters, the water movement is in the same direction as the wind (Pickard and Emery, 1990). Kinematic boundary condition requires that water particles do not escape from the surface as shown by equation (4.13).

$$w = u \frac{\partial \zeta}{\partial x} + v \frac{\partial \zeta}{\partial y} + \frac{\partial \zeta}{\partial t} \quad (4.13)$$

There is a drag between the water and the sea-bottom as water flows over sediments lying on the seabed. The bottom velocity is governed by the bottom stress caused by the roughness of the seabed as shown in equation (4.14).

$$\tau_{bx} = \rho_o N_z \frac{\partial u}{\partial z} \quad \tau_{by} = \rho_o N_z \frac{\partial v}{\partial z} \quad (4.14)$$

The resultant bottom shearing stresses are determined by the bottom drag coefficient C_d as shown in equation (4.15).

$$\tau_{bx} = C_d \sqrt{(u_b^2 + v_b^2)} \cdot u_b \quad \tau_{by} = C_d \sqrt{(u_b^2 + v_b^2)} \cdot v_b \quad (4.15)$$

The vertical profile of velocity can then be calculated from the equations of motion by substituting the horizontal velocity components found in equation (4.14) with the bottom shear stresses in equation (4.15) to obtain equation (4.16).

$$\rho N_z \frac{\partial u}{\partial z} = C_d \sqrt{u_b^2 + v_b^2} \cdot u_b \quad \rho N_z \frac{\partial v}{\partial z} = C_d \sqrt{u_b^2 + v_b^2} \cdot v_b \quad (4.16)$$

From equation (4.16), it is evident that the bottom shear stress is imposed assuming a logarithmic velocity profile whereby the velocity increases logarithmically with distance from the bottom as shown in equation (4.17).

$$u = \frac{u_*}{k_0} \log_e \left(\frac{z'}{z_0} \right) \quad (4.17)$$

where z' is the distance from the bottom, u_* is the friction velocity given by $\sqrt{\frac{\tau_{bx}}{\rho}}$, z_0 is the roughness parameter and k_0 is the von Karman's constant which is approximately equal to 0.41 (Bowden, 1983). The roughness parameter, which is the height above the sea-bottom where the velocity profile becomes zero, is taken as 0.007 m. This value is determined by the grain size of the sediments at the sea-bottom. The bottom drag coefficient shown in equation (4.18) can be derived from the logarithmic law of the wall near boundaries given in equation (4.17) and used in equation (4.16) to determine the vertical velocity.

$$C_d = \left(\frac{k_0}{\log \left(\frac{z'}{z_0} \right)} \right)^2 \quad (4.18)$$

There is no movement of water through the sea-floor as shown by equation (4.19).

$$w = -u \frac{\partial H}{\partial x} - v \frac{\partial H}{\partial y} \quad (4.19)$$

4.3.2 Transport Model

4.3.2.1 Model Equations

The transport model solves an advection-diffusion equation, given in equation (4.20), for the mass conservation of suspended sediment taking into account the bottom exchanges of deposition and erosion. The advection of particles results from the addition of the local velocity, their fall velocity under gravity (Douillet *et al.*, 2001) and diffusion due to turbulence (Harris and Wiberg, 2001).

$$\begin{aligned} & \frac{\partial C}{\partial t} + \frac{\partial(uC)}{\partial x} + \frac{\partial(vC)}{\partial y} + \frac{\partial[(w - W_s)C]}{\partial z} \\ &= \frac{\partial}{\partial x} \left(K_h \frac{\partial C}{\partial x} \right) + \frac{\partial}{\partial y} \left(K_h \frac{\partial C}{\partial y} \right) + \frac{\partial}{\partial z} \left(K_z \frac{\partial C}{\partial z} \right) \end{aligned} \quad (4.20)$$

where C is the suspended sediment concentration, W_s is the settling velocity of particles and K_h and K_z are respectively the horizontal and vertical eddy diffusivity of particles.

The settling velocity for a given type of particle is the rate at which the sediment settles in still fluid (www. wikipedia.org, 2006) and depends on the gravitational forces and on the vertical shear due to settling movement (Cancino and Neves, 1999). The settling velocity may either be measured or derived from Stokes' formula for particles with a diameter less than 100 μm (Douillet *et al.*, 2001) as shown in equation (4.21).

$$W_s = \frac{(s-1)gD_s^2}{18\mu} \quad (4.21)$$

where D_s is the representative diameter of the particles, s is the ratio of the densities of particle and water and μ is the kinematic molecular viscosity of water. Due to the absence of measurements for grain-size distribution within the water column in the Suva Lagoon, the representative diameter of particles is taken as 8 μm in the model. This value provides a settling velocity of $5.76 \times 10^{-5} \text{ m s}^{-1}$.

The horizontal eddy diffusivity of particles K_h is considered a constant ($0.002 \text{ m}^2 \text{ s}^{-1}$) in the model while the vertical eddy diffusivity of particles K_z is generally considered to be proportional to the vertical eddy viscosity N_z according to equation (4.22).

$$K_z = \frac{N_z}{\sigma_c} \quad (4.22)$$

K_z is considered as a constant between the surface and the depth where N_z is maximum. The Schmidt number σ_c assumes that the mass turbulent transfer is similar to momentum and is equal to one.

In addition to the transport of suspended sediments, the model is also able to simulate the transport of salinity from river discharge using equation (4.23).

$$\frac{\partial S}{\partial t} + \frac{\partial(uS)}{\partial x} + \frac{\partial(vS)}{\partial y} + \frac{\partial(wS)}{\partial z} = \frac{\partial}{\partial x} \left(K_h \frac{\partial S}{\partial x} \right) + \frac{\partial}{\partial y} \left(K_h \frac{\partial S}{\partial y} \right) + \frac{\partial}{\partial z} \left(K_z \frac{\partial S}{\partial z} \right) \quad (4.23)$$

where S is salinity. The variations in salinity influence the water density and in turn the velocity field (Balas and Özhan, 2002).

4.3.2.2 Boundary Conditions

A Neumann condition, which specifies the values the derivative of a solution is to take, is imposed on opened lateral boundaries in the case of an outgoing flux, as shown in equation (4.24), and a value of concentration is imposed in the case of an inflow flux.

$$\frac{\partial C}{\partial x_i} = 0 \quad x_i = x, y \quad (4.24)$$

There is no exchange of sediments (for example, dust particles in air) between the water column and the atmosphere as shown by equation (4.25).

$$\left(K_z \frac{\partial C}{\partial z} - W_s C \right)_{\text{surface}} = 0 \quad (4.25)$$

The sediment flux between the water column and the seafloor is given by equation (4.26).

$$\left(K_z \frac{\partial C}{\partial z} - W_s C \right)_{\text{bottom}} = D - E \quad (4.26)$$

where D and E are the exchange rate of particles through the process of deposition and erosion respectively in $\text{kg m}^{-2} \text{s}^{-1}$. No fluxes of salinity are considered at the bottom.

4.3.2.3 Critical Shear Stress for Deposition and Erosion

It is assumed that when bottom shear stress is smaller than a critical value, there is addition of matter to the bottom (deposition) and when the bottom shear stress is higher than the critical value, erosion occurs. Deposition and erosion balance each other between these values. The critical shear stress is determined by factors such as the chemical composition of the bed material, particle size distribution and bioturbation (Gerritsen *et al.*, 2001).

For any given fine sediment, the deposition rate is proportional to the concentration near the bottom and to the settling velocity. The deposition rate formula given in equation (4.27) is based on the assumption that deposition and erosion do not occur simultaneously, that is, a particle reaching the bottom has a probability of remaining there that varies between 0 and 1 as the bottom shear stress varies between a critical shear stress for deposition and zero (Cancino and Neves, 1999).

$$D = W_s C \left(1 - \frac{\tau}{\tau_{cd}} \right) \quad (4.27)$$

where τ is the bed shear stress, τ_{cd} is the critical shear stress for deposition and $1 - \frac{\tau}{\tau_{cd}}$ represents the probability of settling particles to be deposited. The critical shear stress for deposition depends mainly on the size of the flocks (Fernandes, 2005). Flocks are fine clay

mineral sediments which have clumped together. Larger flocks have higher probability of remaining on the sediment bed than smaller flocks and for a flock to stick to the bed, gravitational forces and the electromagnetic properties of clay must be strong enough to withstand the near bed shear stress (Fernandes, 2005).

The combined effects of tides and waves induce stresses at the seabed which simultaneously generate turbulent eddies and sediment erosion (Prandle, 2000). Erosion occurs when the bottom shear stress exceeds the critical shear stress for erosion. The erosion rate formula given in equation (4.28) assumes, like in the case for the deposition rate, that deposition and erosion do not occur simultaneously.

$$E = ke \left(\frac{\tau}{\tau_{ce}} - 1 \right) \quad (4.28)$$

where τ_{ce} is the critical shear stress for erosion, ke is the erosion rate coefficient and $\frac{\tau}{\tau_{ce}} - 1$ is the excess shear stress. The erosion rate is computed at the sediment-water interface and if this layer is eroded, erosion occurs from the underlying sediment layer, which has a higher level of compaction, therefore increasing the erosion shear stress thresholds (Fernandes, 2005).

The percentage of mud to other sediments (for example, sands, corals, coarse grained sediments) by volume at the seabed is assumed to be proportional to the erosion rate coefficient (Douillet *et al.*, 2001) according to equation (4.29).

$$ke = ke_c P_{mud} \quad (4.29)$$

where P_{mud} is the percentage of mud at the seabed and ke_c is a fitting parameter. An averaged value of ke_c is considered and applied to the entire lagoon, except over the reef bottom, which is generally not supplied with fine sediments and where erosion does not occur.

4.4 Transformed Equations and Model Grids

The model equations are solved for locations over the entire study area which is divided into a horizontal grid of 228×99 square cells and 10 vertical σ layers. In the vertical grid, the equations were expressed in terms of z so the equations have to be transformed to σ coordinates. This is because the (x, y, z) coordinate system has certain disadvantages in the vicinity of large bathymetric irregularities (Blumberg and Mellor, 1987) which can be overcome by using σ coordinates which can better resolve the bottom layer (Pietrzak *et al.*, 2002). Also, the vertical advection exchanges are minimized for barotropic flows (Martins *et al.*, 2001). The governing equations are transformed from (x, y, z, t) to (x^*, y^*, σ, t^*) coordinates using equations (4.30) and (4.31).

$$x^* = x \quad y^* = y \quad \sigma = \left(\frac{z + H}{\zeta + H} \right) \quad t^* = t \quad (4.30)$$

$$\frac{\partial}{\partial z} \rightarrow \frac{1}{D} \frac{\partial}{\partial \sigma} \quad (4.31)$$

Using these equations, the hydrodynamic and transport equations (4.5), (4.8), (4.9) and (4.20) are respectively modified to equations (4.32), (4.33), (4.34) and (4.35) to correctly represent the equations in the σ coordinates. Equation (4.36) represents the new vertical velocity.

$$\frac{\partial u D}{\partial x^*} + \frac{\partial v D}{\partial y^*} + \frac{\partial w^* D}{\partial \sigma} + \frac{\partial \zeta}{\partial t} = 0 \quad (4.32)$$

$$\begin{aligned} & \frac{\partial u}{\partial t^*} + u \frac{\partial u}{\partial x^*} + v \frac{\partial u}{\partial y^*} + w^* \frac{\partial u}{\partial \sigma} - f v - \left(\frac{1}{D^2} \right) \cdot \frac{\partial (N_z \partial u)}{\partial \sigma^2} \\ & = \frac{\partial \left(D \int_{\sigma}^1 b \cdot d\sigma \right)}{\partial x^*} - g \frac{\partial \zeta}{\partial x^*} - b \left(\frac{\partial H}{\partial x^*} - \sigma \frac{\partial D}{\partial x^*} \right) + F_x \end{aligned} \quad (4.33)$$

$$\begin{aligned} & \frac{\partial v}{\partial t^*} + u \frac{\partial v}{\partial x^*} + v \frac{\partial v}{\partial y^*} + w^* \frac{\partial v}{\partial \sigma} + fu - \left(\frac{1}{D^2} \right) \cdot \frac{\partial (N_z \partial v)}{\partial \sigma^2} \\ & = - \frac{\partial \left(D \int_{\sigma}^1 b \cdot d\sigma \right)}{\partial y^*} - g \frac{\partial \zeta}{\partial y^*} - b \left(\frac{\partial H}{\partial y^*} - \sigma \frac{\partial D}{\partial y^*} \right) + F_y \end{aligned} \quad (4.34)$$

$$\frac{\partial DC}{\partial t^*} + \frac{\partial u DC}{\partial x^*} + \frac{\partial v DC}{\partial y^*} + \frac{\partial w^* DC}{\partial \sigma} = K_x \frac{\partial^2 DC}{\partial x^2} + K_y \frac{\partial^2 DC}{\partial y^2} + \frac{1}{D} \frac{\partial (K_z \partial C)}{\partial \sigma^2} \quad (4.35)$$

$$w^* = \frac{w}{D} + \frac{u}{D} \left(-\sigma \frac{\partial D}{\partial x^*} + \frac{\partial H}{\partial x^*} \right) + \frac{v}{D} \left(-\sigma \frac{\partial D}{\partial y^*} + \frac{\partial H}{\partial y^*} \right) - \frac{\sigma}{D} \frac{\partial \zeta}{\partial t^*} \quad (4.36)$$

The surface boundary conditions are changed from equations (4.11) and (4.13) to equation (4.37) and equation (4.25) to equation (4.38).

$$\tau_{sx} = \rho_o \frac{N_z}{D} \frac{\partial u}{\partial \sigma} \quad \tau_{sy} = \rho_o \frac{N_z}{D} \frac{\partial v}{\partial \sigma} \quad w^* = 0 \quad (4.37)$$

$$\left(\frac{K_z}{D} \frac{\partial C}{\partial \sigma} - W_s C \right)_{surface} = 0 \quad (4.38)$$

The bottom boundary conditions are changed from equations (4.16) and (4.19) to equation (4.39) and equation (4.26) to equation (4.40).

$$\rho_o \frac{N_z}{D} \frac{\partial u}{\partial \sigma} = C_d \sqrt{u_b^2 + v_b^2} \cdot u_b \quad \rho_o \frac{N_z}{D} \frac{\partial v}{\partial \sigma} = C_d \sqrt{u_b^2 + v_b^2} \cdot v_b \quad w^* = 0 \quad (4.39)$$

$$\left(\frac{K_z}{D} \frac{\partial C}{\partial \sigma} - W_s C \right)_{bottom} = D - E \quad (4.40)$$

The Arakawa C-grid is modified to include the water depths H_x and H_y which allows for automatic treatment of wetting and drying. The staggered arrangement uses u at half-grid points to the east and west of the points where H and ζ are defined and v at half-grid

points to the north and south of H and ζ points, as shown in Fig. 4.1. This arrangement allows the pressure gradient to be determined as a function of the free sea-surface elevation. The quantity σ refers to the depths at which the transport quantities (salinity and SSC and the vertical velocity w) are located. The constant horizontal grid spacing are Δx and Δy and $\Delta\sigma$ is the vertical increment which varies in thickness to accommodate more resolution near the surface and bottom.

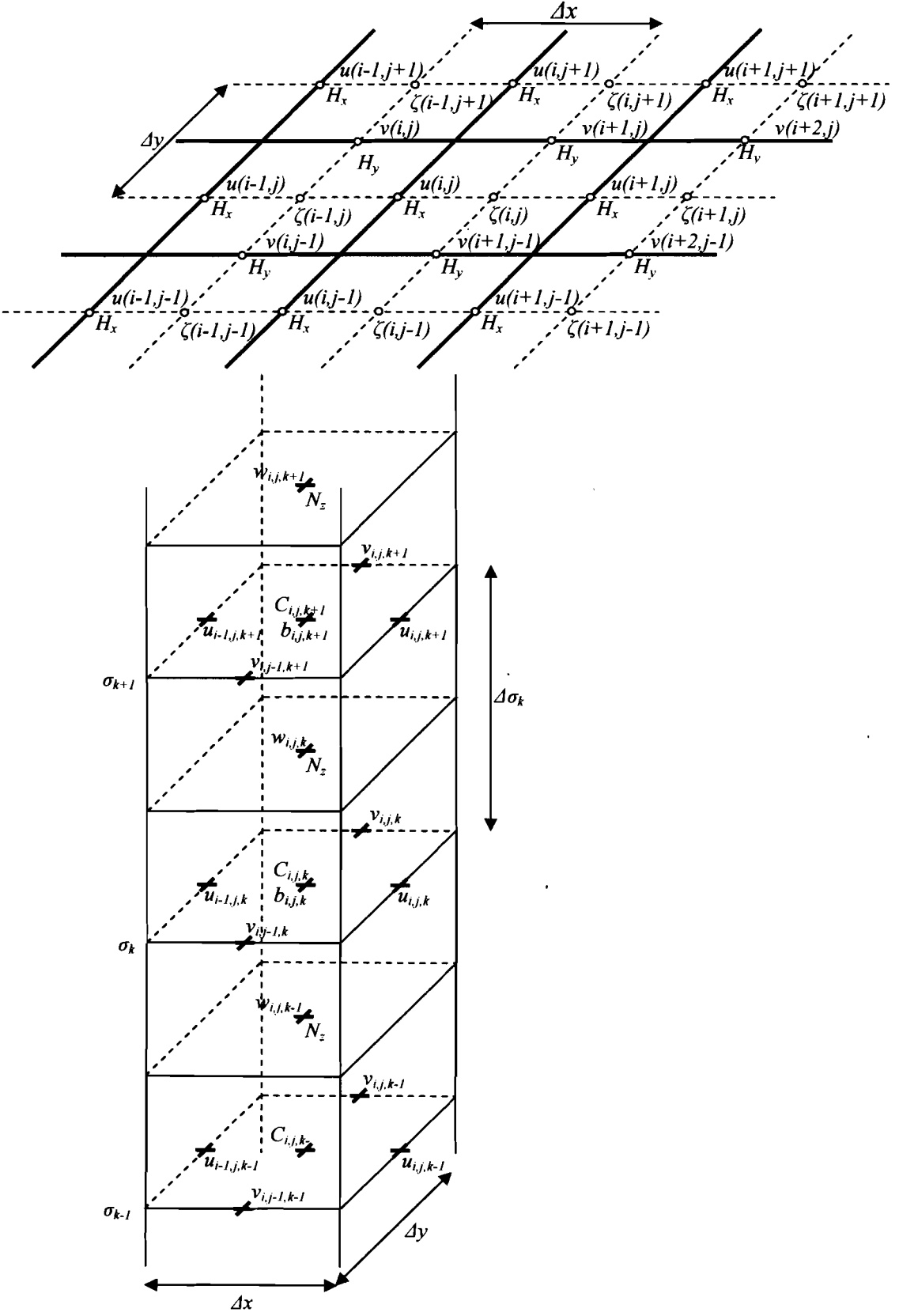


Figure 4.1 Modified Arakawa C-grid.

4.5 Model Bathymetry

The model incorporates realistic coastline and bottom topography. The depth data used in the model were obtained by digitizing the British Admiralty charts and from surveys by the Fiji Hydrographic Services. The depth at the corresponding grid points were determined by an interpolation method and input into the model using a program developed by UR CAMELIA and is shown in Fig. 4.2.

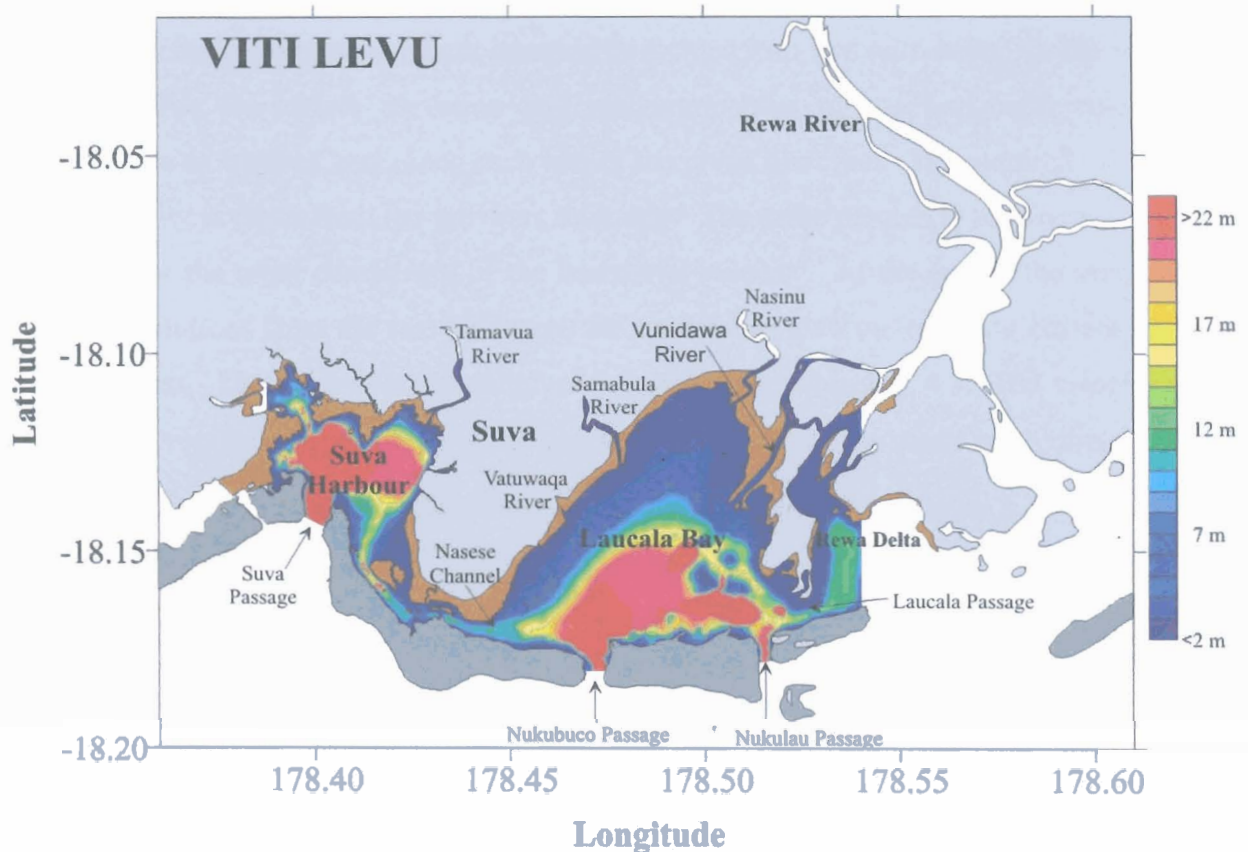


Figure 4.2 Bathymetry of the Suva Lagoon.

4.6 Numerical Discretization

The governing equations form a set of simultaneous partial differential equations which cannot be solved using known analytical methods (Blumberg and Mellor, 1987). The governing equations together with their boundary conditions require numeric computational methods using discretized equations on the Arakawa C-grid. For computational efficiency, a mode splitting technique in time and an implicit numerical scheme in the vertical direction has been adopted. The ADI method is used for time discretization and the finite difference

method is used for space discretization. All governing equations are solved using the finite difference scheme at each of the grid points for each time step until termination of the simulation.

4.6.1 Temporal Discretization

The temporal discretization is carried out by means of the ADI algorithm. The ADI algorithm computes alternatively one component of horizontal velocity implicitly while the other is calculated explicitly. Each iteration is divided into two half-steps. In the first half-step, the free sea-surface elevation and one component of the horizontal velocity are computed in an implicit way along each line of the given direction. The required value of the other velocity is taken from the previous time step. The same process is followed in the next half-step for the other component of the horizontal velocity. At the end of the second half-step, the solutions from the two half-steps are updated to give the resultant current velocity for the points. The order of computation of velocity is shown in Fig. 4.3. The velocity in the west-east direction is represented by u_1 and u_3 , the velocity in the south-north direction is v_2 and v_4 while the sea-surface elevations are ζ_3 , ζ_4 , ζ_1 and ζ_2 at times $t = 1, 2, 3$ and 4 respectively.

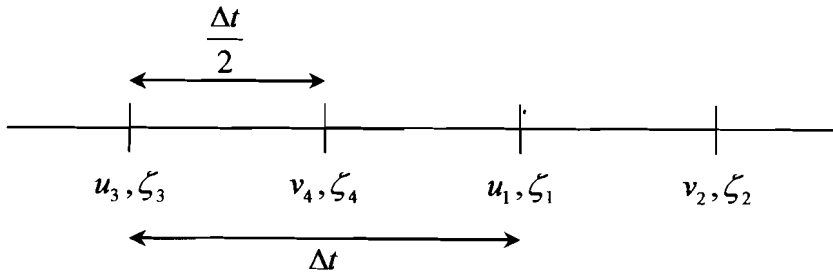


Figure 4.3 ADI algorithm.

The salinity and SSC are also calculated at the end of the second half-step while the vertical velocity is computed from the continuity equation. To incorporate the temporal discretization into the model, equations (4.33), (4.34) and (4.36), which represent the hydrodynamic equations in σ coordinates, have to be transformed respectively to equations (4.41), (4.42) and (4.43) according to the ADI algorithm.

$$\begin{aligned}
 & \frac{u_3 - u_1}{\Delta t} + u_1 \frac{\partial u_1}{\partial x} + v_2 \frac{\partial u_1}{\partial y} + w^* \frac{\partial u_1}{\partial \sigma} - f v_2 - \frac{1}{D_2^2} \frac{\partial \left(N_z \frac{\partial (u_1 + u_3)}{2} \right)}{\partial \sigma^2} \\
 & = - \frac{\partial \left(D_2 \int_{\sigma}^1 b d\sigma \right)}{\partial x} - g \frac{\partial \left(\frac{\zeta_1 + \zeta_3}{2} \right)}{\partial x} - b \left(\frac{\partial H}{\partial x} - \sigma \frac{\partial D_2}{\partial x} \right) + F_x
 \end{aligned} \tag{4.41}$$

$$\begin{aligned}
 & \frac{v_4 - v_2}{\Delta t} + u_3 \frac{\partial v_2}{\partial x} + v_2 \frac{\partial v_2}{\partial y} + w^* \frac{\partial v_2}{\partial \sigma} + f u_3 - \frac{1}{D_3^2} \frac{\partial \left(N_z \frac{\partial (v_2 + v_4)}{2} \right)}{\partial \sigma^2} \\
 & = - \frac{\partial \left(D_3 \int_{\sigma}^1 b d\sigma \right)}{\partial y} - g \frac{\partial \left(\frac{\zeta_2 + \zeta_4}{2} \right)}{\partial y} - b \left(\frac{\partial H}{\partial y} - \sigma \frac{\partial D_3}{\partial y} \right) + F_y
 \end{aligned} \tag{4.42}$$

$$w^* = - \frac{1}{D} \sigma \frac{\partial (\zeta_3 - \zeta_2)}{\Delta t / 2} - \frac{1}{D} \int_0^{\sigma} \left(\frac{\partial D u}{\partial x} + \frac{\partial D v}{\partial y} \right) d\sigma \tag{4.43}$$

The boundary conditions at the free sea-surface and the sea-bottom also need to be changed from equations (4.37) and (4.39) to equations (4.44) and (4.45) respectively.

$$\rho_0 \frac{N_z}{D_2} \frac{\partial u_3}{\partial \sigma} = \tau_{x3} \quad \rho_0 \frac{N_z}{D_3} \frac{\partial v_4}{\partial \sigma} = \tau_{y4} \quad w^* = 0 \tag{4.44}$$

$$\begin{aligned}
 \frac{N_z}{D_2} \frac{\partial \left(\frac{u_1 + u_3}{2} \right)}{\partial \sigma} &= \rho_0 C_d \sqrt{u_{b1}^2 + v_{b2}^2} \left(\frac{u_{b1} + u_{b3}}{2} \right) \\
 \frac{N_z}{D_2} \frac{\partial \left(\frac{v_1 + v_4}{2} \right)}{\partial \sigma} &= \rho_0 C_d \sqrt{u_{b3}^2 + v_{b4}^2} \left(\frac{v_{b2} + v_{b4}}{2} \right) \quad w^* = 0
 \end{aligned} \tag{4.45}$$

To determine the components of velocity at the spatially separated grid points as a function of time, equations (4.41), (4.42) and (4.43) now need to be discretized simultaneously in space.

4.6.2 Spatial Discretization

The spatial discretization is carried out by using the finite difference approximations. New values at a new time are calculated from values at a previous time by using the spatial gradients of quantities. This can be done by using backward difference, forward difference or centered difference approximations using Taylor series expansions. The backward difference and forward difference approximations are first order accurate while the centered difference method is second order accurate. This means that the largest term of the error in the gradient in either the backward or forward approximations, for example, $\frac{\partial u}{\partial x}$ depends on Δx to the first power while the largest error term in the centered difference approximation depends on Δx to the second power. Therefore the error inherited in using the centered difference approximation is smaller than the error inherited when using the backward difference or forward difference approximations. The more accurate approximation of $\frac{\partial u}{\partial x}$ using Taylor series expansion around an arbitrary point x_j is the centered difference approximation (Pond and Pickard, 1983) which is given in equation (4.46).

$$\frac{(u_{j+1} - u_{j-1}))}{2\Delta x} = \frac{\partial u}{\partial x} + \frac{1}{6} \frac{\partial^3 u}{\partial x^3} (\Delta x)^2 + O(\Delta x)^4 \quad (4.46)$$

where derivatives are calculated at x_j and u_{j+1} is the value at x_{j+1} , u_{j-1} is the value at x_{j-1} , Δx is the grid spacing in the x -direction and O is a finite number (Pond and Pickard, 1983). The centered difference approximation is used to transform equation (4.41) to equation (4.47). Similarly, equations (4.42) and (4.43) are approximated using the centered difference approximation.

$$\begin{aligned}
 & \frac{u_{3,i,j,k} - u_{1,i,j,k}}{\Delta t} + u_{1,i,j,k} \left(\frac{u_{1,i+1,k} - u_{1,i-1,k}}{2\Delta x} \right) \\
 & + \left(\frac{v_{2,i,j,k} + v_{2,i+1,j,k} + v_{2,i,j-1,k} + v_{2,i+1,j-1,k}}{4} \right) \left(\frac{u_{1,i,j+1,k} - u_{1,i,j-1,k}}{2\Delta x} \right) \\
 & + \frac{\left(\left(\frac{w_{i+1,j,k-1} + w_{i,j,k-1}}{2} \right) \left(\frac{u_{1,i,j,k} - u_{1,i,j,k-1}}{\Delta \sigma_{k-1}} \right) \right) \Delta \sigma_k + \left(\left(\frac{w_{i+1,j,k} + w_{i,j,k}}{2} \right) \left(\frac{u_{1,i,j,k+1} - u_{1,i,j,k}}{\Delta \sigma_k} \right) \right) \Delta \sigma_{k-1}}{\Delta \sigma_{k-1} + \Delta \sigma_k} \\
 & - f \left(\frac{v_{2,i,j,k} + v_{2,i+1,j,k} + v_{2,i,j-1,k} + v_{2,i+1,j-1,k}}{4} \right) - \frac{1}{2} \frac{1}{\left(H_{x,i,j} + \left(\frac{\zeta_{2,i,j} + \zeta_{2,i+1,j}}{2} \right) \right)^2} \\
 & \times \frac{\left(\left(\frac{N_{z,i,j,k} + N_{z,i+1,j,k}}{2} \right) \left(\frac{u_{1,i,j,k+1} - u_{1,i,j,k}}{\Delta \sigma_k} \right) \right) - \left(\left(\frac{N_{z,i,j,k-1} + N_{z,i+1,j,k-1}}{2} \right) \left(\frac{u_{1,i,j,k} - u_{1,i,j,k-1}}{\Delta \sigma_{k-1}} \right) \right)}{\frac{\Delta \sigma_{k-1} + \Delta \sigma_k}{2}} \\
 & - \frac{1}{2} \frac{1}{\left(H_{x,i,j} + \left(\frac{\zeta_{2,i,j} + \zeta_{2,i+1,j}}{2} \right) \right)^2} \\
 & \times \frac{\left(\left(\frac{N_{z,i,j,k} + N_{z,i+1,j,k}}{2} \right) \left(\frac{u_{3,i,j,k+1}^* - u_{3,i,j,k}^*}{\Delta \sigma_k} \right) \right) - \left(\left(\frac{N_{z,i,j,k-1} + N_{z,i+1,j,k-1}}{2} \right) \left(\frac{u_{3,i,j,k}^* - u_{3,i,j,k-1}^*}{\Delta \sigma_{k-1}} \right) \right)}{\frac{\Delta \sigma_{k-1} + \Delta \sigma_k}{2}} \\
 & = \sum_{m=k}^{k_{\max}-1} \left[\left(\frac{\left((H_{moy,i+1,j} + \zeta_{2,i+1,j}) b_{i+1,j,m} - (H_{moy,i,j} + \zeta_{2,i,j}) b_{i,j,m} \right)}{\Delta x} \right) + \left(\frac{\left((H_{moy,i+1,j} + \zeta_{2,i+1,j}) b_{i+1,j,m+1} - (H_{moy,i,j} + \zeta_{2,i,j}) b_{i,j,m+1} \right)}{\Delta x} \right) \right] \frac{\Delta \sigma_m}{2} \\
 & + \left(\frac{\left((H_{moy,i+1,j} + \zeta_{2,i+1,j}) b_{i+1,j,k_{\max}} - (H_{moy,i,j} + \zeta_{2,i,j}) b_{i,j,k_{\max}} \right)}{\Delta x} \right) (1 - \sigma_{k_{\max}}) \\
 & - \frac{1}{2} g \left(\frac{\zeta_{1,i+1,j} - \zeta_{1,i,j}}{\Delta x} \right) - \frac{1}{2} g \left(\frac{\zeta_{3,i+1,j}^* - \zeta_{3,i,j}^*}{\Delta x} \right) - \left(\frac{b_{i,j,k} + b_{i+1,j,k}}{2} \right) \\
 & \times \left(\left(\frac{H_{moy,i+1,j} - H_{moy,i,j}}{\Delta x} \right) - \sigma_k \left(\frac{H_{moy,i+1,j} + \zeta_{2,i+1,j} - H_{moy,i,j} - \zeta_{2,i,j}}{\Delta x} \right) \right) \\
 & + N_h \left(\frac{u_{1,i+1,k} - 2u_{1,i,j,k} + u_{1,i-1,j,k}}{\Delta x \Delta x} \right) + N_h \left(\frac{u_{1,i,j+1,k} - 2u_{1,i,j,k} + u_{1,i,j-1,k}}{\Delta x \Delta x} \right)
 \end{aligned} \tag{4.47}$$

The solution of equation (4.47) can give the horizontal velocity in the east-west direction at a particular time at any position on the modified Arakawa C-grid. To follow time evolution in the model, the temporal derivatives in the equations need to be approximated. Again a second order accurate approximation is used. The time step Δt is critical since if it is exceeded, there results an explosive growth of small errors inevitably present in the numerical operations (Pond and Pickard, 1983) preventing convergence of a stable solution. To control any instabilities arising during the execution of the model, the time step is continuously compared with the critical time step given in equation (4.48).

$$\Delta t < \frac{2g(\Delta x)^2}{K_r^2 (H + \zeta)_{\max} |u_{\max}|} \quad (4.48)$$

where K_r is the Strikler coefficient equal to $33 \text{ m}^{-1/3} \text{ s}^{-1}$ and $(H + \zeta)_{\max}$ is the maximum depth. The time step used in the model is 25 s. The method of LU factorization is used to solve the algebraic equations that are obtained after discretization. The advantage of using this method is that it is faster than trying to solve using the Gauss elimination method (Rao, 2005).

4.7 Model Validation and Implementation

The main objective of this model study is to simulate suspended sediment transport by mass as realistically as possible. The model computes the hydrodynamic circulation and transport of salinity and SSC based on the model equations and input data. The input data is first filtered for consistency then fed into the model. These data includes wind speed, tidal influence, river runoff, bathymetry and the percentage of fine sediments at the bottom of the lagoon. The wind data is recorded at regular intervals of 10 minutes at a height of 10 m above mean sea-level and the M_2 , S_2 , K_1 and O_1 constituents of tide are used in the model. The river runoff is calculated using equation (3.1) in Chapter 3. The output from the model is written to a file which is then passed to a plotting program for interpretation. The outputs include current velocity, sea-surface elevation, salinity and suspended sediment concentration (SSC – mass of suspended sediments per unit volume of water) at the grid points at discrete time steps.

Verification of the model is achieved through comparison of model output with the *in situ* field data. Model parameters are modified to accommodate any discrepancy arising with the field data. A good verification is achieved when the model output and the field data compare well with each other.

4.8 Conclusions

The MARS3D model has been validated for the water circulation in the southwest lagoon of New Caledonia (Douillet, 1998; Douillet *et al.* 2001; Ouillon *et al.*, 2004; Jouon *et al.*, 2006). An improved version of this model is applied to the Suva Lagoon in this study. This model is able to simulate the transport of fine suspended sediments due to different tidal and wind forcings and river runoffs. The model solves the governing equations using the hydrostatic and Boussinesq approximations. Boundary conditions are imposed at the sea-surface, sea-bottom and along the coastline. The ADI method is used for time discretization and the finite difference method is used for space discretization. A modified Arakawa C-grid is used in the study.

The critical shear stress for deposition (τ_{cd}) and erosion (τ_{ce}) and the erosion rate coefficient (ke) need to be determined in order to verify the model. This is done by comparing the model predicted particle concentration at the bottom with the percentage of mud found in the lagoon for different combinations of τ_{cd} , τ_{ce} and ke : Once these parameters are found, they can be used to predict the distribution of fine suspended sediments in the lagoon. The model predicted results are then compared with the *in situ* data collected and good agreement between the two acts as verification of the model.

The following chapter presents the model verification by determining τ_{cd} , τ_{ce} and ke and using these parameters to predict the water properties in the lagoon. The model predicted results will be compared with the field data to verify the model before running it for the transportation of fine suspended sediments in the Suva Lagoon.



Chapter 5

Model Results and Discussion

5.1 Introduction

In modelling the transport of fine suspended sediments, the values for critical shear stresses for deposition (τ_{cd}) and erosion (τ_{ce}) and the erosion rate coefficient (ke) need to be known. These parameters can be measured directly under controlled flow conditions (Piedra-Cueva *et al.*, 1997) or be chosen so as to provide the best agreement between model results and observations from field data. In this project, the latter case is used. Once these parameters are estimated, they can be used in the model to predict suspended sediment concentration (SSC) and sediment transport in the lagoon. The model results are compared with field data and agreement between the two sets of results will act as verification of the model. After verification, the model can be used to determine the effect of:

- model resolution on salinity distribution;
- the presence of the sandbank in the Rewa Delta on surface salinity distribution; and
- different river discharges on the transport of fine suspended sediments in the lagoon.

The 3D hydrodynamic-sediment transport coupled model used in this project (and discussed comprehensively in Chapter 4), uses the combined effect of the tides, winds and river runoff to simulate the salinity and turbidity distribution in the lagoon. In this chapter, the model will be validated and implemented for the Suva Lagoon.

5.2 Model Parameters

5.2.1 Determination of the Critical Shear Stress for Deposition and Erosion

In the Suva Lagoon, the critical shear stresses for deposition and erosion and the erosion rate coefficient are unknown. Le Normant (1995) and Schaaf (1999) quote the estimates of critical shear stress from several papers ranging from 0.002 N m^{-2} to 0.7 N m^{-2} for τ_{cd} and

from 0.03 N m^{-2} to 1.14 N m^{-2} for τ_{ce} . These ranges are very wide and they generally refer to muddy estuaries (Douillet *et al.*, 2001). In the absence of measurements of these parameters, it is appropriate to assume that τ_{cd} and τ_{ce} are equal to a value called the critical shear stress τ_{cr} . This means that there is always either net deposition or net erosion taking place over a given area. It is also assumed that the net flux over the lagoon seabed can be considered as zero over a tidal scale with mean conditions of wind and tide and no river input. This assumption has two implications:

- the values of the parameters τ_{cr} and ke should provide a balance between deposition and erosion summed up over a tidal cycle under mean tide and wind conditions; and
- the areas of net deposition obtained in simulations using the above parameters should be in best agreement with the areas where fine sediments are dominant at the seabed (Douillet *et al.*, 2001). For that comparison, the distribution of fine sediments in the Suva Lagoon, as measured by Fernandez *et al.* (2006) and shown in Fig. 5.1, will be used.

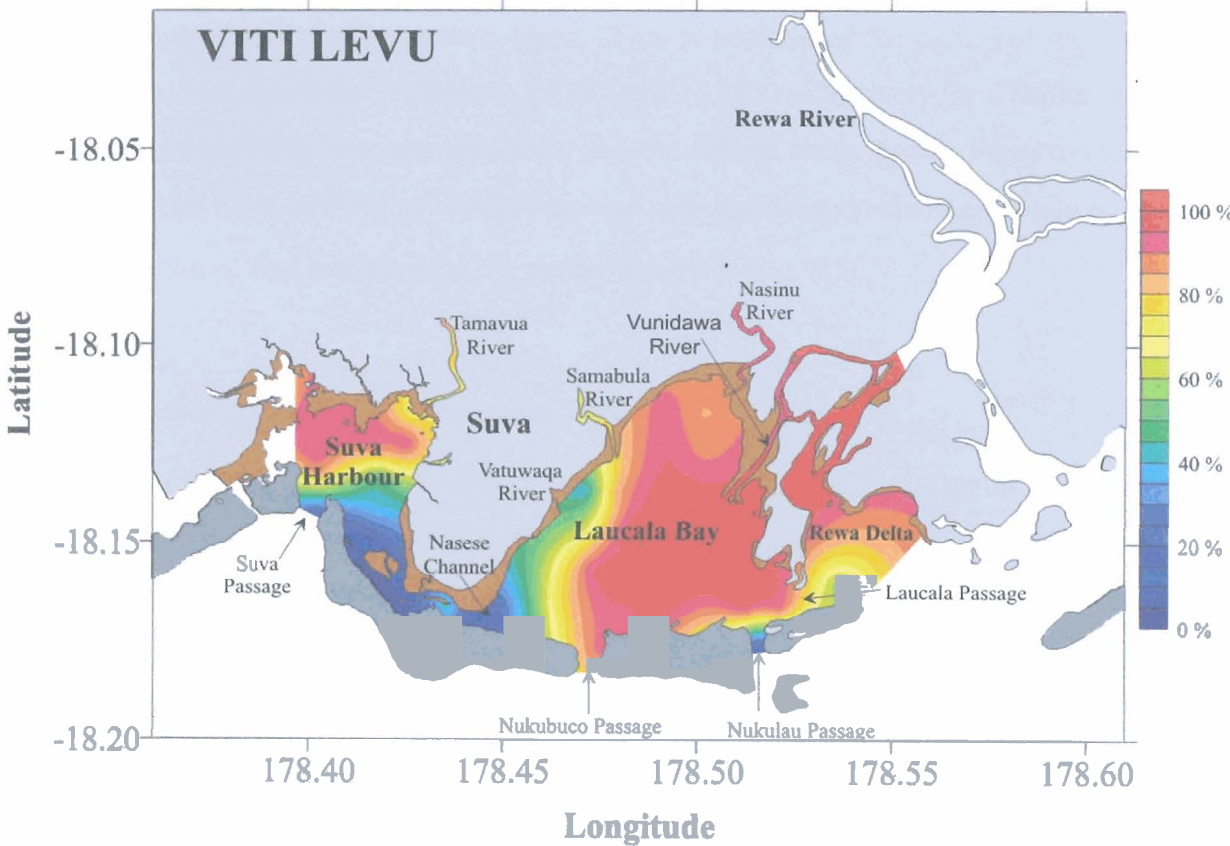


Figure 5.1 The percentage distribution of fine sediments at the bottom in the Suva Lagoon.

Figure 5.1 shows that the eastern half of Laucala Bay contains more than 80% of fine sediments. This demonstrates the tremendous influence of the Rewa River on sediment deposition in the Suva Lagoon. A high percentage of fine sediments can also be seen in the western half of Suva Harbour. The lowest percentage of fine sediments is found through the Nasese Channel.

The M_2 constituent is the major constituent of the tide, thus, only the M_2 constituent is used in this part of the project. The M_2 constituent was initially combined with a mean wind speed of 6 m s^{-1} and computations were performed for different values of τ_{cr} keeping ke constant. To estimate the value of ke , a fitting parameter ke_c was used according to equation (4.29) in Chapter 4. Initial empirical test runs were performed with $\tau_{cr} = 0.017 \text{ N m}^{-2}$ and ke_c varying between $4.0 \times 10^{-5} \text{ g m}^{-2} \text{ s}^{-1}$ and $7.0 \times 10^{-5} \text{ g m}^{-2} \text{ s}^{-1}$. Once ke_c was tentatively determined, a sensitivity study of the model was performed with τ_{cr} varying around 0.017 N m^{-2} .

It was found that whatever value of ke was used, increasing values of τ_{cr} lead to greater deposition zones and smaller erosion areas. This is because of the nature of the deposition and erosion flux formulae [equations (4.27) and (4.28) respectively in Chapter 4], which defines the relationship between the fluxes and the critical shear stress. From model runs, it was found that $\tau_{cr} = 0.020 \text{ N m}^{-2}$ lead to erosion and deposition areas in good agreement with the distribution of fine sediments at the seabed shown in Fig. 5.1.

5.2.2 Determination of the Erosion Rate Coefficient

The value of the erosion rate coefficient ke depends essentially on the nature and porosity of the deposit and can be estimated for each area (Douillet, *et al.* 2001) by changing the model parameters. The influence of the coefficient ke_c was calculated in the presence of the tide and different wind conditions for values in the range of $4.0 \times 10^{-5} \text{ g m}^{-2} \text{ s}^{-1}$ to $7.0 \times 10^{-5} \text{ g m}^{-2} \text{ s}^{-1}$. For comparison purposes, the computed deposition and erosion fluxes (D_f and E_f respectively) were summed up for the whole lagoon over one tidal cycle (12.42 h). These fluxes are expressed in tonnes in Tables 1 – 8 in the Appendix for τ_{cr} ranging between 0.010 N m^{-2} and 0.025 N m^{-2} .

It can be seen from Tables 1 – 8 (in the Appendix) that several combinations of τ_{cr} and ke_c are possible. For deposition and erosion summed up for the whole lagoon to be of a similar value for mean wind and tide conditions requires $ke_c = 6.5 \times 10^{-5} \text{ g m}^{-2} \text{ s}^{-1}$ when $\tau_{cr} = 0.020 \text{ N m}^{-2}$. It can be seen from Table 7 (in the Appendix) that for this same value of ke_c , in the absence of wind, sediments settle whereas under combined tide and wind of 8 m s^{-1} , sediments are eroded. It should be noted that the same equilibrium between deposition and erosion are obtained with other different combinations of τ_{cr} and ke_c . These combinations, together with the minimum percentage difference between the deposition and erosion fluxes are summarized in Table 5.1. The number of possibilities can only be reduced when at least one of these parameters is measured.

Table 5.1 Summary of the minimum percentage difference between deposition and erosion fluxes for mean wind (6 ms^{-1}) and tide (M_2) conditions for several combinations of the critical shear stress τ_{cr} and coefficient of erosion ke_c .

ke_c ($\text{g m}^{-2} \text{ s}^{-1}$)	Percentage Difference							
	$\tau_{cr} \text{ (N m}^{-2}\text{)}$							
	0.010	0.015	0.016	0.017	0.018	0.019	0.020	0.025
4.0×10^{-5}	52	6	4	16	28	41	54	131
4.5×10^{-5}	57	16	6	4	15	26	38	106
5.0×10^{-5}	60	24	15	6	4	14	25	87
5.5×10^{-5}	63	30	22	14	5	5	14	71
6.0×10^{-5}	66	35	28	20	12	3	6	57
6.5×10^{-5}	68	40	33	26	18	10	2	46
7.0×10^{-5}	70	43	37	30	23	16	8	36

The best possible combination between τ_{cr} and ke_c is the one that gives the minimum difference between the deposition and erosion fluxes. It can be deduced from Table 5.1 that the best combination is when the critical shear stress $\tau_{cr} = 0.020 \text{ N m}^{-2}$ and the erosion rate coefficient $ke_c = 6.5 \times 10^{-5} \text{ g m}^{-2} \text{ s}^{-1}$. This combination gives a minimum percentage difference between the deposition and erosion fluxes of 2%.

5.2.3 Sensitivity of the Sediment Fluxes to the Critical Shear Stress

The influence of the critical shear stress for deposition and erosion under several wind and tide conditions were considered. Table 5.2 shows the deposition and erosion fluxes calculated for different values of the critical shear stress τ_{cr} ranging between 0.010 N m^{-2} and 0.025 N m^{-2} for $ke_c = 6.5 \times 10^{-5} \text{ g m}^{-2} \text{ s}^{-1}$.

Table 5.2 Deposition and erosion fluxes (D_f and E_f respectively) calculated by the model for the whole lagoon with different values of the critical shear stress and with $ke_c = 6.5 \times 10^{-5} \text{ g m}^{-2} \text{ s}^{-1}$. D_f and E_f are expressed in tonnes per tidal cycle.

τ_{cr} (N m^{-2})	Wind 6 m s ⁻¹	Wind 8 m s ⁻¹	Tide	Tide + Wind 6 m s ⁻¹	Tide + Wind 8 m s ⁻¹
0.010	$D_f = 1113.3$ $E_f = 3816.6$	$D_f = 2890.1$ $E_f = 42023.1$	$D_f = 1367.3$ $E_f = 1421.7$	$D_f = 1033.3$ $E_f = 3247.9$	$D_f = 807.3$ $E_f = 5756.1$
0.015	$D_f = 1109.1$ $E_f = 1069.8$	$D_f = 2697.2$ $E_f = 27000.6$	$D_f = 1414.7$ $E_f = 776.0$	$D_f = 1122.8$ $E_f = 1857.4$	$D_f = 913.5$ $E_f = 3402.4$
0.016	$D_f = 1129.7$ $E_f = 963.8$	$D_f = 2721.0$ $E_f = 25714.8$	$D_f = 1421.9$ $E_f = 699.5$	$D_f = 1136.9$ $E_f = 1691.2$	$D_f = 930.9$ $E_f = 3117.0$
0.017	$D_f = 1149.2$ $E_f = 873.4$	$D_f = 2698.4$ $E_f = 24124.6$	$D_f = 1428.7$ $E_f = 633.3$	$D_f = 1150.1$ $E_f = 1546.5$	$D_f = 947.3$ $E_f = 867.6$
0.018	$D_f = 1167.2$ $E_f = 795.0$	$D_f = 2677.1$ $E_f = 22713.1$	$D_f = 1435.1$ $E_f = 575.5$	$D_f = 1162.6$ $E_f = 1419.7$	$D_f = 962.8$ $E_f = 2647.9$
0.019	$D_f = 1184.1$ $E_f = 727.0$	$D_f = 2656.9$ $E_f = 21451.9$	$D_f = 1441.1$ $E_f = 524.7$	$D_f = 1174.4$ $E_f = 1307.8$	$D_f = 977.5$ $E_f = 2453.3$
0.020	$D_f = 1200.2$ $E_f = 667.9$	$D_f = 2637.6$ $E_f = 20318.5$	$D_f = 1446.9$ $E_f = 479.9$	$D_f = 1185.6$ $E_f = 1208.5$	$D_f = 991.5$ $E_f = 2279.9$
0.025	$D_f = 1273.8$ $E_f = 1064.0$	$D_f = 2552.1$ $E_f = 16028.4$	$D_f = 1472.2$ $E_f = 319.2$	$D_f = 1234.4$ $E_f = 845.7$	$D_f = 1052.3$ $E_f = 1638.9$

It can be seen from Table 5.2 that for the tide (M_2 constituent only) alone, erosion is weak when τ_{cr} is greater than 0.011 N m^{-2} (through extrapolation) and deposition, which depends on the initial concentration field, is strong. This means that the area over which τ is lower than τ_{cr} is greater, thus more deposition. With wind alone, deposition is greater than erosion when τ_{cr} is greater than 0.015 N m^{-2} for a wind of 6 m s^{-1} . Erosion is very strong for a wind of 8 m s^{-1} and the critical shear stress needs to be a lot higher for the deposition and erosion to be of the same order of magnitude. Considering a combination of tide and wind of 8 m s^{-1} , erosion increases rapidly when τ_{cr} decreases. This is because the currents due to the combined forcings generates stronger bed shear stresses and the area where τ is greater than τ_{cr} is greater.

5.2.4 Discussion of Deposition and Erosion for Different Forcings

Using the values of the critical shear stress ($\tau_{cr} = 0.020 \text{ N m}^{-2}$) and erosion rate coefficient ($ke_c = 6.5 \times 10^{-5} \text{ g m}^{-2} \text{ s}^{-1}$) obtained above, the distribution of the deposition and erosion areas calculated for different forcings can now be compared with the percentage distribution of fine sediments at the bottom from Fig. 5.1. Comparing the deposition and erosion areas for each process, and those obtained with the tide and wind combined, should be helpful in identifying the respective role of each process. Figure 5.2 shows the deposition and erosion fluxes cumulated during one tidal cycle for the different forcings.

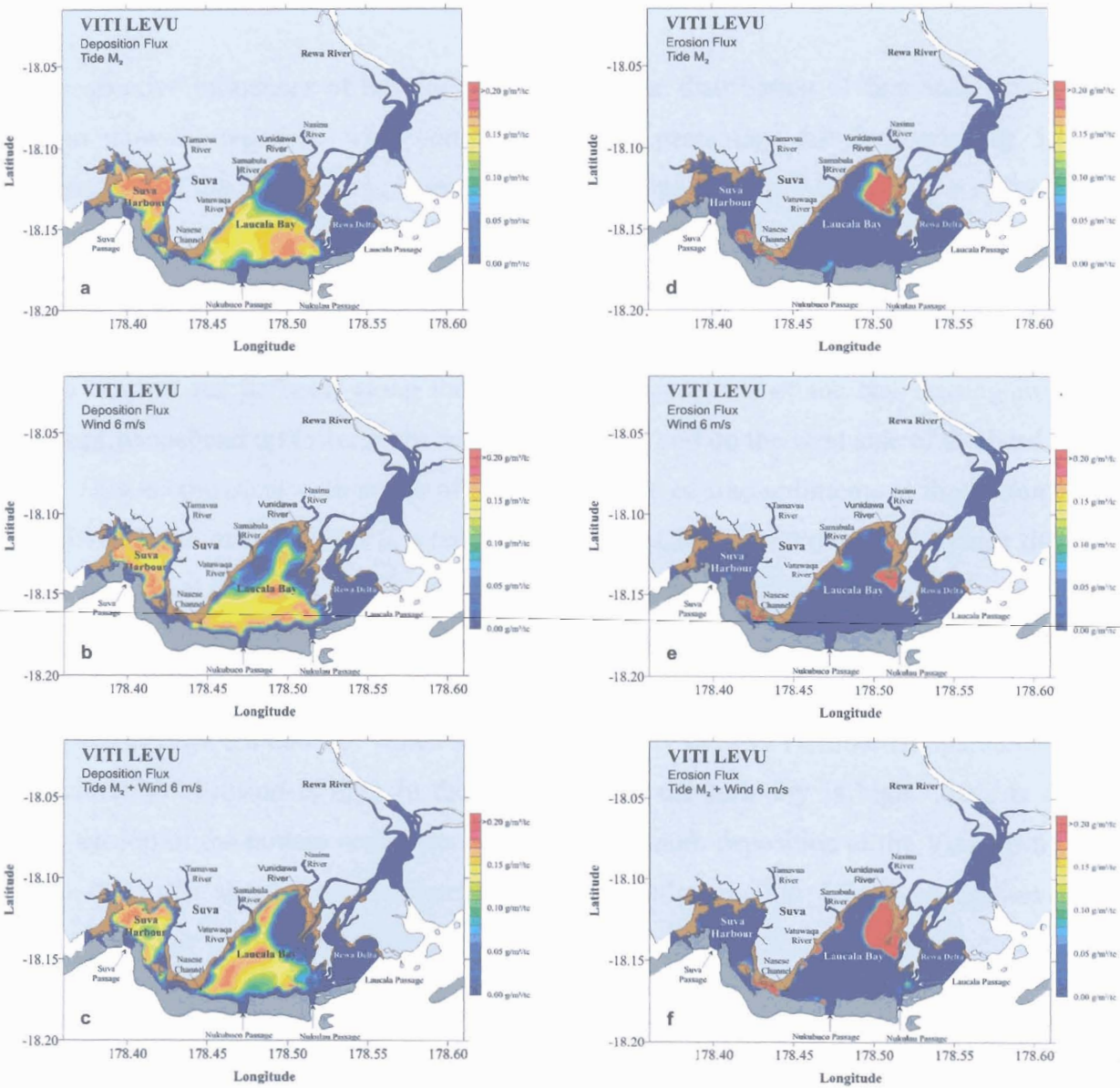


Figure 5.2 Model distribution of the deposition flux (left column) and erosion flux (right column) cumulated over a tidal cycle for different forcings (a and d) tide, (b and e) wind 6 m s^{-1} and (c and f) tide and wind 6 m s^{-1} .

For the tide alone (Fig. 5.2a), deposition is weak at the head of Laucala Bay, through Nasese Channel and at the Suva, Nukubuco and Nukulau Passages. Maximum deposition can be seen at the head of Suva Harbour gradually decreasing to a minimum near the Suva Passage. Maximum deposition can also be seen off the Nasigasiga Reef, decreasing towards the middle of the bay. Along the coast on the west side of the bay, the concentration of fine sediments found at the bottom is high. For the wind alone (Fig. 5.2b), deposition is weak near the Vunidawa River mouth, at the head of the bay extending along the coast towards and through the Nasese Channel. Maximum deposition can be seen off the Nasigasiga, Nukubuco, Sosoikula, Vunivau and Nukusaga Reefs, near the middle of the bay and at the head of the harbour.

The respective influences of the tide and wind on the distribution of fine sediments at the bottom show discrepancies when compared with the percentage distribution in Fig. 5.1. A combination of the two forcings is essential to determine the distribution of fine sediments at the bottom.

Combining the tide with a wind of 6 m s^{-1} (Fig. 5.2c), maximum deposition can be observed at the head of the harbour, along the coast on the west side of the bay starting from the Nasese Channel end up towards the middle of the bay and on the west side of the head of the bay. This is consistent with zones of high percentage of fine sediments at the bottom from Fig. 5.1. Minimum deposition is seen through Nasese Channel, on the east side near the head of the bay and at the Vunidawa River mouth. The distribution of the deposition flux resulting from the combination of tide and wind appears to be in good agreement with zones of high percentage of fine sediments at the bottom seen in Fig. 5.1. This is consistent with field data presented in Figs. 3.8 and 3.9, which show low turbidity in Suva Harbour compared to that in Laucala Bay. Erosion is high in the bay therefore the turbidity is high. This is due to resuspension of the bottom sediments. There is minimum deposition at the Vunidawa River mouth due to the absence of river discharge in the simulations (Fig. 5.2a, b, c). However, the high percentage of fine sediments found at the bottom at the Vunidawa River mouth (Fig. 5.1) is due to the suspended sediment input from the river.

Favorable areas of deposition are dominated by fine sediments while erosion occurs preferably over areas where the percentage of coarse sediments at the bottom is greatest

(www.ozestuaries.org, 2006). Erosion areas, for the tide alone (Fig. 5.2d), are limited to the Nasese Channel, to the east side at the head of Laucala Bay, the Vunidawa River mouth and to some extent, near the Nukubuco Passage. Strong currents generated at the Nukubuco Passage and through the narrow Nasese Channel create strong bed shear stresses, which is greater than the critical shear stress, causing erosion of bottom sediments. At the Vunidawa River mouth, the shallow depths allow resuspension of bottom sediments due to the changing currents during the tidal cycle. For the wind alone (Fig. 5.2e), the erosion areas are confined to the shallow waters at Nasese Channel and at the Vatuwaqa, Samabula, Nasinu and Vunidawa River mouths. The current induced by the wind effect at the surface resuspends bottom sediments at the shallow depths causing erosion of bottom sediments.

The combination of tide and wind (Fig. 5.2f) shows that the influence of the individual forcings is significant in determining the overall erosion flux in the lagoon. The zones where low percentages of fine sediments are found (from Fig. 5.1) are consistent with the areas of erosion under the combined forcing of tide and wind, especially in the Nasese Channel and at the river mouths. The high amount of erosion near the head of the bay and at the river mouth is due to the resuspension phenomenon. Figure 5.2f shows that there is good agreement between the erosion fluxes and the zones where there is low percentage of fine sediments at the bottom of the lagoon. It can be seen from Fig. 5.2 that the tidal influence is greater in the deeper parts of the lagoon, where the tide operates as the main regulator, while the effect of wind is more dominant at shallower depths.

5.3 Model Verification

Verification of the model was carried out by comparing field data (presented in Chapter 3) with the model output. The model salinity and turbidity profiles were extracted for sites where field data were collected and compared with the field salinity and turbidity profiles at those sites. A successful comparison would be achieved if the profiles derived from the model follow the field profiles. The field data used for comparison was data collected from *Cruise 1* (on 15th March 2006).

To ensure a realistic representation, the model used the M_2 , S_2 , K_1 and O_1 constituents of tide, wind data from the weather station at the School of Marine Studies (SMS) for the simulation

period and river discharges from the Rewa, Nasinu, Samabula, Vatuwaqa and Tamavua Rivers. The discharge used for the Rewa River was $200 \text{ m}^3 \text{ s}^{-1}$ and was calculated using equation (3.1). Due to the unavailability of individual discharge data for the Nasinu, Samabula, Vatuwaqa and Tamavua Rivers, these discharges were each approximated to $5 \text{ m}^3 \text{ s}^{-1}$ based upon the size, width and depth of these rivers compared to the Rewa River. The freshwater introduced into the model had an initial salinity of 0 psu and turbidity of 20 FTU. This value of turbidity is obtained from field results (discussed in Chapter 3) and the fact that high rainfall introduces a high amount of terrigenous input into the river. The reference salinity of ocean water used in the model was 35.0 psu. This value was taken from measurements at a point outside the Suva Passage. Initial test runs of the model using 34.5 psu and 35.5 psu for the salinity of ocean water showed considerable discrepancies from the field data. This is because salinity near the coastal areas is generally lower than that found in deeper regions away from the coast. The model used 10 vertical σ layers, where the vertical axis k equivalent to 0 represents the bottom and the value equivalent to 1 represents the surface. The model results are taken 120 hours after the introduction of freshwater into the model.

5.3.1 Salinity Profiles

Four sites were chosen to represent salinity distribution in the lagoon. These were at Suva Harbour, Nukubuco Passage, Laucala Bay and Rewa Delta. Figure 5.3 shows the field and model salinity profiles at each of the four sites.

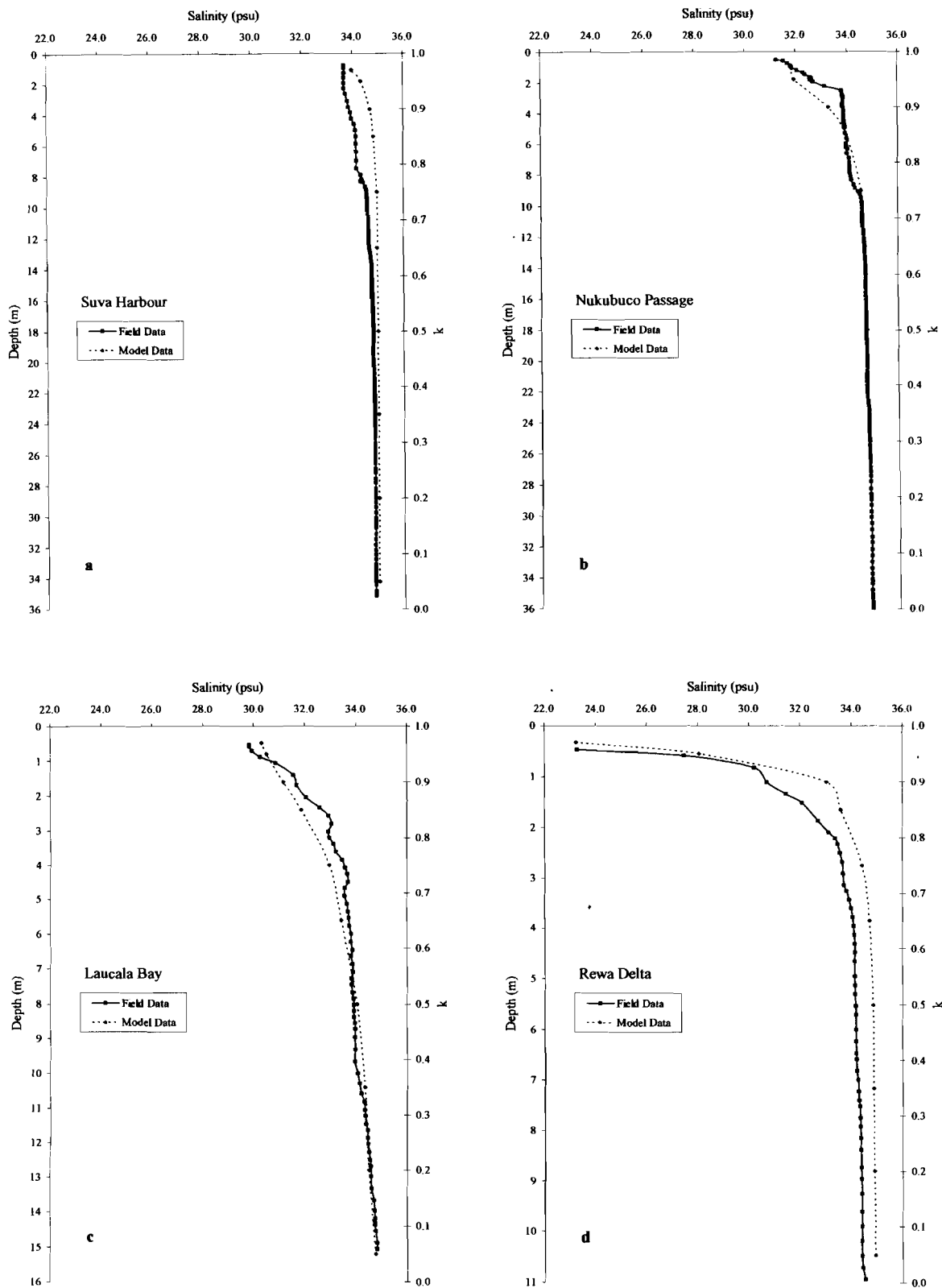


Figure 5.3 Field and model salinity profiles for $\sigma = 10$ levels at different locations in the Suva Lagoon using the same range for salinity at (a) Suva Harbour, (b) Nukubuco Passage, (c) Laucala Bay and (d) Rewa Delta.

The model salinity in Suva Harbour (Fig. 5.3a) shows a slight deviation from the field salinity at the surface. This can be attributed to the estimated discharge of $5 \text{ m}^3 \text{ s}^{-1}$ from the Tamavua River used in the model. The discharge is probably more and using a higher value for the discharge will decrease the model salinity and generate a more accurate salinity profile. The model salinity at Nukubuco Passage and Laucala Bay (Fig. 5.3c, d respectively) follow the field salinity with an average deviation of 0.2 psu. The model salinity is generally lower than the field salinity at the surface due to the continuous river discharges used in the model. Instead of using a constant rate of river discharge, more realistic and instantaneous runoffs would increase the model salinity generating more accurate profiles. The salinity profiles show a good comparison between model output and field data in the Rewa Delta (Fig. 5.3d).

The bottom salinity at the four sites shows better agreement between model results and field data than at the surface. This means that the discharge from the rivers influences the surface salinity more than the bottom salinity. This is similar to Rao's (2005) findings. The model and field salinity profiles in Fig. 5.3 follow each other in a similar manner showing that the model is reasonably capable of representing the salinity distribution in the Suva Lagoon fairly accurately and that the model has been verified for salinity distribution. The model used 10 vertical σ layers to represent the salinity distribution. The effect of increasing the model resolution on salinity distribution is discussed next.

5.3.2 Effect of Model Resolution on Salinity Distribution

In validating the model for salinity distribution, 10 vertical σ layers were used. To observe the effect of increasing the model resolution on salinity distribution, 23 vertical σ layers are used. The same parameters that were used to validate the model for salinity distribution using $\sigma = 10$ levels from above are used for $\sigma = 23$ levels. Figure 5.4 shows the model salinity profiles at different locations in the Suva Lagoon 120 hours after the introduction of freshwater into the model using both 10 and 23 vertical σ layers.

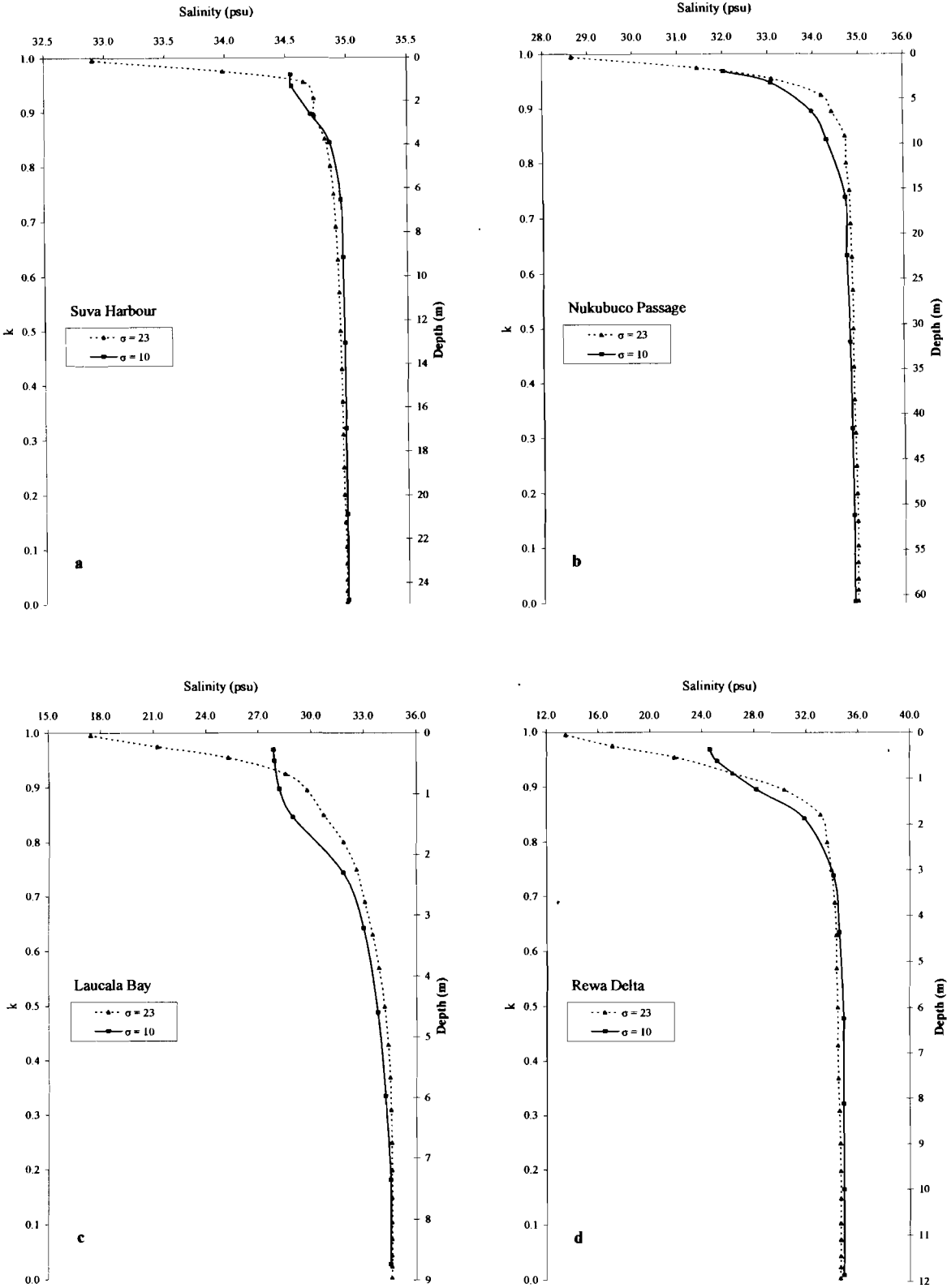


Figure 5.4 Model salinity profiles for $\sigma = 10$ levels and $\sigma = 23$ levels at different locations in the Suva Lagoon (a) Suva Harbour, (b) Nukubucu Passage, (c) Laucala Bay and (d) Rewa Delta.

The model salinity profiles in Fig. 5.4 show that there is better representation of the vertical profile when $\sigma = 23$ levels than when $\sigma = 10$ levels because of the larger number of data points. The surface salinity for $\sigma = 23$ levels has more data points than for $\sigma = 10$ levels (7 compared to 4 for the first 2 m of a total depth of 10 m) therefore the surface salinity for $\sigma = 23$ levels is better resolved. This can be seen in Fig. 5.4 where surface salinity for $\sigma = 23$ levels is more defined than for $\sigma = 10$ levels. In the deeper areas of the lagoon, for example in the Nukubuco Passage (Fig. 5.4b), representation of the vertical profile for $\sigma = 23$ levels is more realistic because the thickness of the freshwater plume on the surface is better resolved. There is greater resolution at the surface and at the bottom than in the middle of the vertical profile. However, the middle layer is conserved as the thickness between the levels is not very large so resolution is not lost.

5.3.3 Turbidity Profiles

The four sites chosen for the verification of turbidity distribution were the same as that for salinity distribution, that is, at Suva Harbour, Nukubuco Passage, Laucala Bay and Rewa Delta. Figure 5.5 shows the field and model turbidity profiles at each of the four sites. It is to be noted that the field turbidity profiles have been adjusted to account for the background turbidity of water discussed earlier in Section 3.4.5 (Chapter 3).

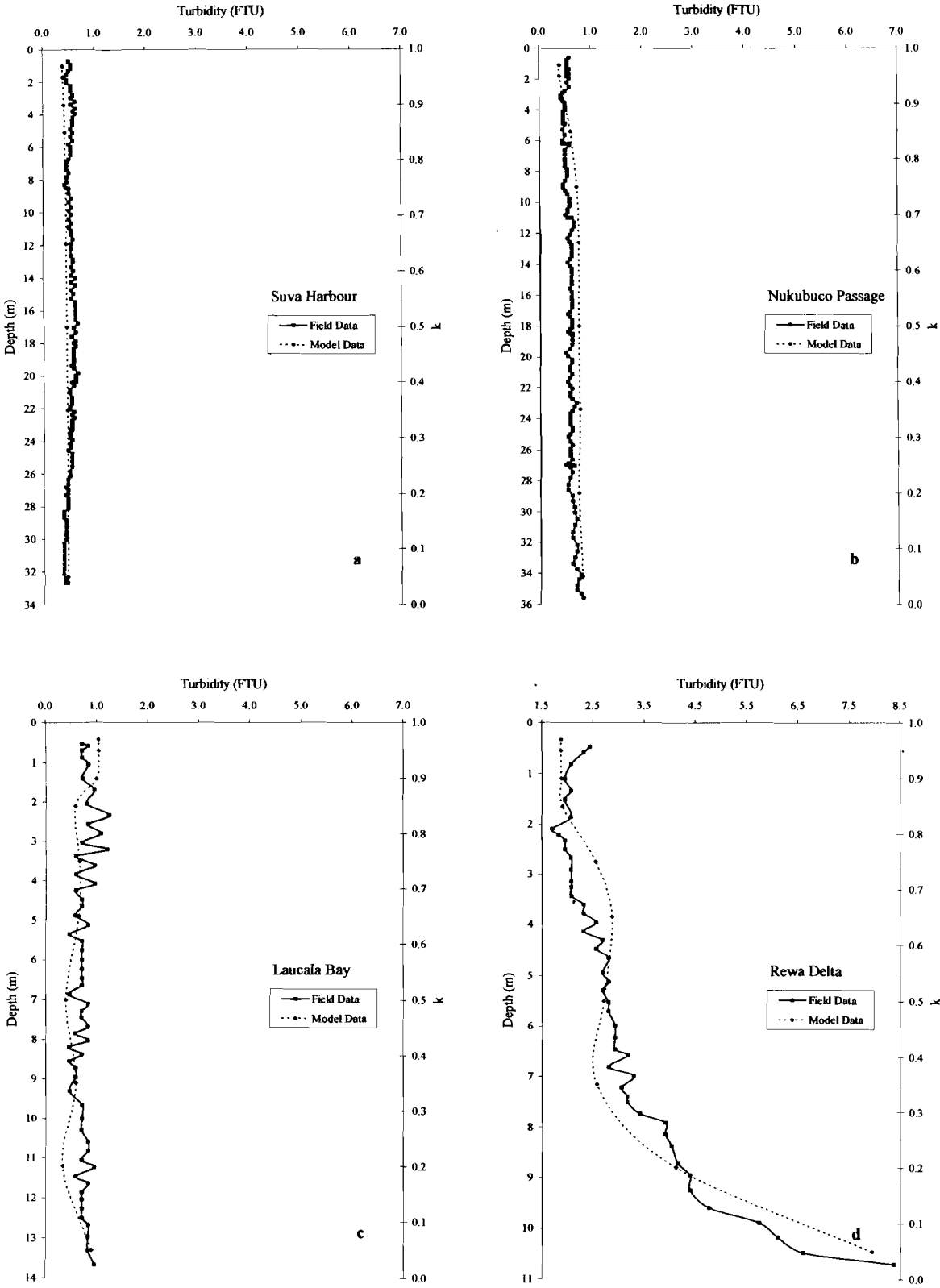


Figure 5.5 Field and model turbidity profiles for $\sigma = 10$ levels at different locations in the Suva Lagoon using the same range for turbidity at (a) Suva Harbour, (b) Nukubuco Passage, (c) Laucala Bay and (d) Rewa Delta.

The model and field turbidity in the Suva Lagoon generally show good agreement with each other. The model turbidity at Suva Harbour and Nukubuco Passage (Fig. 5.5a, b respectively) can be seen to follow the field turbidity with an average deviation of less than 0.1 FTU. The field turbidity profile in Laucala Bay shows that turbidity generally stays constant at about 0.9 FTU. The model turbidity at this site also stays constant with an average value of about 0.8 FTU. Near the bottom, resuspension of bottom sediments increases the turbidity and this can be seen in the Rewa Delta (Fig. 5.5d). This phenomenon is not seen in Suva Harbour and Nukubuco Passage because of the low percentage of fine sediments found at the bottom. The bottom model turbidity in the Rewa Delta shows high turbidity. This is what is also observed from the field turbidity profile. The above comparisons show that the model is able to represent turbidity distribution in the Suva Lagoon fairly reasonably and therefore the model has been verified for turbidity distribution.

The model used 10 vertical σ layers to represent turbidity distribution. It would be difficult to observe the effect of increasing the model resolution on turbidity distribution in the vertical layer. This is because of the following reason. For the vertical transport of fine sediments in the water column, the vertical velocity is multiplied by the time step. If the number of σ layers is increased, $\Delta\sigma$ decreases (as depth is conserved). Since settling velocity is conserved, the vertical transport of fine sediments will take place from one σ level to another. This will not conserve the vertical profile of sediment transport and in the first σ level ($\sigma = 1$), that is, at the bottom of the seabed, the sediment particle will go straight through the bottom. This is particularly common in shallow waters where $\Delta\sigma$ is relatively small. To avoid this from happening, the time step will have to be reduced. Doing this will conserve the vertical transport of fine sediments in the water column, that is, in $\Delta\sigma$. However, decreasing the time step implies more computations and a longer time to run the model, which cannot be handled by a normal computer. A larger and faster processor is required. Therefore, only 10 σ levels were used for the calculation of suspended sediment concentration in this project.

5.4 Implementation of the Model to the Suva Lagoon

The verified model can be used to simulate the distribution of salinity and turbidity under different conditions in the Suva Lagoon. In the model, real-time wind data for the study period from SMS and the M_2 , S_2 , K_1 and O_1 constituents of tide are used. The effect of the presence of the sandbank in the Rewa Delta and different river discharges on the water quality in the Suva Lagoon will be determined.

5.4.1 Effect of the Presence of the Sandbank on Salinity Distribution

Campbell *et al.* (1982) stated that the Vunidawa River channels 15% of the total discharge of the Rewa River into Laucala Bay, while the remainder flows into the Rewa Delta. However, it is to be noted that the Rewa Delta is generally closed due to the formation of sandbanks and these sandbanks can play a significant role in determining the amount of freshwater that enters Laucala Bay and Rewa Delta.

Freshwater discharges from rivers carry sediments to the coastal areas from where they are either deposited or transported further. Sometimes rivers carry more sediments to the coastal areas than longshore currents can distribute (Trujillo and Thurman, 2005). As a result, the depositional processes exceed coastal erosion and transportation processes and these rivers develop a delta (triangular) deposit at their mouths (Trujillo and Thurman, 2005). These deltas then grow through the formation of distributaries, which radiate out over the delta and become choked with sediment when they get too long (Trujillo and Thurman, 2005).

To determine the influence of the sandbank on salinity distribution in the lagoon, especially in Laucala Bay, several model runs were made for different river discharges, with and without the presence of the sandbank in the Rewa Delta, and the results are presented 120 hours after the introduction of freshwater into the model in Fig. 5.6. In the model simulations, wind data from the weather station at SMS, the M_2 , S_2 , K_1 and O_1 constituents of tide and $\sigma = 23$ levels are used. The freshwater introduced into the model had an initial salinity of 0 psu.

River. The individual discharges from the smaller rivers (Nasinu, Samabula, Vatuwaqa and Tamavua Rivers) were each considered to be $5 \text{ m}^3 \text{ s}^{-1}$. However, since the discharge from the Vunidawa River ($12 \text{ m}^3 \text{ s}^{-1}$) has a small effect on surface salinity distribution in Laucala Bay, these individual discharges from the Nasinu, Samabula, Vatuwaqa and Tamavua Rivers on surface salinity variation in the lagoon can be considered as insufficient to make a significant change in the surface salinity distribution.

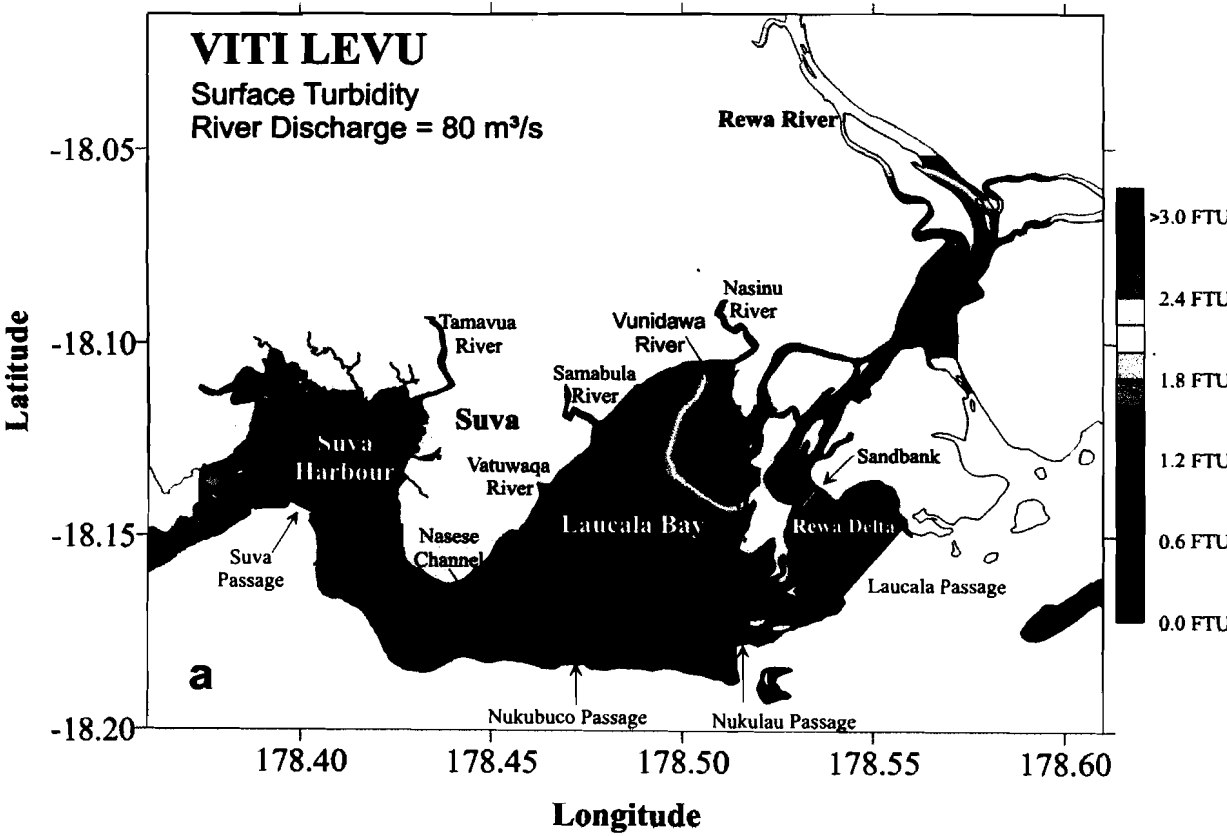
The influence of the sandbank on surface salinity distribution is greater for a river discharge of $200 \text{ m}^3 \text{ s}^{-1}$ (Fig. 5.6c, d) from the Rewa River (to represent high river discharge). The surface salinity distribution in Laucala Bay, with the presence of the sandbank, extends up to the entrance of Nasese Channel (Fig. 5.6c). However, in the absence of the sandbank, surface salinity distribution is only up to the middle of Laucala Bay and the Nukubuco Reef, near Nukubuco Passage (Fig. 5.6d). The effect of the presence of the sandbank in the Rewa Delta is most clearly observable for a higher discharge from the Rewa River of $400 \text{ m}^3 \text{ s}^{-1}$ (Fig. 5.6e, f). In the presence of the sandbank, surface salinity in the bay varies between 25.0 psu at the head of the bay to 29.0 psu at the Nasese Channel (Fig. 5.6e). High salinity waters at the surface can be seen to accumulate along Laucala Bay coast. In the absence of the sandbank, surface salinity in the bay is higher, varying between 28.0 psu at the head of the bay to 32.0 psu at the Nasese Channel (Fig. 5.6f). Surface salinity in the Rewa Delta is higher when the sandbank is present in comparison to when there is no sandbank.

The presence of the sandbank plays an important role in the distribution of surface salinity in the lagoon, especially during periods of high freshwater discharge. In the presence of the sandbank, more freshwater is channeled from the Rewa River into Laucala Bay (via the Vunidawa River) than into the Rewa Delta. Therefore, surface salinity in the bay is low. In the absence of the sandbank, there is less amount of freshwater entering the bay and more freshwater channeled into the Rewa Delta, therefore surface salinity in the bay is high.

5.4.2 Effect of River Discharge on the Transport of Fine Suspended Sediments

As mentioned earlier, salinity in the Suva Lagoon is largely influenced by the freshwater discharge from the Rewa River. The Rewa River discharges not only low salinity waters but

also freshwater which include high amounts of terrigenous input. As rivers flow seaward, they carry sediments with them from the land (www.southsloughestuary.org, 2005). These sediments enter the lagoon and are either deposited or transported further depending on the current velocity. (A brief summary of the water circulation in the Suva Lagoon from Rao's (2005) work is presented in Chapter 2.) Model simulations to study the effect of different river discharges on the transport of fine sediments in the Suva Lagoon are shown in Fig. 5.7. The freshwater introduced into the model had an initial suspended sediment concentration of 20 FTU and the model simulations are taken 120 hours after the input of freshwater into the model. The wind data was taken from the weather station at SMS and the M_2 , S_2 , K_1 and O_1 constituents of tide were used in the simulations.



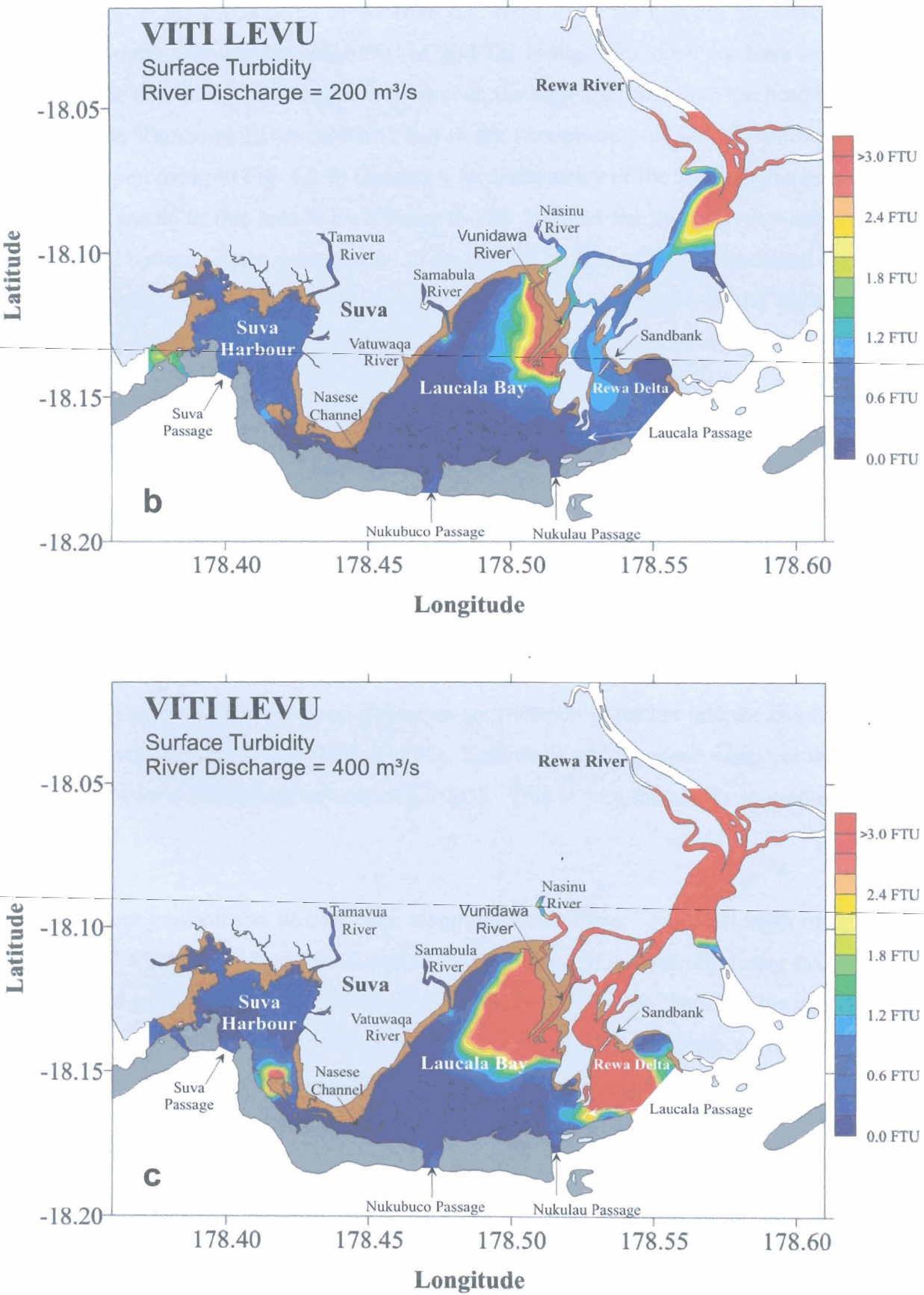


Figure 5.7 Model surface turbidity distribution for a river discharge of (a) 80 m³ s⁻¹, (b) 200 m³ s⁻¹ and (c) 400 m³ s⁻¹.

The small river discharge of $80 \text{ m}^3 \text{ s}^{-1}$ from the Rewa River (to find out the effect of lower river discharge), carrying an initial SSC of 20 FTU in Fig. 5.7a, does not have a significant effect on the SSC in the Suva Lagoon. However, the high SSC seen near the head of Laucala Bay and the Vunidawa River mouth is due to the resuspension of bottom sediments in the shallow region (refer to Fig. 4.2 in Chapter 4 for bathymetry of the lagoon). The percentage of fine sediments in this area is high (refer to Fig. 5.1) and the tidal currents and the wind effect at the bottom causes resuspension of the bottom sediments. It is to be noted that this is consistent with the areas of erosion shown in Fig. 5.2f. The turbidity in the lagoon is high, even during low river discharges near the Vunidawa River mouth due to the resuspension phenomenon.

For a higher discharge from the Rewa River of $200 \text{ m}^3 \text{ s}^{-1}$ (to represent high river discharge) shown in Fig. 5.7b, the turbidity near the Vunidawa River mouth and the head of Laucala Bay is lower than for a discharge of $80 \text{ m}^3 \text{ s}^{-1}$ (Fig. 5.7a). However, it is to be noted that the turbidity gradient along the surface in Fig. 5.7b is more defined than that in Fig. 5.7a. This means that at the river mouth, the freshwater rushes into the bay but as it moves further into the bay, the velocity decreases. As this happens, the coarser grained sediments settle near the river mouth while the finer grained sediments are transported further into the bay before they eventually settle to the bottom (Segar, 1998). Sediments are deposited wherever the currents are slowed (www.southsloughestuary.org, 2005). This is why the sediment gradient is seen in Fig. 5.7b.

The sediment gradient can also be seen along the Rewa River. For discharges of $80 \text{ m}^3 \text{ s}^{-1}$ and $200 \text{ m}^3 \text{ s}^{-1}$, the SSC along the Rewa River (Fig. 5.7a, b) is relatively lower than the SSC at the initial point (20 FTU) of introduction of freshwater into the model. This is because of two reasons. Firstly, the percentage of fine sediments at the bottom used in the model covered Laucala Bay and Suva Harbour and not the Rewa River and Rewa Delta. Therefore, there is no resuspension of bottom sediments along the Rewa River. And secondly, the initial discharges introduce high SSC but since the discharges are relatively small ($80 \text{ m}^3 \text{ s}^{-1}$ and $200 \text{ m}^3 \text{ s}^{-1}$), the river currents are also small and the sediments are deposited rather than transported downstream. The discharge from the smaller rivers (Nasinu, Samabula, Vatuwaqa and Tamavua) is much smaller (taken as $5 \text{ m}^3 \text{ s}^{-1}$) than the discharge from the Rewa River ($80 \text{ m}^3 \text{ s}^{-1}$). Thus, the amount of suspended sediments that are introduced by

these smaller rivers, settle along the river channel before they reach the river mouths and empty into the lagoon. Therefore, the effect of the smaller rivers on the SSC in the Suva Lagoon can be considered to be insufficient to make a significant change in SSC in the lagoon. Higher discharges transport the suspended sediments further downstream. This can be seen in Fig. 5.7a, b where the sediments transported from the initial point of introduction of freshwater for a discharge of $200 \text{ m}^3 \text{ s}^{-1}$ is further downstream than that for a discharge of $80 \text{ m}^3 \text{ s}^{-1}$.

During much higher river discharges, for example, $400 \text{ m}^3 \text{ s}^{-1}$ (shown in Fig. 5.7c), the SSC in the bay is more than during smaller discharges ($80 \text{ m}^3 \text{ s}^{-1}$ and $200 \text{ m}^3 \text{ s}^{-1}$ in Fig. 5.7a, b). The high initial discharge carries the suspended sediments further downstream and is introduced into Laucala Bay via the Vunidawa River. This scenario was not observed for smaller discharges of $80 \text{ m}^3 \text{ s}^{-1}$ and $200 \text{ m}^3 \text{ s}^{-1}$ (Fig. 5.7a, b respectively). The high river currents at the river mouth carry the suspended sediments introduced from the river and the resuspended sediments from the bottom further into Laucala Bay and this accounts for the high SSC found in the bay. The tides and the wind help in the distribution of suspended sediments, as discussed earlier in Section 5.2.4.

The model simulations discussed above show that the SSC in Laucala Bay is influenced by the resuspension of the bottom sediments in the bay. The Rewa River influences the SSC in the bay during high river discharges. These suspended sediments are transported not only by the river currents but also by the effect of winds and tides. The tide and the wind are important parameters in the transport of fine sediments as they contribute to the overall turbidity in the lagoon.

5.5 Conclusions

Several combinations of the critical shear stress τ_{cr} and the erosion rate coefficient ke_c were obtained through model runs. The number of possibilities can only be reduced when at least one of these parameters is determined from field measurements. However, values of $\tau_{cr} = 0.020 \text{ N m}^{-2}$ and $ke_c = 6.5 \times 10^{-5} \text{ g m}^{-2} \text{ s}^{-1}$ were chosen as this combination gave the minimum percentage difference between deposition and erosion fluxes cumulated for the whole lagoon over one tidal cycle. A combination of the tide and wind forcings provides the

best agreement between the fluxes and the percentage of fine sediments found at the bottom as opposed to the individual forcings. The tide and wind are the main regulators in determining the deposition and erosion fluxes of sediments at the seabed.

The model was verified for salinity and turbidity distribution using data gathered from field measurements (discussed in Chapter 3). The model salinity profiles were seen to follow the field salinity profiles fairly accurately. Using the values of τ_{cr} and ke_c mentioned above, the model was verified for suspended sediment concentration distribution. It was found that the model turbidity profiles depicted the field turbidity profiles to a reasonable amount of accuracy.

Both the field results and model output showed that the surface layer shows more variation in salinity distribution than the middle or bottom layers. This is due to the wind effect in transporting the freshwater entering the lagoon. Increasing the model resolution from 10 to 23 σ levels has a considerable effect on the salinity profiles, especially at the surface layer. This is because there are relatively more data points in the upper layer. The middle and bottom layers are conserved and increasing the model resolution in these layers has little effect on the salinity profiles.

The presence of the sandbank in the Rewa Delta plays a very significant role in the distribution of surface salinity in the Suva Lagoon, especially during high freshwater discharges from the Rewa River. A higher volume of freshwater enters Laucala Bay rather than the Rewa Delta when there is a sandbank present. This affects the salinity distribution in the lagoon considerably, especially in Laucala Bay. For a river discharge of $400 \text{ m}^3 \text{ s}^{-1}$, the freshwater effect reaches beyond the Nasese Channel in the presence of the sandbank but only up to the middle of Laucala Bay in the absence of the sandbank (Fig. 5.6e, f).

The transport of fine suspended sediments in the Suva Lagoon is influenced by three main factors:

- the tide, which resuspends the bottom sediments due to the shear stresses acting at the bottom;
- the wind, which transports the suspended sediments introduced through river discharges and the resuspended sediments along the surface; and

- the large river currents during high river discharges, which carry the suspended and resuspended sediments further into Laucala Bay.

The tides are an important component in the resuspension of bottom sediments. The tidal range during the sampling period at Suva (*Cruise 1* on 15th March 2006, which was during the spring tide) was 1.2 m. This is the period that was used in the model simulations as an example. Although the sampling period is close to equinox (21st March, which falls during the neap tide), the tidal range is not very large since the solar influence on tides is only 47% of the lunar effect. The maximum tidal range during the month of March 2006 was 1.7 m and the minimum tidal range was 0.8 m. Therefore, the tidal range during the sampling period was close to the average value for March 2006. If the model was run for the period of higher tidal range, the tidal currents would be stronger and this would generate stronger shear stresses at the bottom causing erosion of the underlying sediments. Therefore, the suspended sediment concentration in the water column would be high. For a lower tidal range, the tidal currents would be smaller and the smaller shear stress generated would cause less erosion and the concentration of suspended sediments in the water column would be low.

The wind effect at the surface also causes resuspension of bottom sediments, especially in the shallow areas. The wind speed during the sampling period (*Cruise 1* on 15th March 2006) averaged 3.8 m s^{-1} . The mean monthly wind speed during the 2005 – 2006 wet-warm season was in the range of $3.3 - 4.5 \text{ m s}^{-1}$ (discussed earlier in Section 3.2 in Chapter 2). Therefore, the average wind speed during the sampling period was close to the mean value for the wet-warm season. In the model simulations, realistic wind data was used from the weather station at the School of Marine Studies. If the model was run for the period of higher wind speeds ($> 3.8 \text{ m s}^{-1}$), there would be increased erosion of the bottom sediments as the wind effect at the bottom would be more due to the strong currents generated at the surface. This can be seen clearly in Tables 1 – 8 in the Appendix for a wind of 8 m s^{-1} . The erosion fluxes are very big compared to that for a wind of 6 m s^{-1} . Consequently, lower wind speeds used in the model ($< 3.8 \text{ m s}^{-1}$) would cause less erosion.

It is to be noted that when the tidal range and the wind speed are higher in the modelling period, there is also more deposition of the suspended sediments. This is because an increase in the erosion flux results in an increase in the amount of suspended sediments in the water

column. The deposition flux is proportional to the settling velocity and the concentration of fine sediments in the water column [refer to equation (4.27) in Chapter 4]. Therefore, where there is increased erosion, there is also increased deposition. This can be seen in Tables 1 – 8 in the Appendix.

The discharge from the Rewa River is the major source of sediments in the Suva Lagoon. Sediments are carried into the lagoon by the river currents. The transport of these sediments from the Rewa River into the Suva Lagoon is highly dependent on the discharge rate of the Rewa River. During low river discharge (for example $80 \text{ m}^3 \text{ s}^{-1}$), river currents will be slower since discharge and current velocity obey the relationship given by equation (5.1).

$$R_D = A \times v_{av} \quad (5.1)$$

where R_D is the river discharge in $\text{m}^3 \text{ s}^{-1}$, A is the cross-sectional area of the river mouth or any cross-section considered in m^2 and v_{av} is the average current velocity in the cross-sectional area A in m s^{-1} . Therefore, the sediments that are introduced into the river system at the source are deposited in the river channel. The suspended sediments barely make their way downstream and into the Suva Lagoon. However, during much higher discharges during the wet-warm season (approximately $200 \text{ m}^3 \text{ s}^{-1}$), the suspended sediments in the Rewa River make their way further downstream, than for a lower discharge rate (for example, $80 \text{ m}^3 \text{ s}^{-1}$). But the river currents are not that strong enough and the sediments again settle, but further, along the river channel. It is only during very high discharge rates, for example $400 \text{ m}^3 \text{ s}^{-1}$, that the effect of the discharge from Rewa River on SSC can be seen more clearly in the Suva Lagoon. The suspended sediments are carried by the strong river currents downstream where they enter Laucala Bay via the Vunidawa River. These sediments also make their way into the Rewa Delta. The suspended sediments are then either deposited or transported further depending on the tides and the winds. The concentration of suspended sediments in the Suva Lagoon would be higher during tropical cyclones as there would be high rainfall resulting in high river runoff.

The tidal and wind effect on suspended sediments in the Suva Lagoon is always there, as the contribution from nature. The suspended sediment concentration near the mouth of the

Vunidawa River is always high, even during low discharge rates. This is due to the high percentage of fine sediments found at the bottom. However, it is the high discharge from the Rewa River which is the major influence on the transportation of fine suspended sediments in the Suva Lagoon. As can be seen from equation (3.1) in Chapter 3, rainfall has a direct relationship with river discharge. This means that rainfall is the deciding influence on SSC in the Suva Lagoon. In general, the amount of rainfall is somehow controlled by the El Niño/La Niña period in the Pacific Region. According to the southern oscillation index (SOI) records, the study period (March 2006) has a positive SOI value. Consequently, the results from the model simulations represent the transport of fine suspended sediments of a neutral period in the Suva Lagoon area.



Chapter 6

Conclusions

6.1 What has been done in the Suva Lagoon?

Numerous studies in various fields (including physical, biological and chemical oceanography, geomorphology and geology) have been conducted in the Suva Lagoon since the establishment of the University of the South Pacific (USP) in the 1960s at the Laucala Bay foreshores. More recently, a symposium held at USP from 30th March – 1st April 2005 discussed the ongoing research and its results on the science and management of the Suva Lagoon. Being the first of its kind on the study of the Suva Lagoon to be held at USP, this important event was organized by the Institute of Applied Sciences at USP and the School of Earth and Environmental Science of the University of Wollongong. Proceedings of this symposium was published in “*At the Crossroads-Science and Management of the Suva Lagoon*” and edited by Morrison and Aalbersberg (2006). Subsequently, a list of pioneers in the study of the Suva Lagoon has been quoted in Chapter 2.

Amongst all these research work, the field of physical oceanography at USP has grown rapidly within the past decade. For example, Kumar (2000) applied a 2D hydrodynamic model, built by the Institut de Recherche pour le Développement (IRD), to the Suva Lagoon. Five years later, Rao (2005) used an improved version of the model used by Kumar (2000), and modified by IRD, to study the water circulation in the lagoon using a 3D hydrodynamic model. The present work uses an extension of the model used by Rao (2005) to study the transport of fine suspended sediments in the lagoon. The model used is a 3D hydrodynamic-sediment transport coupled model, which belongs to the Institut Français de Recherche pour l'Exploitation de la Mer (IFREMER). The model is able to simulate the effects of bathymetry, bottom friction, turbulence, river runoff, tides and wind forcing on the salinity and suspended sediment concentration in the Suva Lagoon for the completeness of the model.

Most of the research work done previously on the Suva Lagoon has been briefly summarized in Chapter 2 as literature review. This will assist in any future studies undertaken for the Suva Lagoon area.

6.2 Outcomes of this Project

Having gathered the river discharge and rainfall data and collected wind, CTD and turbidity data, a thorough analysis of these data was conducted. Consequently, the present work has contributed the following findings in developing a further understanding of the physical processes taking place in the Suva Lagoon:

- The mean wind direction over the Suva Lagoon is generally from the southeast direction all throughout the year. Stronger winds persist in the dry-cool season than in the wet-warm season. The mean wind speed is between $4.4 - 5.6 \text{ m s}^{-1}$ in the dry-cool season and between $3.3 - 4.5 \text{ m s}^{-1}$ during the wet-warm season. The wind data has been collected since it was setup at the School of Marine Studies by the Institut de Recherche pour le Développement (IRD) in 2003. These wind data can be used for many other purposes also.
- The Rewa River discharge is influenced by individual runoffs from the contributing tributaries and has a direct relationship with the rainfall. Higher rainfall results in higher river discharge and vice versa for lower rainfall. A relationship between river discharge and rainfall has been determined and can be used in future for further and other studies. The relationship is given by equation (3.1) in Chapter 3.
- The discharge from the Rewa River is the major source of variations in salinity, temperature and turbidity in the Suva Lagoon. The runoff from the Vunidawa River, one of the tributaries of the Rewa River, greatly influences the water quality in Laucala Bay. Suva Harbour is isolated from the effects of the discharge from the Rewa River, however, variations in the water properties in the harbour is due to the freshwater discharge from the Tamavua River. Therefore, Laucala Bay and Suva Harbour can be said to exist as two separate water bodies, which are separated by the narrow Nasese Channel. Table 6.1 summarizes the salinity, temperature and turbidity range at the surface at various locations in the Suva Lagoon during the different seasons.

Table 6.1 Summary of the salinity, temperature and turbidity range at the surface in Suva Harbour, Nasese Channel, Laucala Bay and Rewa Delta during the wet-warm and dry-cool seasons.

Water Property	Season	Suva Harbour	Nasese Channel	Laucala Bay	Rewa Delta
Salinity (psu)	Wet-warm	33.7 – 34.4	33.2 – 34.7	31.2 – 33.3	23.6 – 32.8
	Dry-cool	33.8 – 34.3	33.2 – 34.2	32.5 – 34.5	28.7 – 32.6
Temperature (°C)	Wet-warm	28.9 – 29.4	29.1 – 29.6	29.2 – 30.2	29.6 – 30.0
	Dry-cool	24.5 – 24.8	24.5 – 25.0	24.5 – 25.4	24.8 – 25.2
Turbidity (FTU)	Wet-warm	0.4 – 0.8	0.5 – 0.6	0.6 – 1.9	0.8 – 2.6
	Dry-cool	0.1 – 0.2	0.2 – 0.4	0.1 – 1.9	0.8 – 2.2

The effects of the different parameters influencing the water quality in the Suva Lagoon were studied by using a 3D hydrodynamic-sediment transport coupled model. The following are the findings from the model output:

- The critical shear stress τ_{cr} and erosion rate coefficient ke_c for the Suva Lagoon was estimated to be 0.020 N m^{-2} and $6.5 \times 10^{-5} \text{ g m}^{-2} \text{ s}^{-1}$ respectively. Several combinations of τ_{cr} and ke_c are possible, however, this combination gives the minimum percentage difference between the deposition and erosion fluxes calculated over the whole lagoon for one tidal cycle. The number of possibilities can only be reduced when at least one of these parameters is measured.
- The individual influence of the tide and wind are the main regulators in determining the deposition and erosion fluxes of sediments at the bottom. However, the combined effect of the tide and wind provides the best agreement with the estimated percentage of fine sediments that are found at the bottom of the lagoon.
- The effect of model resolution on salinity distribution in the lagoon is significant, especially in the surface layer. Increasing the model resolution increases the number of data points and the salinity, especially at the surface, is better resolved. The middle and bottom layers of the salinity profile are conserved and do not show much difference when the model resolution is increased. More computational power is needed to increase the resolution for turbidity distribution.
- The sandbank in the Rewa Delta is very influential in determining the surface salinity distribution in the lagoon, especially during high freshwater discharges from the Rewa River. More freshwater is channeled into Laucala Bay, via the Vunidawa River, than into the Rewa Delta in the presence of the sandbank as opposed to when there is no sandbank present. This causes the surface salinity in Laucala Bay to drop significantly.

- The suspended sediment concentration (SSC) in the Suva Lagoon is controlled by the combined effect of the tides, wind and river discharge. The SSC in Laucala Bay during low discharges from the Rewa River is less than for higher discharges. For a river discharge of $80 \text{ m}^3 \text{ s}^{-1}$, the SSC at the mouth of the Vunidawa River is about 7 FTU and for a discharge of $200 \text{ m}^3 \text{ s}^{-1}$, the SSC at the river mouth is more than 12 FTU. The high concentration of suspended sediments in Laucala Bay during low discharges (~ 7 FTU) is due to resuspension of bottom sediments from the effect of the tides and winds. This means that the amount of suspended sediments in Laucala Bay, especially at the mouth of the Vunidawa River, is always high even during low discharge rates from the Rewa River. For much higher discharges of $400 \text{ m}^3 \text{ s}^{-1}$, the SSC at the Vunidawa River mouth is more than 18 FTU. This high value is attributed to the sediments introduced into Laucala Bay from the discharge of the Rewa River. The Rewa River discharge is the main source of suspended sediments in the Suva Lagoon.

6.3 Contributions to the study of the Suva Lagoon

During the course of this project, two oral presentations on the results from the earlier part of this study were presented at international conferences and a paper was published internationally. These are listed as follows:

- *Water quality management in the Suva Lagoon* was presented at the 21st Pacific Science Congress held in Okinawa, Japan from 12th – 18th June, 2007.
- *Water properties in the Suva Lagoon, Fiji* was presented at the 4th Annual Meeting of the Asia Oceania Geosciences Society held in Bangkok, Thailand from 30th July – 4th August, 2007. A paper on this presentation has been submitted for publication in Advances in Geosciences: Collected papers from the 4th Annual Meeting of the Asia Oceania Geosciences Society, World Scientific Publishing Company, Singapore.
- Singh, A. and T. Aung, 2008. Salinity, Temperature and Turbidity Structure in the Suva Lagoon, Fiji. *American Journal of Environmental Sciences* 4 (4): 252-261.

More papers on the results of this project are under preparation for submission.

6.4 Final Remarks

Personally, I have gained tremendously by doing this research project. I have learnt about field data collection and analysis, considerable knowledge of coastal modelling, the pros and cons of numerical methods and above all, I have improved my scientific judgment in this area and general analytical thinking, organizational skills, endurance and perseverance for future work. Now a similar type of work, as the one done in this project, can be done in other lagoons or on a much larger scale in other coastal areas. The training undertaken while conducting this project is a valuable and worthwhile experience in my life. Eventually it was realized that burning the midnight oil is part of daily life in doing research!

In any kind of study, one adds something to existing knowledge, while another adds something else. I believe that I have contributed a little more for those who are interested in the study of the Suva Lagoon. An addition, however small it may be, is a lot especially since no work of this kind has been done in this area. I conclude by quoting the words of **Buddha** on the way of practice in life:

“First they should have right ideas of things, ideas that are based on careful observation, and understand causes and effects and their significance correctly.”

In accordance with this teaching, I have exerted all my effort into the present study.



Bibliography

- Balas, L. and E. Özhan, 2002. Three-dimensional modelling of stratified coastal waters. *Estuarine, Coastal and Shelf Science* 54: 75-87.
- Blumberg, A.F. and G.L. Mellor, 1987. A description of a three-dimensional coastal ocean circulation model. In N.S. Heaps (ed.) *Three dimensional coastal ocean models*. American Geophysical Union, Washington, DC: 1-16.
- Bowden, K.F., 1983. *Physical oceanography of coastal waters*, Ellis Horwood Limited, Chichester, West Sussex, England.
- Brierley, G.J. and K.A. Fryirs, 2005. *Geomorphology and river management: Applications of the river styles framework*. Blackwell Publishing, Victoria, Australia.
- Burchard, H., 2002. *Applied turbulence modelling in marine waters*. Springer, Berlin.
- Campbell, L.E., P.R. Cock and R.A. Corris, 1982. Kinoya sewage treatment plant: Report on receiving water study. Report prepared by Commonwealth Department of Transport and Construction and Caldwell Connell Engineers for Public Works Department, Ministry of Works and Communications, Suva, Fiji.
- Cancino, L. and R. Neves, 1999. Hydrodynamic and sediment suspension modelling in estuarine systems Part 1: Description of the numerical models. *Journal of Marine Systems* 22: 105-116.
- Cohesive Sediment Mechanics*, available online <<http://www.kuleuven.be/hydr/CohesiveSed.htm>> (date accessed: 31st November 2007).
- Deleersnijder, E. and J.M. Beckers, 1992. On the use of σ -coordinate system in regions of large bathymetric variations. *Journal of Marine Systems* 3: 381-390.

- Douillet, P., 1998. Tidal dynamics of the south-west lagoon of New Caledonia: Observations and 2D numerical modelling. *Oceanologica Acta* 21(1): 69-79.
- Douillet, P., S. Ouillon and E. Cordier, 2001. A numerical model for fine suspended sediment transport in the southwest lagoon of New Caledonia. *Coral Reefs* 20: 361-372.
- Estournel, V., P. Knodrachoff and R. Vehil, 1997. The plume of the Rhone: Numerical simulation and remote sensing. *Continental Shelf Research* 8: 889-924.
- Fernandes, L.D.F., 2005. *Modelling of arsenic dynamics in the Tagus estuary*. MSc thesis. Instituto Superior Técnico, Universidade Técnica de Lisboa, Portugal.
- Fernandez, J.M., G. Cadiou, B. Moreton, R. Legendre, R. Fichez and C. Badie, 2006. Overview of the metal distribution in surface deposits and sedimentary records in Suva Lagoon. In R.J. Morrison and B. Aalbersberg (eds.) *At the crossroads: Science and Management of the Suva Lagoon*. Proceedings of a symposium, University of the South Pacific, Suva, Fiji: 110-111.
- Gendronneau, L., 1985. Physical oceanography at the Institute of Marine Resources: First dynamic study in Suva Harbour and Laucala Bay, Institute of Marine Resources, University of the South Pacific, Suva.
- Gerritsen, H., J.G. Boon, T. van der Kaaij and R.J. Vos, 2001. Integrated modelling of suspended matter in the North Sea. *Estuarine, Coastal and Shelf Science* 53: 581-594.
- Harmonic Constituents*, available online <http://tidesandcurrents.noaa.gov/data_menu.shtml?unit=0&shift=&format=Apply+Change&stn=1910000+Suva%2C+Suva+Harbor%2C++&type=Harmonic+Constituents> (date accessed: 26th July 2006).
- Harris, C.K. and P.L. Wiberg, 2001. A two-dimensional, time-dependent model of suspended sediment transport and bed reworking for continental shelves. *Computers and Geosciences* 27: 675-690.

- Hu, H. and K.H. Wang, 1998. *Modelling suspended sediment transport in open channels*, Department of Civil and Environmental Engineering, University of Houston, available online <http://gem1.cive.uh.edu/content/conf_exhib/00_poster/3.htm> (date accessed: 29th October 2004).
- Jouon, A., P. Douillet, S. Ouillon and P. Fraunié, 2006. Calculations of hydrodynamic time parameters in a semi-opened coastal zone using a 3D hydrodynamic model. *Continental Shelf Research* 26: 1395-1415.
- Julien, P.Y., 1998. *Erosion and sedimentation*. Cambridge University Press, United States of America.
- Kumar, N., 2000. *Definition of the water circulation in the Suva Lagoon: The budget of the water volume transport and its variations*. MSc thesis. University of the South Pacific, Suva, Fiji.
- Lazure, P. and J.C. Salomon, 1991. Coupled 2D and 3D modelling of coastal hydrodynamics. *Oceanologica Acta* 14: 173-180.
- Le Normant, C., 1995. *Modélisation numérique tridimensionnelle des processus de transport des sédiments cohésifs en environnement estuarien*. PhD thesis. Institute National Polytech Toulouse, France.
- Leendertse, J.J., 1967. *Aspects of computational model for long-period water-wave propagation*, The Rand Corporation, Santa Monica, CA, Rep RM-5294-PR.
- Li, C.W. and J. Gu, 2001. 3D layered-integrated modelling of mass exchange in semi-enclosed water bodies. *Journal of Hydraulic Research* 39(4): 403-411.
- Martins, F., P. Leitão, A. Silva and R. Neves, 2001. 3D modelling in the Sado estuary using a new generic vertical discretization approach. *Oceanologica Acta* 24(Supplement).

- Mellor, G.L., and T. Yamada, 1982. Development of a turbulence closure model for geophysical fluid problems. *Reviews of Geophysics and Space Physics* 20(4): 851-875.
- Morrison, R.J., 2006. Science and management of coastal lakes and lagoons. In R.J. Morrison and B. Aalbersberg (eds.) *At the crossroads: Science and Management of the Suva Lagoon*. Proceedings of a symposium, University of the South Pacific, Suva, Fiji: 110-111.
- Morrison, R.J. and B. Aalbersberg, 2006. *At the crossroads: Science and management of the Suva Lagoon*. Proceedings of a symposium, University of the South Pacific, Suva, Fiji.
- N'Yeurt, A.D.R., 2001. Marine algae from the Suva Lagoon and reef, Fiji. *Australian Systematic Botany* 14: 689-691.
- Naidu, S., W.G.L. Alersberg, J.E. Brodie, V.A. Fuavao, M. Maata, M. Naqasima, P. Whippy and R.J. Morrison, 1991. Water quality studies on selected South Pacific lagoons. UNEP Regional Seas Reports and Studies No. 136 and SPREP Reports and Studies No. 49, South Pacific Environmental Programme, Suva, Fiji.
- Numerical Modelling*, available online <<http://www.aslenv.com/modelling.html>> (date accessed: 28th September 2004).
- Ouillon, S., P. Douillet and S. Andréfouët, 2004. Coupling satellite data with in situ measurements and numerical modelling to study fine suspended-sediment transport: a study for the lagoon of New Caledonia. *Coral Reefs* 23: 109-122.
- Penn, N., 1983. *The environmental consequences and management of coral sand dredging in the Suva region, Fiji*. PhD thesis. University of Wales.
- Pickard, G.L. and W.J. Emery, 1990. *Descriptive physical oceanography: An introduction*. 5th edition. Butterworth-Heinemann Limited, Great Britain.

- Piedra-Cueva, I., M. Mory and A. Temperville, 1997. A race-track recirculating flume for cohesive sediment research. *Journal of Hydraulic Research* 35: 377-396.
- Pietrzak, J., J.B. Jakobson, H. Burchard, H.J. Vested and O. Peterson, 2002. A three-dimensional hydrostatic model for coastal and ocean modelling using a generalised topography following co-ordinate system. *Ocean Modelling* 4: 173-205.
- Pond, S. and G.L. Pickard, 1983. *Introductory dynamical oceanography*. 2nd edition. Butterworth-Heinemann, Exeter.
- Prandle, D., 2000. Introduction operational oceanography in coastal waters. *Coastal Engineering* 41: 3-12.
- Raj, R., 2004. *Integrated flood management– Case study on Fiji Islands: Flood management– Rewa River basin*, World Meteorological Organization/Global Water Partnership Associated Programme on Flood Management, available online <http://www.apfm.info/pdf/case_studies/cs_fiji.pdf> (date accessed: 13th June 2006).
- Rao, S.A., 2005. *Determination of the hydrodynamic circulation of the Suva Lagoon*. MSc thesis. University of the South Pacific, Suva, Fiji.
- Ruddick, K.G., E. Deleersnijder, P.J. Luyten and J. Ozer, 1995. Haline stratification in the Rhine-Meuse freshwater plume: A three-dimensional model sensitivity analysis. *Continental Shelf Research* 15(13): 1597-1630.
- Schaaf, E., 1999. Remise en suspension des sédiments du Golfe du Lion: Expériences et modélisation. *DEA Science Environment Mar*, Université Méditerranée, Marseille, France.
- Schneider, W., I. Schmelzer and J. Wurtz, 1995. Sedimentological interplay of siliciclastic Rewa River input and organic carbonate production of the Suva barrier reef, Laucala Bay, Fiji. Technical Report, Marine Studies Programme, University of the South Pacific, Suva, Fiji 95(4).

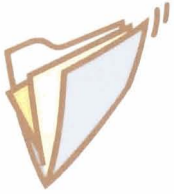
- Sediment Transport*, available online <<http://www.qeallc.com/html/sediment.html>> (date accessed: 25th May 2006).
- Sediment Transport and Deposition*, available online <<http://www.southsloughestuary.org/EFS/sediment.htm>> (date accessed: 10th February 2005).
- Sediment Transport and Morphology*, available online <<http://www.dhi.dk/Consulting/RiversLakes/Sediments/index.html>> (date accessed: 25th May 2006).
- Segar, D.A., 1998. *Introduction to ocean sciences*. Wadsworth Publishing Company, USA.
- Settling*, available online <<http://en.wikipedia.org/wiki/Settling>>, (date accessed: 29th June 2006).
- Shorten, G.G., 1993. *Geotechnical analysis of recent estuarine organo-calcareous silts, Fiji: New considerations for investigations of soft marine clays*. PhD thesis. University of Sydney, Australia.
- Smith, R., S. Young and G. Frost, 1994. Aanderaa current meter deployment Suva Harbour, Laucala Bay, Viti Levu, Fiji. Preliminary Report 70 prepared by SOPAC for the South Pacific Applied Geoscience Commission Coastal Program, Suva, Fiji.
- Squires, D.F., 1962. Corals at the mouth of the Rewa River, Viti Levu, Fiji. *Nature* 195(4839): 361-362.
- The Climate of Fiji*, available online <<http://www.met.gov.fj/climate.html>> (date accessed: 22nd November 2005).
- The World Factbook-Fiji*, available online <<http://www.cia.gov/library/publications/the-world-factbook/geos/fj.html>> (date accessed: 26th June 2007).
- Trujillo, A.P. and H.V. Thurman, 2005. *Essentials of Oceanography*. 3rd edition. Pearson Education Incorporated, New Jersey, USA.

Turbidity, available online <<http://www.lenntech.com/turbidity.html>> (date accessed: 27th July 2006).

Turbidity, available online <<http://www.ozestuaries.org/indicators/turbidity.jsp>> (date accessed: 20th November 2006).

Turbidity, available online <<http://waterontheweb.org/under/waterquality/turbidity.html>> (date accessed: 27th July 2006).

Viti Levu, available online <<http://www.factbites.com/topics/Viti-Levu>> (date accessed: 22nd November 2005).



Deposition and Erosion Fluxes

Table 1 Deposition and erosion fluxes (D_f and E_f respectively) calculated by the model over the whole lagoon with different values of the coefficient of erosion and with $\tau_{cr} = 0.010 \text{ N m}^{-2}$. D_f and E_f are expressed in tonnes per tidal cycle.

ke_c ($\text{g m}^{-2} \text{ s}^{-1}$)	Wind 6 m s ⁻¹	Wind 8 m s ⁻¹	Tide	Tide + Wind 6 m s ⁻¹	Tide + Wind 8 m s ⁻¹
4.0×10^{-5}	$D_f = 1010.7$	$D_f = 1988.8$	$D_f = 1307.4$	$D_f = 962.8$	$D_f = 735.1$
	$E_f = 2349.9$	$E_f = 25860.4$	$E_f = 874.9$	$E_f = 1998.7$	$E_f = 3542.2$
4.5×10^{-5}	$D_f = 1031.2$	$D_f = 2169.0$	$D_f = 1319.4$	$D_f = 976.9$	$D_f = 749.5$
	$E_f = 2634.6$	$E_f = 29092.9$	$E_f = 984.3$	$E_f = 2248.5$	$E_f = 3985.0$
5.0×10^{-5}	$D_f = 1051.7$	$D_f = 2349.3$	$D_f = 1331.3$	$D_f = 991.0$	$D_f = 764.0$
	$E_f = 2937.4$	$E_f = 32325.4$	$E_f = 1093.6$	$E_f = 2498.4$	$E_f = 4427.8$
5.5×10^{-5}	$D_f = 1072.2$	$D_f = 2529.6$	$D_f = 1343.3$	$D_f = 1005.1$	$D_f = 778.4$
	$E_f = 3231.1$	$E_f = 35558.0$	$E_f = 1203.0$	$E_f = 2748.2$	$E_f = 4870.6$
6.0×10^{-5}	$D_f = 1092.7$	$D_f = 2709.8$	$D_f = 1355.3$	$D_f = 1019.2$	$D_f = 792.9$
	$E_f = 3524.8$	$E_f = 38790.5$	$E_f = 1312.3$	$E_f = 2998.0$	$E_f = 5313.4$
6.5×10^{-5}	$D_f = 1113.3$	$D_f = 2890.1$	$D_f = 1367.3$	$D_f = 1033.3$	$D_f = 807.3$
	$E_f = 3816.6$	$E_f = 42023.1$	$E_f = 1421.7$	$E_f = 3247.9$	$E_f = 5756.1$
7.0×10^{-5}	$D_f = 1133.8$	$D_f = 3070.4$	$D_f = 1379.3$	$D_f = 1047.4$	$D_f = 821.7$
	$E_f = 4112.3$	$E_f = 45255.6$	$E_f = 1531.1$	$E_f = 3497.7$	$E_f = 6198.9$

Table 2 Deposition and erosion fluxes (D_f and E_f respectively) calculated by the model over the whole lagoon with different values of the coefficient of erosion and with $\tau_{cr} = 0.015 \text{ N m}^{-2}$. D_f and E_f are expressed in tonnes per tidal cycle.

ke_c ($\text{g m}^{-2} \text{ s}^{-1}$)	Wind 6 m s ⁻¹	Wind 8 m s ⁻¹	Tide	Tide + Wind 6 m s ⁻¹	Tide + Wind 8 m s ⁻¹
4.0×10^{-5}	$D_f = 1087.1$	$D_f = 1938.1$	$D_f = 1373.6$	$D_f = 1070.5$	$D_f = 853.7$
	$E_f = 658.3$	$E_f = 16615.8$	$E_f = 477.5$	$E_f = 1143.0$	$E_f = 2093.8$
4.5×10^{-5}	$D_f = 1091.5$	$D_f = 2089.9$	$D_f = 1381.8$	$D_f = 1080.9$	$D_f = 865.6$
	$E_f = 740.6$	$E_f = 18692.8$	$E_f = 537.2$	$E_f = 1285.9$	$E_f = 2355.5$
5.0×10^{-5}	$D_f = 1095.9$	$D_f = 2278.3$	$D_f = 1390.0$	$D_f = 1091.4$	$D_f = 877.6$
	$E_f = 822.9$	$E_f = 21891.4$	$E_f = 596.9$	$E_f = 1428.8$	$E_f = 2617.2$
5.5×10^{-5}	$D_f = 1100.3$	$D_f = 2425.8$	$D_f = 1398.2$	$D_f = 1101.8$	$D_f = 889.5$
	$E_f = 905.2$	$E_f = 23285.7$	$E_f = 656.6$	$E_f = 1571.7$	$E_f = 2879.0$
6.0×10^{-5}	$D_f = 1104.7$	$D_f = 2545.4$	$D_f = 1406.5$	$D_f = 1112.3$	$D_f = 901.5$
	$E_f = 987.5$	$E_f = 24923.7$	$E_f = 716.3$	$E_f = 1714.5$	$E_f = 3140.7$
6.5×10^{-5}	$D_f = 1109.1$	$D_f = 2697.2$	$D_f = 1414.7$	$D_f = 1122.8$	$D_f = 913.5$
	$E_f = 1069.8$	$E_f = 27000.6$	$E_f = 776.0$	$E_f = 1857.4$	$E_f = 3402.4$
7.0×10^{-5}	$D_f = 1113.4$	$D_f = 2849.1$	$D_f = 1422.9$	$D_f = 1133.2$	$D_f = 925.4$
	$E_f = 1152.1$	$E_f = 29077.6$	$E_f = 835.6$	$E_f = 2000.3$	$E_f = 3664.1$

Table 3 Deposition and erosion fluxes (D_f and E_f respectively) calculated by the model over the whole lagoon with different values of the coefficient of erosion and with $\tau_{cr} = 0.016 \text{ N m}^{-2}$. D_f and E_f are expressed in tonnes per tidal cycle.

ke_c ($\text{g m}^{-2} \text{ s}^{-1}$)	Wind 6 m s^{-1}	Wind 8 m s^{-1}	Tide	Tide + Wind 6 m s^{-1}	Tide + Wind 8 m s^{-1}
4.0×10^{-5}	$D_f = 1108.4$	$D_f = 1941.0$	$D_f = 1383.4$	$D_f = 1087.3$	$D_f = 873.1$
	$E_f = 593.1$	$E_f = 15824.5$	$E_f = 430.5$	$E_f = 1040.7$	$E_f = 1918.2$
4.5×10^{-5}	$D_f = 1112.7$	$D_f = 2097.0$	$D_f = 1391.1$	$D_f = 1097.2$	$D_f = 884.7$
	$E_f = 667.3$	$E_f = 17802.5$	$E_f = 484.3$	$E_f = 1170.8$	$E_f = 2157.9$
5.0×10^{-5}	$D_f = 1116.9$	$D_f = 2253.0$	$D_f = 1398.8$	$D_f = 1107.2$	$D_f = 896.2$
	$E_f = 741.4$	$E_f = 19780.6$	$E_f = 538.1$	$E_f = 1300.9$	$E_f = 2397.7$
5.5×10^{-5}	$D_f = 1121.2$	$D_f = 2409.0$	$D_f = 1406.5$	$D_f = 1117.1$	$D_f = 907.8$
	$E_f = 815.6$	$E_f = 21758.6$	$E_f = 591.9$	$E_f = 1431.0$	$E_f = 2637.5$
6.0×10^{-5}	$D_f = 1125.4$	$D_f = 2565.0$	$D_f = 1414.2$	$D_f = 1127.0$	$D_f = 919.3$
	$E_f = 889.7$	$E_f = 23736.7$	$E_f = 645.7$	$E_f = 1561.1$	$E_f = 2877.3$
6.5×10^{-5}	$D_f = 1129.7$	$D_f = 2721.0$	$D_f = 1421.9$	$D_f = 1136.9$	$D_f = 930.9$
	$E_f = 963.8$	$E_f = 25714.8$	$E_f = 699.5$	$E_f = 1691.2$	$E_f = 3117.0$
7.0×10^{-5}	$D_f = 1133.9$	$D_f = 2877.0$	$D_f = 1429.6$	$D_f = 1146.8$	$D_f = 942.4$
	$E_f = 1038.0$	$E_f = 27692.8$	$E_f = 753.4$	$E_f = 1821.3$	$E_f = 3356.8$

Table 4 Deposition and erosion fluxes (D_f and E_f respectively) calculated by the model over the whole lagoon with different values of the coefficient of erosion and with $\tau_{cr} = 0.017 \text{ N m}^{-2}$. D_f and E_f are expressed in tonnes per tidal cycle.

ke_c ($\text{g m}^{-2} \text{ s}^{-1}$)	Wind 6 m s^{-1}	Wind 8 m s^{-1}	Tide	Tide + Wind 6 m s^{-1}	Tide + Wind 8 m s^{-1}
4.0×10^{-5}	$D_f = 1128.7$	$D_f = 1934.6$	$D_f = 1392.5$	$D_f = 1103.1$	$D_f = 891.5$
	$E_f = 537.5$	$E_f = 14845.9$	$E_f = 389.7$	$E_f = 951.7$	$E_f = 1764.7$
4.5×10^{-5}	$D_f = 1132.8$	$D_f = 2087.4$	$D_f = 1399.7$	$D_f = 1112.5$	$D_f = 902.6$
	$E_f = 604.6$	$E_f = 16701.7$	$E_f = 438.4$	$E_f = 1070.7$	$E_f = 1985.3$
5.0×10^{-5}	$D_f = 1136.9$	$D_f = 2240.1$	$D_f = 1407.0$	$D_f = 1121.9$	$D_f = 913.8$
	$E_f = 671.8$	$E_f = 18557.4$	$E_f = 487.1$	$E_f = 1189.6$	$E_f = 2205.8$
5.5×10^{-5}	$D_f = 1141.0$	$D_f = 2392.9$	$D_f = 1414.2$	$D_f = 1131.3$	$D_f = 925.0$
	$E_f = 739.0$	$E_f = 20413.1$	$E_f = 535.9$	$E_f = 1308.6$	$E_f = 2426.4$
6.0×10^{-5}	$D_f = 1145.1$	$D_f = 2545.6$	$D_f = 1421.5$	$D_f = 1140.7$	$D_f = 936.1$
	$E_f = 806.2$	$E_f = 22268.9$	$E_f = 584.6$	$E_f = 1427.6$	$E_f = 2647.0$
6.5×10^{-5}	$D_f = 1149.2$	$D_f = 2698.4$	$D_f = 1428.7$	$D_f = 1150.1$	$D_f = 947.3$
	$E_f = 873.4$	$E_f = 24124.6$	$E_f = 633.3$	$E_f = 1546.5$	$E_f = 2867.6$
7.0×10^{-5}	$D_f = 1153.2$	$D_f = 2851.1$	$D_f = 1435.9$	$D_f = 1159.5$	$D_f = 958.4$
	$E_f = 940.6$	$E_f = 25980.3$	$E_f = 682.0$	$E_f = 1665.5$	$E_f = 3088.2$

Table 5 Deposition and erosion fluxes (D_f and E_f respectively) calculated by the model over the whole lagoon with different values of the coefficient of erosion and with $\tau_{cr} = 0.018 \text{ N m}^{-2}$. D_f and E_f are expressed in tonnes per tidal cycle.

ke_c ($\text{g m}^{-2} \text{ s}^{-1}$)	Wind 6 m s^{-1}	Wind 8 m s^{-1}	Tide	Tide + Wind 6 m s^{-1}	Tide + Wind 8 m s^{-1}
4.0×10^{-5}	$D_f = 1147.5$	$D_f = 1928.7$	$D_f = 1401.0$	$D_f = 1117.9$	$D_f = 908.8$
	$E_f = 489.3$	$E_f = 13977.3$	$E_f = 354.1$	$E_f = 873.7$	$E_f = 1629.5$
4.5×10^{-5}	$D_f = 1151.4$	$D_f = 2078.4$	$D_f = 1407.8$	$D_f = 1126.9$	$D_f = 919.6$
	$E_f = 550.4$	$E_f = 15724.5$	$E_f = 398.4$	$E_f = 982.9$	$E_f = 1833.2$
5.0×10^{-5}	$D_f = 1155.4$	$D_f = 2228.0$	$D_f = 1414.6$	$D_f = 1135.8$	$D_f = 930.4$
	$E_f = 611.6$	$E_f = 17471.6$	$E_f = 442.7$	$E_f = 1092.1$	$E_f = 2036.9$
5.5×10^{-5}	$D_f = 1159.3$	$D_f = 2377.7$	$D_f = 1421.4$	$D_f = 1144.7$	$D_f = 941.2$
	$E_f = 672.7$	$E_f = 19218.8$	$E_f = 486.9$	$E_f = 1201.3$	$E_f = 2240.6$
6.0×10^{-5}	$D_f = 1163.2$	$D_f = 2527.4$	$D_f = 1428.3$	$D_f = 1153.7$	$D_f = 952.0$
	$E_f = 733.9$	$E_f = 20965.9$	$E_f = 531.2$	$E_f = 1310.5$	$E_f = 2444.3$
6.5×10^{-5}	$D_f = 1167.2$	$D_f = 2677.1$	$D_f = 1435.1$	$D_f = 1162.6$	$D_f = 962.8$
	$E_f = 795.0$	$E_f = 22713.1$	$E_f = 575.5$	$E_f = 1419.7$	$E_f = 2647.9$
7.0×10^{-5}	$D_f = 1171.1$	$D_f = 2826.7$	$D_f = 1441.9$	$D_f = 1171.6$	$D_f = 973.6$
	$E_f = 859.2$	$E_f = 24460.3$	$E_f = 619.7$	$E_f = 1528.9$	$E_f = 2851.6$

Table 6 Deposition and erosion fluxes (D_f and E_f respectively) calculated by the model over the whole lagoon with different values of the coefficient of erosion and with $\tau_{cr} = 0.019 \text{ N m}^{-2}$. D_f and E_f are expressed in tonnes per tidal cycle.

ke_c ($\text{g m}^{-2} \text{ s}^{-1}$)	Wind 6 m s^{-1}	Wind 8 m s^{-1}	Tide	Tide + Wind 6 m s^{-1}	Tide + Wind 8 m s^{-1}
4.0×10^{-5}	$D_f = 1165.2$	$D_f = 1923.1$	$D_f = 1408.9$	$D_f = 1131.9$	$D_f = 925.3$
	$E_f = 447.4$	$E_f = 13201.2$	$E_f = 322.9$	$E_f = 804.8$	$E_f = 1509.7$
4.5×10^{-5}	$D_f = 1169.0$	$D_f = 2069.9$	$D_f = 1415.4$	$D_f = 1140.4$	$D_f = 935.7$
	$E_f = 503.3$	$E_f = 14851.3$	$E_f = 363.3$	$E_f = 905.4$	$E_f = 1698.5$
5.0×10^{-5}	$D_f = 1172.7$	$D_f = 2216.6$	$D_f = 1421.8$	$D_f = 1148.9$	$D_f = 946.2$
	$E_f = 559.2$	$E_f = 16501.5$	$E_f = 403.6$	$E_f = 1006.0$	$E_f = 1887.2$
5.5×10^{-5}	$D_f = 1176.5$	$D_f = 2363.4$	$D_f = 1428.2$	$D_f = 1157.4$	$D_f = 956.6$
	$E_f = 615.1$	$E_f = 18151.6$	$E_f = 444.0$	$E_f = 1106.6$	$E_f = 2075.9$
6.0×10^{-5}	$D_f = 1180.3$	$D_f = 2510.1$	$D_f = 1434.7$	$D_f = 1165.9$	$D_f = 967.1$
	$E_f = 671.1$	$E_f = 19801.8$	$E_f = 484.3$	$E_f = 1207.2$	$E_f = 2264.6$
6.5×10^{-5}	$D_f = 1184.1$	$D_f = 2656.9$	$D_f = 1441.1$	$D_f = 1174.4$	$D_f = 977.5$
	$E_f = 727.0$	$E_f = 21451.9$	$E_f = 524.7$	$E_f = 1307.8$	$E_f = 2453.3$
7.0×10^{-5}	$D_f = 1187.8$	$D_f = 2803.7$	$D_f = 1447.6$	$D_f = 1182.9$	$D_f = 988.0$
	$E_f = 782.9$	$E_f = 23102.1$	$E_f = 565.1$	$E_f = 1408.4$	$E_f = 2642.0$

Table 7 Deposition and erosion fluxes (D_f and E_f respectively) calculated by the model over the whole lagoon with different values of the coefficient of erosion and with $\tau_{cr} = 0.020 \text{ N m}^{-2}$. D_f and E_f are expressed in tonnes per tidal cycle.

ke_c ($\text{g m}^{-2} \text{ s}^{-1}$)	Wind 6 m s^{-1}	Wind 8 m s^{-1}	Tide	Tide + Wind 6 m s^{-1}	Tide + Wind 8 m s^{-1}
4.0×10^{-5}	$D_f = 1182.1$ $E_f = 411.0$	$D_f = 1917.8$ $E_f = 12503.7$	$D_f = 1416.4$ $E_f = 295.3$	$D_f = 1145.1$ $E_f = 743.7$	$D_f = 941.0$ $E_f = 1403.0$
4.5×10^{-5}	$D_f = 1185.7$ $E_f = 462.4$	$D_f = 2061.8$ $E_f = 14066.6$	$D_f = 1422.5$ $E_f = 332.2$	$D_f = 1153.2$ $E_f = 836.6$	$D_f = 951.1$ $E_f = 1578.4$
5.0×10^{-5}	$D_f = 1189.4$ $E_f = 513.7$	$D_f = 2205.7$ $E_f = 15629.6$	$D_f = 1428.6$ $E_f = 362.2$	$D_f = 1161.3$ $E_f = 929.6$	$D_f = 961.2$ $E_f = 1753.7$
5.5×10^{-5}	$D_f = 1193.0$ $E_f = 565.1$	$D_f = 2349.7$ $E_f = 17192.6$	$D_f = 1434.7$ $E_f = 406.1$	$D_f = 1169.4$ $E_f = 1022.5$	$D_f = 971.3$ $E_f = 1929.1$
6.0×10^{-5}	$D_f = 1196.6$ $E_f = 616.5$	$D_f = 2493.7$ $E_f = 18755.5$	$D_f = 1440.8$ $E_f = 443.0$	$D_f = 1177.5$ $E_f = 1115.5$	$D_f = 981.4$ $E_f = 2104.5$
6.5×10^{-5}	$D_f = 1200.2$ $E_f = 667.9$	$D_f = 2637.6$ $E_f = 20318.5$	$D_f = 1446.9$ $E_f = 479.9$	$D_f = 1185.6$ $E_f = 1208.5$	$D_f = 991.5$ $E_f = 2279.9$
7.0×10^{-5}	$D_f = 1203.9$ $E_f = 719.2$	$D_f = 2781.6$ $E_f = 21881.4$	$D_f = 1453.0$ $E_f = 516.8$	$D_f = 1193.7$ $E_f = 1301.4$	$D_f = 1001.6$ $E_f = 2455.2$

Table 8 Deposition and erosion fluxes (D_f and E_f respectively) calculated by the model over the whole lagoon with different values of the coefficient of erosion and with $\tau_{cr} = 0.025 \text{ N m}^{-2}$. D_f and E_f are expressed in tonnes per tidal cycle.

ke_c ($\text{g m}^{-2} \text{ s}^{-1}$)	Wind 6 m s^{-1}	Wind 8 m s^{-1}	Tide	Tide + Wind 6 m s^{-1}	Tide + Wind 8 m s^{-1}
4.0×10^{-5}	$D_f = 1223.3$ $E_f = 654.8$	$D_f = 1893.7$ $E_f = 9863.6$	$D_f = 1448.5$ $E_f = 196.4$	$D_f = 1201.9$ $E_f = 520.5$	$D_f = 1009.1$ $E_f = 1008.6$
4.5×10^{-5}	$D_f = 1233.4$ $E_f = 736.6$	$D_f = 2025.4$ $E_f = 11096.6$	$D_f = 1453.2$ $E_f = 221.0$	$D_f = 1208.4$ $E_f = 585.5$	$D_f = 1017.7$ $E_f = 1134.6$
5.0×10^{-5}	$D_f = 1243.5$ $E_f = 818.4$	$D_f = 2157.1$ $E_f = 12329.5$	$D_f = 1458.0$ $E_f = 245.5$	$D_f = 1214.9$ $E_f = 650.6$	$D_f = 1026.4$ $E_f = 1260.7$
5.5×10^{-5}	$D_f = 1253.6$ $E_f = 900.3$	$D_f = 2288.7$ $E_f = 13562.5$	$D_f = 1462.7$ $E_f = 270.1$	$D_f = 1221.4$ $E_f = 715.6$	$D_f = 1035.0$ $E_f = 1386.8$
6.0×10^{-5}	$D_f = 1263.7$ $E_f = 982.1$	$D_f = 2420.4$ $E_f = 14795.4$	$D_f = 1467.5$ $E_f = 294.7$	$D_f = 1227.9$ $E_f = 780.7$	$D_f = 1043.6$ $E_f = 1512.8$
6.5×10^{-5}	$D_f = 1273.8$ $E_f = 1064.0$	$D_f = 2552.1$ $E_f = 16028.4$	$D_f = 1472.2$ $E_f = 319.2$	$D_f = 1234.4$ $E_f = 845.7$	$D_f = 1052.3$ $E_f = 1638.9$
7.0×10^{-5}	$D_f = 1283.9$ $E_f = 1145.8$	$D_f = 2683.8$ $E_f = 17261.3$	$D_f = 1477.0$ $E_f = 343.8$	$D_f = 1240.9$ $E_f = 910.8$	$D_f = 1060.9$ $E_f = 1765.0$